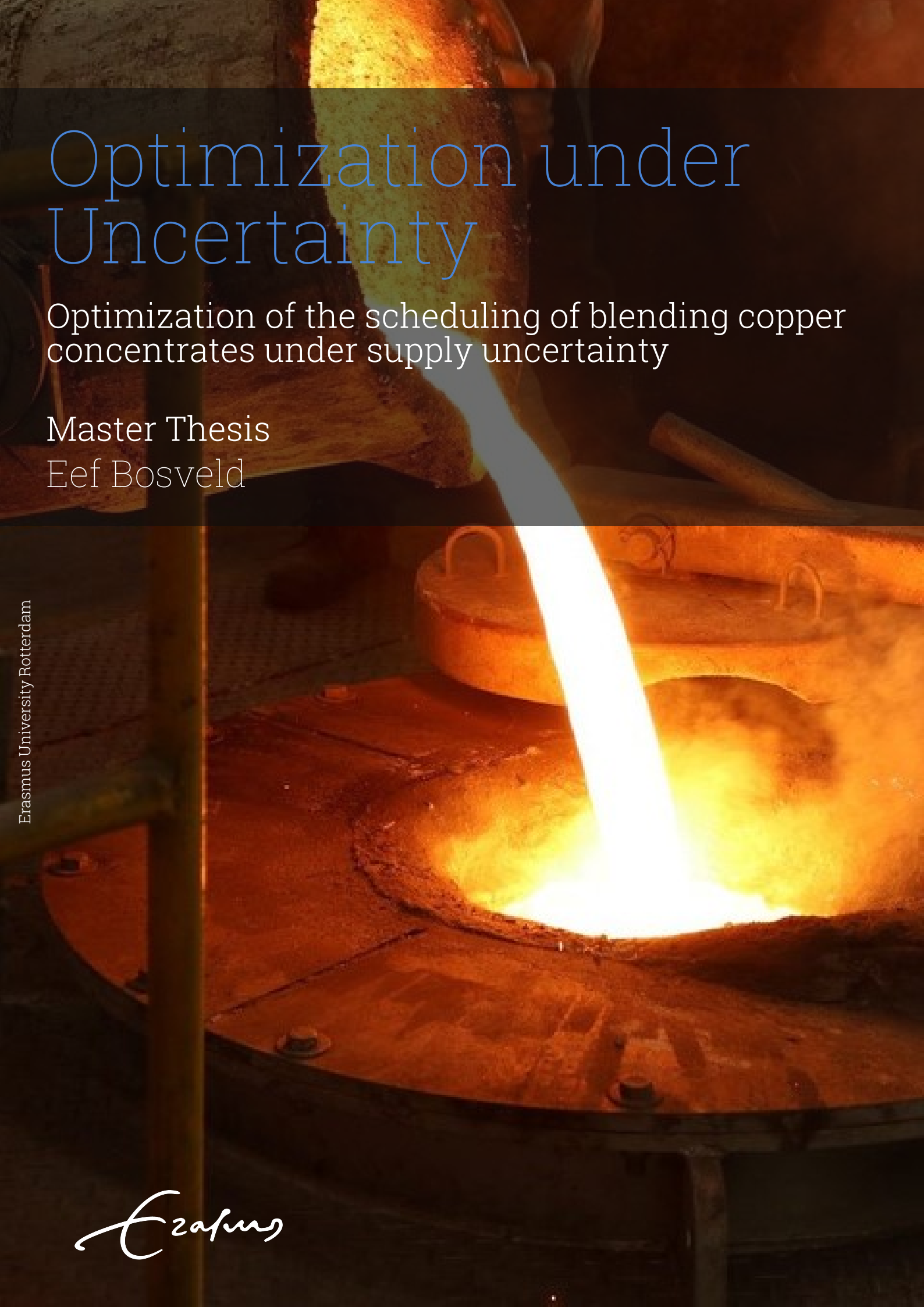

Optimization under Uncertainty

Optimization of the scheduling of blending copper concentrates under supply uncertainty

Master Thesis

Eef Bosveld

Erasmus University Rotterdam

Erasmus University Rotterdam
Erasmus School of Economics
Master Thesis Analytics and Operations Research in Logistics

Optimization of the scheduling of blending copper concentrates under supply uncertainty

Eef Bosveld (622070)

Supervisor:	Dr. O. Kuryatnikova
Second assessor:	Dr. E.R. van Beesten
Date final version:	Friday 26th April, 2024

Abstract

The optimization of the scheduling the blending of copper concentrates problem (SBCP) under supply uncertainty is studied. The SBCP has a multistage nature and seeks optimal blends of copper concentrates that satisfy the smelter throughput and elemental flow constraints and schedules them over a scheduling horizon, resulting in an optimal blending schedule. The arrival of copper concentrates and the continuously feeding of the flash smelting furnace are large-scale processes, involving strict production constraints. Additionally, there are frequent deviations in the expected mass of a copper concentrate, mass fraction of elements in a copper concentrate, and arrival time of a copper concentrate, denoted as supply uncertainty, proving the scheduling and optimization of these processes to be challenging.

The study aims to analyze how the supply uncertainty influences the feasibility of the SBCP and to create an optimization model that provides a robust solution, indicating a blending schedule that remains feasible for the entire scheduling horizon after the uncertainty realization. First, a discrete-time linear model is created to model the nominal SBCP. Afterward, successfully three optimization models are designed considering each one type of supply uncertainty. The models are tested across five generated data instances. A one-stage robust mass model is created which captures the mass uncertainty with a box uncertainty set, resulting in feasibility ratios of 100.0 evaluated across different mass uncertainty realizations. The mass fraction uncertainty is captured by a budgeted uncertainty set for each element having mass fraction uncertainty, denoted as the one-stage robust mass fraction model. This models results in feasibility ratios ranging from 70.0 to 100.0, decreasing by a larger scheduling horizon. The SBCP reacts sensitive to mass fraction uncertainty, especially for element 2 and element 7. Then, a one-stage and multistage stochastic model are formulated utilizing both a reduced scenario tree where for each copper concentrate two possible delays are selected. A reduced scenario tree is utilized because otherwise, the model becomes computationally too extensive. The resulting feasibility ratios obtained by the stochastic models which include no delay or the maximum delay of each copper concentrate vary between 50.0 and 100.0 due to over-conservatism of the model. Overall, the SBCP reacts very sensitively to arrival time uncertainty. Ultimately, the results illustrate that using robust blending schedules that consider supply uncertainty directly into the model improves the feasibility ratios of the solution for the SBCP under supply uncertainty, whereas, for both mass and mass fraction uncertainty, this can be obtained against a minor profit reduction and for arrival time uncertainty this proves to be more challenging and results in a significant profit reduction.

For further research, it is recommended to look into which scenarios are included in the stochastic model and look at how the current optimization methods can be applied and evaluated for instances with a larger scheduling horizon. Lastly, it is recommended to perform a sensitivity analysis on the capacity and start inventory present in the instances and validate the current results with actual (raw) data of a refinery.

Contents

1 Introduction

This chapter introduces the scheduling of the blending of copper concentrates problem (SBCP) under supply uncertainty. We explain the main concepts of the copper industry, the blending of copper concentrates, and the importance of considering supply uncertainty. We then proceed to introduce the research questions.

1.1. Supply chain uncertainty

Recent events such as the COVID-19 pandemic and the blockage of the Suez Canal have emphasized the sensitivity of supply chains to disruptions. A supply chain (SC) functions as a network facilitating the delivery of products and services from suppliers of raw materials to end customers through an integrated flow of information, material, and cash (Cox and Blackstone, 2002). Disruptions, characterized by being a low likelihood and high impact risk, significantly affect supply chains especially given the global nature of most supply chains nowadays (Suryawanshi and Dutta, 2022). However, these disruptions are not the only risks supply chains are exposed to. Supply chains are frequently exposed to uncertainties, characterized as a low-impact but high-likelihood risk, such as uncertainties in demand, supply, and lead time (Torabi et al., 2015).

Due to the unavoidable presence of uncertainties in the supply chain, uncertainties are an important concept to consider in supply chain management. Supply chain management (SCM) involves managing the flow of goods and services to and from a business, including all processes that transform raw material into final products (investopedia, 2024). Effective SCM is crucial for optimizing profits for stakeholders in the SC. Mathematical optimization methods can serve as valuable tools for finding (near) optimal solutions to SCM problems. Lately, the interest has increased in SCM in considering the uncertainties a SC faces by creating robust supply chains. Robustness provides systems with the strength to handle likely disturbances (Bundschuh et al., 2003). For finding robust solutions, many methods have been developed such as robust optimization and stochastic optimization. In academia, this field is called optimization under uncertainty and studies decision-making in the presence of uncertain parameters. The goal of this research field is to find solutions that perform well across a range of possible scenarios or real-world conditions.

Nevertheless, at the moment few businesses use optimization methods for their SCM and when they implement them they still rely much on deterministic nominal optimization methods. These methods do not consider parameter uncertainty, treating the expected value, also called the nominal value, as the actual value of a parameter. Therefore, the performance of the nominal solution is often worse than indicated due to real-world parameter uncertainty. A gap can thus be defined between the theoretical development of the optimization under uncertainty methods and the practical implementation of the optimization under uncertainty methods to real-world problems. It is intriguing to study if the developed optimization under uncertainty techniques effectively addresses uncertainties, yielding an optimal solution that ensures a robust supply chain for real-world problems.

1.2. Copper industry

This study considers copper production at a given refinery as a case study to analyze the effects of considering uncertainty directly in the optimization of a real-world problem. The thesis is written in cooperation with an individual company who could provide advise on the problem and assess whether the suggested model was realistic. This section provides an introduction to the copper industry. We introduce the metal copper, explain the main steps of copper production, describe the latest trends in the copper industry, and introduce the current optimization methods in the copper industry.

The metal copper

Copper is man's oldest used metal and is still highly used in industry. Around 9000 before common era the metal copper was discovered[1]. It was used early in man's history because copper is one of the few metals that occurs in nature in a directly usable metallic form. Because copper has properties like high thermal and electrical conductivity, good corrosion resistance, and malleability the metal is used to a great extent in industry (Langner, 2011). The main sectors where copper is used are construction, transport, power generation, energy transport, and electronics[2].

Copper production

Deposits of copper ore captured in sand and stone are located worldwide. A map of these deposits is presented in Figure 1.1; Chile dominates global copper resources and reserves, followed by the United States and Peru. Copper is produced from sulfide-copper ores or oxide-copper ores, which are mined from the deposits. Sulfide-copper ores are processed using pyrometallurgy; the extraction and purification of metals by processes involving the application of heat. Oxide-copper ores are processed using hydrometallurgy. This process uses aqueous solutions to extract and purify copper from oxide-copper ores at ordinary temperatures. In addition to the production of copper by mining copper ores, it is also possible to recycle copper, by melting old copper scrap. Copper can be recycled repeatedly without loss of quality[2].

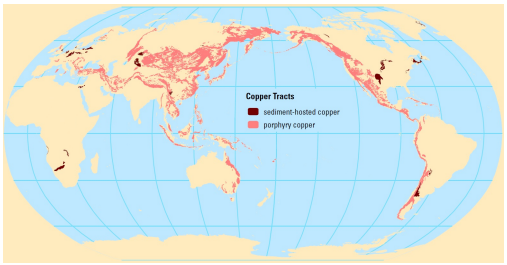

Figure 1.1: Map shows copper in sediment-hosted and porphyry deposits around the world (adapted from USGS science for a changing world, 2016)

This research studies the production of copper from sulfide-copper ores. The pyrometallurgy production process of copper consists of multiple steps, where the main steps are the formulation of copper concentrate, smelting, and electrolysis. The raw material of this production process is sulfide-copper ore and the final product is copper cathode. Sulfide-copper ore is mined and generally consists of 1 mass percent of copper element. Then this sulfide-copper ore is crushed and separated from the rock. The resulting product is called copper concentrate, a material that looks like fine sand and consists generally of 20 to 30 mass percent copper element combined with a mixture of other elements. Each copper concentrate has thus a distinct composition of elements. Next, a blend is created by combining various copper concentrates, which are all fed to the flash smelting furnace. After the copper concentrates have been smelted, they are further processed with the use of electrolysis into copper cathode. Copper cathode consists generally of 99.99 mass percent copper (Langner, 2011). The copper cathode is the final result of the refinery and is also called refined copper. The refined copper can be used to produce for instance copper wires, copper tubes, copper plates, or chips (Barros et al., 2022).

Trends in copper industry

The total worldwide copper mine production amounted to an estimated 22 million metric tons in 2022[3]. This makes it fourth in the list of most mined metals. Global copper production has seen steady growth over the past decade, rising from 16 million metric tons in 2010[3]. To meet the increasing demand, more copper has to be mined. Lately, in addition to the increase in demand for copper, there has been a gradual decrease in the grade of mined copper ores. Copper concentrates have become more

[1] worldatlas.com, 2023
[2] https://copperalliance.org/, 2023
[3] Statista.com, 2023

complex with higher impurity and rock content, and thus a lower concentration of copper. This trend has had a large effect on smelters as they have to increase throughput to maintain copper metal production while increasing operating costs due to processing the increased amounts of secondary products, like slag and acid, and the stabilization of waste streams. Therefore the need for optimization of the current processes in the copper industry has risen (Flores et al., 2020).

Optimization of copper production

This study focuses on the optimization of the first production step for a refinery; the feeding of the smelter with copper concentrates. This step is crucial for the production of copper because it determines the speed of the other sequential processes. In the flash smelting furnace chemical processes take place. To maintain them it is of high importance that the smelter works continuously. Therefore at every moment in time, a feasible blend of copper concentrates should be present at the site, which can be fed into the smelter. When the smelter can not be fed continuously, it leads to downtime, resulting in significant costs for the refinery. This is indicated as an infeasible solution. In addition to this scheduling problem, the profit of processing the copper concentrates can be maximized, by optimizing which copper concentrates are put in the blend. The corresponding problem, which optimizes when and which blend of copper concentrates should be fed to the smelter over a scheduling horizon, is called the scheduling of the blending of copper concentrates problem (SBCP).

Currently, the refinery uses a linear deterministic nominal optimization model to solve the SBCP over a three-month time horizon. This model optimizes both the SBCP and subsequent batch processes. Although this model is useful for analyzing copper concentrate trends, extending the scheduling horizon to capture long-term trends is hindered by computational constraints. At the moment it takes multiple hours to solve the model for a mid-term horizon. Despite generating an optimal blending schedule, direct implementation at the site is often impractical due to discrepancies between actual and expected supply parameters, denoted as supply uncertainty. Historical data reveals that supply uncertainty comprises three elements; uncertainty in the mass of a copper concentrate, uncertainty in the mass fraction of elements in a copper concentrate, and uncertainty in the arrival time of a copper concentrate. To accommodate this supply uncertainty, an additional linear model schedules blender operations within a shorter time horizon of a few days. However, even with the utilization of this second model, numerous adjustments are still required to find a feasible blend for the actual supply parameters. As a result, current blending operations heavily rely on human experience.

The refinery faces significant capacity and feasibility issues due to challenges in scheduling the blending of copper concentrates. Without effective long-term scheduling, this leads to the accumulation of specific copper concentrates on-site and leads to infeasible blending schedules, resulting in substantial costs during smelter downtime. These challenges underscore the limitations of current models in describing and optimizing the SBCP under supply uncertainty. The refinery desires to know what the effect of supply uncertainty is on the SBCP. The refinery aims to quantify the impact of supply uncertainty on the SBCP and assess the risk of infeasibility due to this uncertainty. With *quantifying* the impact is meant that an indicator is introduced which expresses for which part of uncertainty realizations the solution remains feasible over the entire scheduling horizon. Ultimately, the refinery aims to determine how to schedule the blending operations to be robust against supply uncertainty. Here, a robust blending schedule indicates that it remains feasible after supply uncertainty realization. To find a robust solution there is a pressing need for an optimization model capable of effectively optimizing the SBCP while considering supply uncertainty over a mid-term scheduling horizon. The optimization model must be computationally efficient so that eventually the scheduling horizon can be extended.

1.3. Research Questions

To address the identified research gap and refinery objective, the following main research question has been formulated. To be able to answer this research question thoroughly, we formulate four additional sub-questions, indexed further by (a) through (d).

"What is the influence of supply uncertainty on the feasibility of the SBCP and how can we find a robust solution to the SBCP, indicating a feasible blending schedule for the entire scheduling horizon after the uncertainty realization, with the use of optimization for a mid-term scheduling horizon?"

(a) How can the SBCP be modeled as a linear nominal optimization problem?

(b) Which optimization under uncertainty methods can best be applied to consider supply uncertainty for the SBCP? What are the drawbacks and benefits of the different optimization methods?

   i. Which optimization method is best suited to address uncertainty in the mass of a copper concentrate?

   ii. Which optimization method is best suited to address uncertainty in the mass fraction of elements in a copper concentrate?

   iii. Which optimization method is best suited to address uncertainty in the arrival time of a copper concentrate?

(c) How does the SBCP react to supply uncertainty? How can we quantify the risks associated with different uncertainty types and what is the quantified risk of the infeasibility of the *nominal* solution due to supply uncertainty for the SBCP?

   i. What is the quantified risk of the infeasibility of the *nominal* solution due to uncertainty in the mass of a copper concentrate?

   ii. What is the quantified risk of the infeasibility of the *nominal* solution due to uncertainty in the mass fraction of elements in a copper concentrate?

   iii. What is the quantified risk of the infeasibility of the *nominal* solution due to uncertainty in the arrival time of a copper concentrate?

(d) We call a solution to SBCP obtained via optimization under uncertainty a *robust* solution. The final sub-question is, what is the quantified risk of the infeasibility of the *robust* solution due to supply uncertainty for the SBCP? How much has the performance improved in comparison with the *nominal* solution?

   i. What is the quantified risk of the infeasibility of the *robust* solution due to uncertainty in the mass of a copper concentrate?

   ii. What is the quantified risk of the infeasibility of the *robust* solution due to uncertainty in the mass fraction of elements in a copper concentrate?

   iii. What is the quantified risk of the infeasibility of the *robust* solution due to uncertainty in the arrival time of a copper concentrate?

Chapter 3 and Chapter 4 address sub-question (a) and sub-question (b). In Chapter 3, we select the most suitable models to model the nominal SBCP and the SBCP while directly considering the supply uncertainty based on the reviewed literature. Thereafter, Chapter 4 outlines the implementation of these models. Subsequently, Chapter 6 and Chapter 7 address sub-question (c) and sub-question (d), respectively. We test the models on various instances, which are introduced in Chapter 5. Then in Chapter 6, we discuss the numerical results and draw relevant conclusions. Finally, we formulate answers to the research questions in Chapter 7 and discuss the limitations of the models and recommendations for further research in Chapter 8.

2

Problem description

To provide more insight into the complexity and comprehensiveness of copper production, Section 2.1 gives an explanation of the pyrometallurgy production of copper from sulfide-copper ores. Thereafter, Section 2.2 describes the consequent SBCP which is related to the first and second production processes of refining copper.

2.1. Pyrometallurgy copper production

The pyrometallurgy production process consists of six main steps. Figure 2.1 shows a schematic representation of this production process.

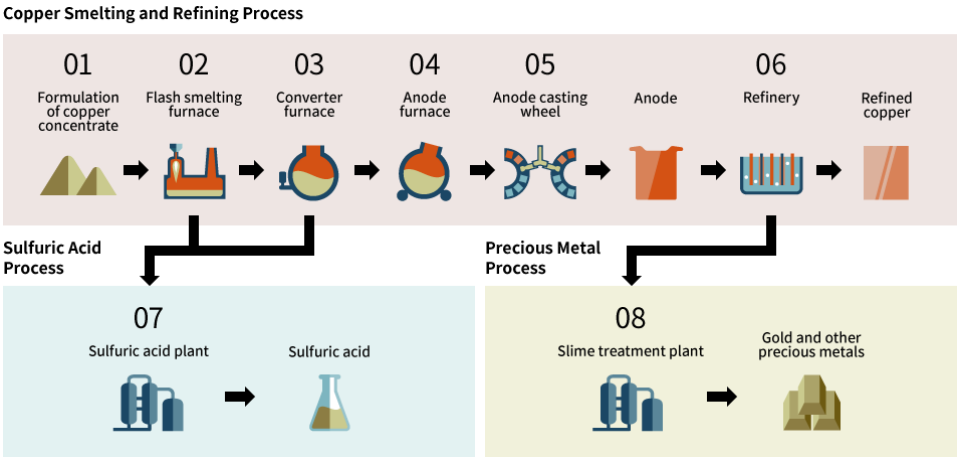

Figure 2.1: Schematic representation of copper smelting and refining process (adapted from Pan Pacific Copper, 2024)

As a first step, the sulfide-copper ore is extracted from a mine and is formulated into copper concentrate (Figure 2.1, step 1). At the mine, the extracted sulfide-copper ores are crushed into fine sand and are then separated from rock through froth flotation. This process adds a mixture of water and chemicals to the ores. The chemicals bind to the copper particles, which makes them hydrophobic. The tank is then aerated, causing hydrophobic copper particles to attach to the air bubbles that rise to the tank's top which separates the copper particles from the rock. Afterwards, excess water is removed, to thicken the material which leaves behind copper concentrate.

In the subsequent step, a blend of various copper concentrates and additional raw materials is created and is fed to the flash smelting furnace (Figure 2.1, step 2). Within the flash smelting furnace, the blend undergoes heating up to 1300 °C, transforming into a molten liquid. Following the smelting process, the residue consists of copper matte and slag. Copper matte is a mixture of copper, sulfur, and iron, while slag is a dense, glassy substance composed of iron, silica, and other impurities. The copper matte undergoes further heating in the converter, where sulfur and iron are burned off (Figure

2.1, step 3). This results in blister copper, which has a yellow color. The slag is a secondary byproduct.

As a next step, the oxygen is burned off the blister copper in the anode furnace (Figure 2.1, step 4), which results in a product called anode copper. The anode copper is molded in the anode casting wheel into large sheets (Figure 2.1, step 5), such that it can undergo the final production step involving electrolysis for refinement (Figure 2.1, step 6). Anode slabs are suspended in a sizable tank containing an electrolyte solution comprising copper sulfate and sulfuric acid for 14 days. During this period, copper ions migrate from the anode to the cathode, while other metals and impurities exit the anode, settling at the tank's base. These impurities are gathered and can be further refined to recover additional precious metals such as silver and gold. The ultimate products are sheets of refined copper cathodes (Pan Pacific Copper, 2024).

2.2. The scheduling of blending copper concentrates problem (SBCP)

This study focuses on the transition from the first to the second step of the pyrometallurgy copper production process (Figure 2.1): the formulation of copper concentrates and their processing in the flash smelting furnace. During this transition, a blend of various copper concentrates has to be made that eventually is fed into the flash smelting furnace. This section provides a detailed description of the resulting SBCP.

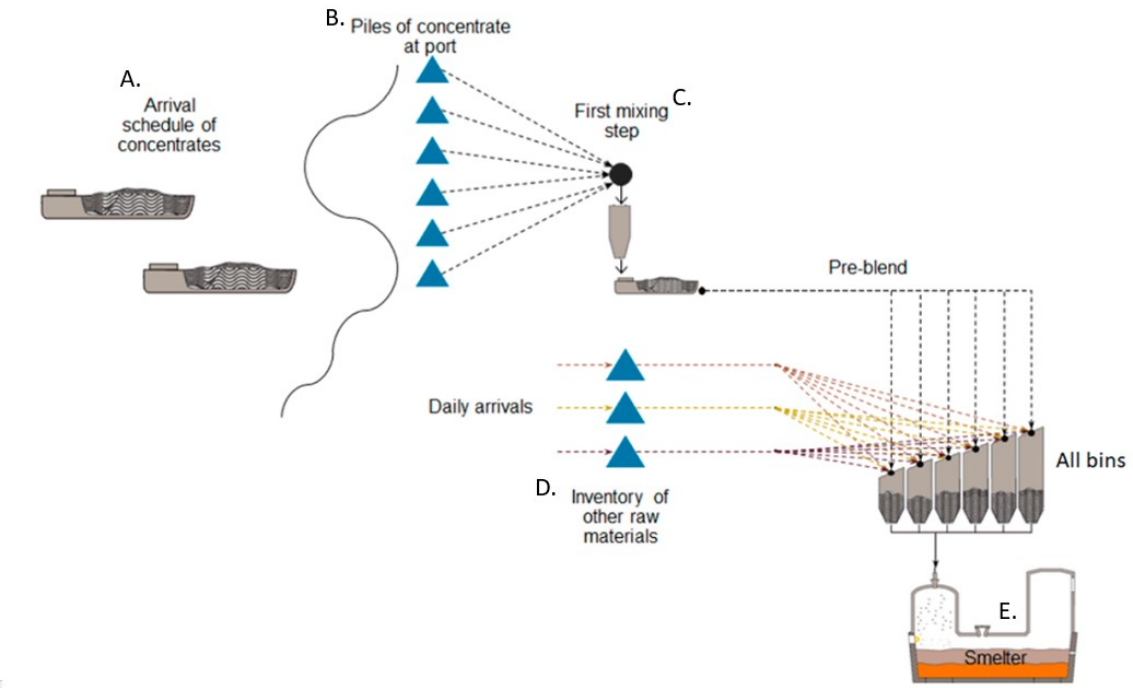

Figure 2.2: Schematic representation of the arrival and blending of copper concentrates (adapted from Song et al., 2018)

Figure 2.2 illustrates the SBCP, which comprises five sub-processes denoted by letters A to E. The SBCP begins with the arrival of copper concentrates at the site via maritime vessels (Figure 2.2, A). These concentrates may be transported on multiple vessels, and vice-versa, there may be multiple concentrates on a single vessel. The refinery purchases these copper concentrates from mines worldwide. The refinery procures these concentrates from mines worldwide through long-term contracts with suppliers and traders. These contracts specify expected parameters such as the mass of a copper concentrate, the mass fractions of elements in a copper concentrate, and the arrival time of a copper concentrate. However, it is common for the actual parameters to deviate from the agreed-upon expected values, a phenomenon often referred to as supply uncertainty. Notably, we assume that the actual supply parameters are independent of each other.

Upon arrival at the site, a copper concentrate is stored in a stockpile (Figure 2.2, B). A capacity limit, denoted as Q, is imposed on the total inventory of all stockpiles. The initial inventory at the start of the scheduling horizon, known as the start inventory, contains known values for both its actual mass and the mass fraction of elements, eliminating uncertainty in these parameters. Moving to the third step of the SBCP, a pre-blend of various copper concentrates is created periodically (Figure 2.2, C). Selected copper concentrates are transported to the pre-blender, where they are mixed. Parts of the copper concentrate inventory in a stockpile can be utilized for this process. Then the pre-blend is transported to the blender.

In the fourth step, the blend of copper concentrates is mixed with non-copper concentrates in the blender. Non-copper concentrates, including materials such as sand and recyclable materials, arrive daily at the site and are stored in raw material stockpiles (Figure 2.2, D). It is essential to ensure that the total amount of non-copper concentrates does not accumulate over time, with the total amount at the end of the time horizon being smaller or equal to MD. This combination of concentrates forms the final blend. Finally, in the fifth step, the final blend is fed into the smelter, where it transforms into a molten liquid form (Figure 2.2, E). Afterward, it undergoes further processing with the use of various batch processes as outlined in the pyrometallurgy copper production process (Section 2.1), ultimately yielding refined copper.

Profit is generated through the smelting of concentrates in the flash smelting furnace. The primary objective of the refinery is to maximize this total profit by finding an optimal blend of various concentrates. Each ton of concentrate processed in the smelter is associated with a profit parameter α_c depending on the composition of the copper concentrate. Copper concentrate typically contains high concentrations of copper, iron, and sulfur, along with lower concentrations of fluor, mercury, nickel, lead, and other elements (Muthumariappan and David, 2019). However, it is important to note that the composition of each copper concentrate varies, leading to variations in the related profit parameter α_c. For example, higher concentrations of precious metals, such as gold and silver, result in higher profit parameters. Conversely, copper concentrates containing elements that require removal, like pollutants, tend to have lower profit parameters. Furthermore, recyclable non-copper concentrates generally have lower profit parameters (Flores et al., 2020).

In addition to maximizing profit, ensuring that blends satisfy all smelter constraints is crucial. The smelter imposes strict elemental constraints, including upper bound constraints and interdependency constraints. The upper bound constraints ensure that a specific product quality is maintained and the interdependency constraints facilitate the correct chemical reactions and ensure that the heat is controlled in the smelter. To be able to meet these elemental constraints, various copper concentrates are blended to create a feasible blend allowed to enter the smelter. Operational constraints, such as employee shifts, limit the frequency of blend changes per day.

Ensuring the availability of a feasible blend in every period is crucial for the smelter to operate at its maximum capacity flow rate $\widehat{F}$. From the initial start-up period ET the smelter has to work exactly at the maximum capacity flow rate. The throughput per period can not exceed the maximum capacity of the smelter, nor can it fall below this capacity, as any decrease indicates downtime for the smelter, which should be avoided at all costs. After experiencing downtime, it takes multiple days to restart the chemical processes correctly. Therefore, preventing smelter downtime is essential, with failure costs amounting to 1,000,000 euros for each day the smelter is down.

To ensure continuous smelter operation, the blending of copper concentrates is scheduled in advance over a mid-term time horizon. This time horizon allows for potential corrective measures, such as adjusting the mass of purchased copper concentrates for future orders. Additionally, the optimization model with the mid-term time horizon for the SBCP is re-optimized every week. This enables the refinery to adapt its scheduling based on evolving knowledge of the supply uncertainty. The SBCP has thus a multistage nature; knowledge of uncertainties evolves and decisions can be made at multiple points in time. In summary, the SBCP is both an optimization and scheduling problem with a multistage nature. It seeks optimal blends of copper concentrates and schedules them over a time horizon, resulting in an optimal blending schedule that satisfies all smelter constraints.

3

Theoretical Background and Literature review

This chapter provides a review of the existing literature on the SBCP and a theoretical background for optimization under uncertainty. First, Section 3.1 reviews the literature on the SBCP. After that, Section 3.2 provides an overview of the main concepts in the field of optimization under uncertainty. From this theoretical background, we motivate the modeling choices in this study.

3.1. State-of-the-art optimization of the SBCP

This section provides an overview of existing literature on optimizing the SBCP under supply uncertainty. The refining of copper, as discussed in Section 2.1, involves multiple large-scale processes, each controlled by strict production constraints. Planning and scheduling these processes prove to be challenging due to factors such as insufficient measurement data, complex logistics, high raw-material variability, frequent disturbances, and maintenance operations that significantly impact ideal process cycles (Iiro Harjunkoski et al., 2006). Consequently, various studies have focused on optimizing processes within the copper industry. However, our review reveals a gap in specific research addressing the SBCP, particularly under supply uncertainty. This emphasizes the need to study the SBCP and develop optimization models capable of handling supply uncertainty effectively. The discussion begins with a review of the nominal optimization of the SBCP and then examines optimization models for the SBCP considering supply uncertainty. Due to the limited literature on the SBCP, this review broadens to include optimization of other copper industry processes and related business contexts.

Research has been done in multiple fields related to the SBCP. Derpich et al., 2019 optimized mine production using a linear model. In this context, mine production denotes the mining of copper ore and processing into copper concentrate. Although, the main restrictions of this problem are also dependent on the copper concentrate grade, denoting the availability of elements in the ores, the production constraints are different. Therefore, this model is not applicable to describe the SBCP. Similarly, Suominen et al., 2016 explored nonlinear optimization for scheduling the process in the converter. While related to the SBCP and enduring similar elemental constraints, the model is limited to batch processes, not able to capture the continuous working of the flash smelting furnace, which is critical for the SBCP.

Furthermore, the zinc industry addresses a blending composition problem, as explored in Savi et al., 2016. The study proposes a linear model that incorporates technical, environmental, and economic constraints. The linear model effectively captures the conflicting requirements of the problem and identifies optimal batches for zinc production that satisfy all these constraints. However, the model overlooks the scheduling aspect crucial for the SBCP and has different specific elemental constraints. Nevertheless, this study underscores the potential of linear models in addressing blending composition problems, offering promising insights for the SBCP.

In recent years, there has been a growing emphasis on concurrently optimizing multiple processes within the copper industry. Currently, it is common to schedule the processes manually, and a global overview of the overall production process is usually missing. This results in productivity losses since

the overall process efficiency may be far from optimal as many batches end up unnecessarily waiting for equipment in the next production stage (Iiro Harjunkoski et al., 2006). Both Suominen et al., n.d. and Iiro Harjunkoski et al., 2006 propose a mixed-integer linear optimization formulation (MILP) to concurrently optimize the batch process scheduling in the copper industry, aiming to increase the throughput compared to individual process optimization. These formulations have as main decision variables the batch processing times of the smelter, converter, and anode processes, with computational efficiency being a key consideration due to the need for frequent re-scheduling in response to uncertainty. However, it is important to note the limitations of these models in the context of the SBCP. While they demonstrate effectiveness in improving throughput compared to local optimization approaches, they are primarily designed for batch processes and do not inherently account for the continuous feeding of the smelter. Additionally, they assume unlimited material availability, overlooking the dynamic relationship between copper concentrate arrival and smelter feeding. As such, these linear batch optimization models are not directly applicable to the SBCP. Nevertheless, the focus on computationally efficient models and maximizing throughput remains noteworthy. Furthermore, these studies align with the overarching goal of enhancing the efficiency of copper refinement in response to current industry trends.

The long-term planning of the concentrate ingredient list in the copper industry is the focus of study in Zhang et al., 2022. This problem involves optimizing the SBCP while also considering the circular use of byproducts such as slag. To address the limitations of current short-term planning, a long-term planning model for the concentrate ingredient list is proposed, aiming to stabilize smelter production and maximize concentrate feeding duration. Given a large number of production constraints and the non-linear nature of the optimization objective, exact methods for optimizing the large-scale ingredient planning are challenging (Zhang et al., 2022). The number of stages, denoting the blends that are made, and the ingredient list itself are variable, leading to variable decision variables and constraints. A multistage dynamic optimization method is proposed to tackle this, utilizing multi-stage stochastic object coding. The model succeeds in finding solutions with longer concentrate feeding duration, which also have a lower variation in objective values making the solutions more robust. However, the model requires high computational effort to solve, although currently it does not consider supply uncertainty. Considering supply uncertainty will make the model more complex and hard to solve. Studying the effect of supply uncertainty on the SBCP being our main objective, we choose not to apply the above approach and model the SBCP in a more interpretable way by maximizing the profit generated by the throughput in the smelter instead of the feeding duration.

Ultimately, Song et al., 2018 proposes a discrete-time formulation to model the nominal SBCP. Compared to continuous-time models, discrete-time models offer advantages in terms of speed, comprehension, and operational implementation (Song et al., 2018). The resulting model is a large-scale, non-convex mixed-integer nonlinear program, incorporating logistic operation constraints. To address the computational complexity of this model, a two-step MILP-NLP decomposition procedure is introduced. The model provides a tight MILP relaxation so that the optimality gap is close to 0 %. However, the model's size is large and requires a large computational effort because there are many variables. For the industrial example, an additional relax-and-fix rolling horizon with nearby time windows overlaps is needed to solve the model. In summary, the MILP-NLP captures the SBCP sufficiently and performs well in finding near-optimal solutions however at the cost of high computational effort. To our knowledge no other paper proposed a discrete-time model for the SBCP.

Our objective is to develop a straightforward model for the nominal SBCP requiring minimal computational resources, enabling us to assess the effects of supply uncertainty. From the above-introduced literature we can conclude that not many formulations have been proposed for the SBCP, but a linear discrete-time model appears to be suitable for capturing the main concepts of the SBCP while maintaining computational efficiency. To achieve this, we will utilize the discrete-time model proposed in Song et al., 2018, with some simplifications to enhance its usability. Specifically, we will remove nonlinearity and omit operational and logistic constraints, focusing solely on the core aspects of the SBCP. While limited research has focused on optimizing the SBCP, even fewer studies explored the impact of supply uncertainty on its optimization. This is noteworthy, considering that the SBCP often operates under conditions of information uncertainty, necessitating frequent adjustments to solutions before implementation. Next, the studies that do analyze the SBCP under supply uncertainty will be discussed.

In Imanbekova et al., 2015, an intelligent network is proposed to control the blending and melting of copper concentrates in a electric furnace, employing an adapted neuro-fuzzy model. Intelligent systems offer advantages such as shorter computation times compared to large mathematical models typically used in the copper industry processes. The study successfully captures the mass fraction uncertainty with the use of a neuro-fuzzy models and uses it to effectively control the production process. Even though this is a promising result, this study chooses to not implement any intelligent model, because ultimately we want to be able to implement the created models on the existing optimization models of the refinery. In addition, a neural network does not provide easy to interpret insights into the relation of supply uncertainty and the feasibility of the SBCP. Therefore, the use of a neural network does not correspond with our research objective and will not be exploited.

Additionally, in Goodfellow and Dimitrakopoulos, 2016, the impact of mass fraction uncertainty on the production planning of multiple mines is examined. The study formulates a two-stage stochastic global optimization model, employing three different meta-heuristics as solving approaches. Results indicate a significant 22.6 percent deviation in objective value compared to conventional deterministic mine planning software. While these findings are promising, the use of meta-heuristics in solving the model may not align with our research objectives. However, it shows that considering the mass fraction uncertainty into the optimization method significantly increased the efficiency of the solution.

Finally, Pengfei Chenga et al., 2020 delves into mass fraction uncertainty specifically within the SBCP context. A continuous-time formulation is proposed, resulting in a large-scale non-convex mixed-integer nonlinear model. To tackle the complexity, a two-step MILP-NLP decomposition technique is employed, resulting in a robust model capable of obtaining optimal solutions while ensuring quality requirements under moderate uncertainty. The study underscores the significant challenge of solving the SBCP posed by the problem's complexity and the substantial impact of uncertainty on element constraints(Pengfei Chenga et al., 2020). While the paper provides promising formulations for addressing mass fraction uncertainty in the SBCP, it is important to note its limitations. Specifically, the study only considers uncertainty in a maximum of three elements simultaneously and neglects uncertainty related to the mass and arrival time of copper concentrate.

In conclusion, the SBCP has received relative little attention as a research area, despite its importance in the copper industry. Key challenges in this domain include the need to develop computationally efficient models that can effectively account for comprehensive production constraints and ensure the required continuous working of the flash smelting furnace. Notably, an emerging field of research pertains to considering supply uncertainty in optimization models for the SBCP, with a focus on mass fraction uncertainty being the primary area of study thus far. However, there remains a significant gap in the literature regarding other types of uncertainty, such as mass uncertainty and arrival time uncertainty, which warrant further exploration. Addressing these uncertainties could provide valuable insights into optimizing the SBCP process and enhancing its efficiency and reliability in real-world applications. Overall, while significant progress has been made in understanding and modeling the SBCP, there is still much to be done to fully realize its potential and address the challenges it presents in the context of supply uncertainty.

3.2. Framework optimization under uncertainty

This section provides an overview of the main concepts of optimization under uncertainty. Section 3.2.1 and Section 3.2.2 introduce the concepts of feasibility and the objective function under uncertainty and the formulation of one-stage and multistage models. Thereafter, Section 3.2.3 and Section 3.2.4 introduce the two main approaches in the optimization under uncertainty field; robust optimization and stochastic optimization. There exists more optimization under uncertainty approaches, however, these are not considered in this study because the two main approaches provide enough concepts to start addressing the uncertainty in the SBCP.

3.2.1. Feasibility and objective function under uncertainty

Problems in the field of optimization under uncertainty are characterized by the fact that decisions have to be made without knowing what their full effect will be (Sahinidis, 2004). This is caused by the fact

that some parameters are uncertain; only their expected value, called nominal value, is known at the moment of decision-making, and not their actual value. This is denoted as parameter uncertainty or data uncertainty. Sometimes the parameters are random or stochastic, but actual data can also be different due to for instance a measurement error. The field of optimization under uncertainty makes an effort to consider this uncertainty directly in the optimization method. When the objective function and/or feasibility set are dependent on the uncertain parameter, this implies that for different realizations of the uncertainty the objective and/or the feasibility is different (Figure 3.1, Bakker et al., 2020). This leads to different optimal solutions for different realizations of the uncertainty. If the solution must be feasible for all possible realizations of the uncertainty, this reduces the feasibility space. This results in a more conservative solution; for a maximization problem such as the SBCP, this implies a lower optimal objective.

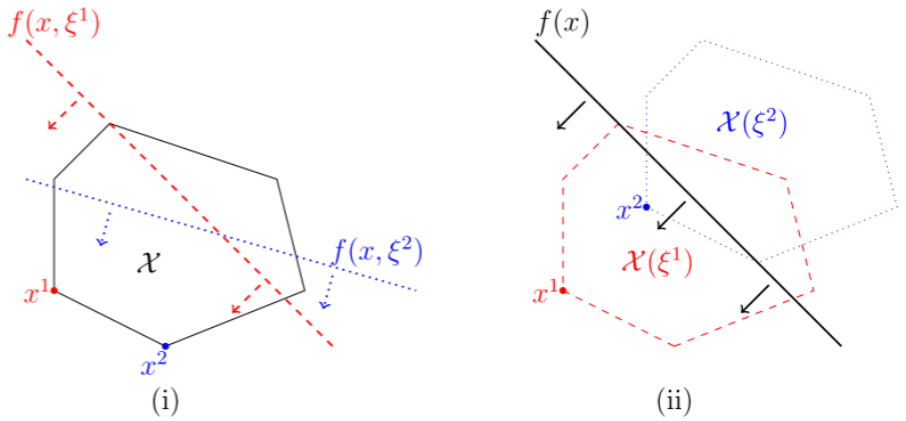

Figure 3.1: For different realizations of the uncertainty the objective (i) and feasibility set (ii) can be different. This leads to different optimal solutions. Here, $\mathcal{X}$ and $f(x)$ represent the feasible region and objective function under the nominal values of the uncertain parameter ζ. Further, $\mathcal{X}(\zeta)$ and $f(x,\zeta)$ represent the feasible region and objective function under alternative realizations of the uncertain parameter ζ (adapted from Bakker et al., 2020).

3.2.2. One-stage and multi-stage models

An important concept in optimization under uncertainty is the definition of stages; the partitioning of the decision variables in sets. In a multi-period optimization problem, a problem where decisions have to be made for multiple periods, one can model the problem as either a one-stage or a multistage model. A problem has a multistage nature when more uncertainty is known over time and at multiple points in time decisions can be made (Pflug and lois Pichler, 2014). A multistage model uses these characteristics, by dividing the decision variables into different sets, adding flexibility to the model by providing that certain decisions can be made after some uncertainty is known. In contrast, a one-stage formulation requires all decisions to be made before uncertainty is known.

The timeline of a multistage problem is shown in equation (3.1). Here, x_t denotes a decision at a decision period t. The parameter ξ_t denotes the random observed uncertainty after decision period t, but before decision period $t+1$. The uncertainty thus becomes known in the time frame $[t,\ t+1]$. Therefore at decision period x_{t+1} a decision can be made based on more information than in period t (Pflug and lois Pichler, 2014).

$$x_0 \rightarrow \xi_1 \rightarrow x_1 \rightarrow ... \rightarrow x_{T-1} \rightarrow \xi_T \tag{3.1}$$

Decision x_0 has to be made before any uncertainty is known, such decisions are called here-and-now decisions. The decisions that are made after the random events of the previous stage have presented themselves are called wait-and-see decisions. The objective is to choose the here-and-now variables in a way that the sum of the here-and-now objective value and the expected value of the uncertain random wait-and-see objective is optimized (Pflug and lois Pichler, 2014).

The SBCP is a multi-period problem that has a multistage nature. So as outlined in the above literature the problem can be modeled both as a one-stage and multistage model. Multi-stage models yield the

potential to lead to better solutions than their one-stage alternative formulations due to more flexibility, but translating this advantage into an actual improvement remains often a challenge (Bakker et al., 2020). Multistage models are comprehensive and often computationally hard to solve. Therefore, a one-stage model is sometimes more suitable to implement. Per optimization approach applied to the SBCP, it will be decided if it is worth modeling the more complex multistage formulation.

3.2.3. Stochastic optimization

One of the main approaches in optimization under uncertainty is stochastic optimization. In stochastic optimization, it is assumed that the uncertainty is random or stochastic and the probability distribution of the uncertainty is known. Consequently, this information is used to optimize the expected objective. The idea of stochastic optimization is to optimize the problem such that it performs optimally on average, considering the uncertainty (Birge and Louveaux, 2011). The field of stochastic optimization started in 1950 when the concept of a chance constraint was introduced (Kucukyavyz and Jiang, 2022). A chance constraint guarantees that a constraint holds with a certain probability α. This is formulated as follows,

$$P(Ax \leq b) \geq \alpha, \tag{3.2}$$

where both the parameter matrix A and the right-value parameter b can be uncertain following a probability distribution $\mathcal{G}$. A chance constraint reflects well the idea of stochastic optimization, however, due to the probability distributions in the formulations chance constraints are often computationally intractable to solve. The feasibility space may become even non-convex (Birge and Louveaux, 2011). Therefore, this research does not implement chance constraints.

When a discrete parameter is uncertain, a natural approach to describe the uncertainty is as a finite set of scenarios $\mathcal{Z}$. Each scenario z denotes a possible realization of the uncertain parameters and occurs with a certain probability p_z. The probability p_z can be calculated with the use of the probability distribution $\mathcal{G}$ of the uncertain parameter. When we substitute the uncertain parameters for their finite set of scenarios in the mathematical formulation, we formulate a deterministic equivalent problem (Birge and Louveaux, 2011). Problem (3.3) shows an example of a deterministic equivalent formulation for a multistage model, where the number of stages is two.

$$\begin{aligned} \max_{x,y} \quad & c^T x + \sum_{z=1}^{Z} p_z (q^{zT} y^z) && && (3.3)\\ \text{s.t.} \quad & Ax = b, \\ & T^z x + W^z y^z = h^z && \forall 1, ..., Z \\ & x \geq 0, \quad y^z \geq 0 && \forall 1, ..., Z \end{aligned}$$

Here, x denotes the here-and-now decisions and y denotes the wait-and-see decisions. The wait-and-see decisions y can vary depending on the realization of the uncertainty, and these variables are thus defined for each scenario z. The parameters T, W, and h are uncertain and the constraints have to hold for all the scenarios z of these parameters. The objective maximizes the objective value of the here-and-now variables and the expected objective value of the wait-and-see variables. The latter is calculated by multiplying the expected objective value of a scenario, which is denoted as $q^{zT} y^z$, with the probability of that scenario p_z and summing this value for all scenarios $z \in \mathcal{Z}$. The deterministic equivalent problem is still a linear model, however, when the number of scenarios increases, these models can become very large. Especially for multistage models, if the number of stages increases, even if only a few realizations are allowed in each stage, the model can be extremely large (Birge and Louveaux, 2011). Therefore methods that solve directly the deterministic equivalent problem are often computationally intensive.

Research has explored more efficient methods for solving the deterministic equivalent problem. Some multistage models lend themselves to be modeled as a dynamic programming problem. In dynamic programming, the problem is broken down into simpler sub-problems in a recursive way (Birge and Louveaux, 2011). To be able to implement dynamic programming the decisions of the new stage must be only dependent on the realization of the uncertainty in the previous step. For the SBCP the current decisions are dependent on the realizations of the uncertainty of all the previous stages, therefore it

is not convenient to implement dynamic programming. It is also possible to exploit other structures of the problem, by implementing other decomposition approaches (Birge and Louveaux, 2011). However, these decomposition approaches are not applied to the SBCP because the extensiveness of these methods is beyond the scope of this research.

Another way of simplifying the deterministic equivalent program is by excluding some scenarios. By solving problem (3.3) for a smaller set of scenarios $\overline{\mathcal{Z}} \subset \mathcal{Z}$, an approximation of the deterministic equivalent problem is solved. The challenge is to find such a reduced set of scenarios $\overline{\mathcal{Z}}$ so that the solution of the approximation still provides a well-performing solution. In general, there are two ways to define the reduced set of scenarios $\overline{\mathcal{Z}}$. Firstly, one can sample scenarios from the probability distribution $\mathcal{G}$ that describes the uncertain parameter. This method aims to formulate a smaller set of scenarios that effectively covers a significant portion of the probability space. Alternatively, the reduced set $\overline{\mathcal{Z}}$ can be strategically designed by selectively including scenarios. For example, it might encompass all worst-case scenarios or only realizations of the uncertainty with a high probability of occurring.

For the SBCP we will model the arrival time uncertainty with the use of stochastic optimization with a reduced set of scenarios $\overline{\mathcal{Z}}$, as described above. The created linear nominal model for the SBCP is a discrete-time model, as will be explained in Section 4.1.2, making the representation in scenarios well-suited for capturing the discrete arrival time uncertainty. Stochastic optimization is possible for the SBCP because the probability distributions of the uncertainties are known. Moreover, optimizing the expected objective aligns closely with the repetitive nature of the SBCP over time. We will begin by modeling a one-stage stochastic model, aiming to provide a simplified representation of the SBCP. However, we anticipate that the SBCP may be very sensitive to arrival time uncertainty. As a result, the one-stage formulation may produce overly conservative models or even infeasible solutions. To address this concern, we will also implement a multistage stochastic model specifically for arrival time uncertainty. For the other two supply uncertainties, namely the mass uncertainty and the mass fraction uncertainty, we choose to not model them using stochastic optimization. This is because the possible realizations of these uncertainties are less suitable to describe with a finite number of scenarios.

3.2.4. Robust optimization

The idea of the second approach, robust optimization, is to provide a robust solution that is, a solution that is immune against the effect of uncertainty in the parameters. The advantage of robust optimization is that the uncertainty does not have to be of stochastic nature. The probability distribution of the uncertainty is not needed, and the constraints will not hold for a certain probability as in the chance constraints. Instead, it is guaranteed that the solution is feasible against all realizations of the uncertainty. Therefore, the solution performs well in the worst-case scenario and consequently is a conservative solution (Ben-Tal et al., 2009). In robust optimization, the uncertainty is represented by an uncertainty set $\mathcal{U}$. This is a set that summarizes the available information about the actual realizations of the uncertain parameters. Equation (3.4) shows the definition of an uncertain Linear Optimization ($LO_{\mathcal{U}}$). It is the collection of LP programs with the data (c, A, b) varying in a given uncertainty set $\mathcal{U}$.

$$\left\{ \max_x \{c^T x : Ax \leq b\} \right\}_{(c,A,b)\in\mathcal{U}} \tag{3.4}$$

The vector of decision variables is defined as $x \in \mathbb{R}^n$, $c \in \mathbb{R}^n$ is the vector in the objective, A is an m×n constraint matrix, and $b \in \mathbb{R}^m$ is the right-hand side vector. Equation (3.5) presents the resulting robust constraint, where the vector $x \in \mathbb{R}^n$ should satisfy all the realizations from the uncertainty set.

$$Ax \leq b \quad \forall (c, A, b) \in \mathcal{U} \tag{3.5}$$

From the worst-case perspective, the robust objective $\widehat{c}(x)$ is defined as the smallest value of the true objective over all realizations of the data from the uncertainty set as formulated in equation (3.6).

$$\widehat{c}(x) = \min_{(c,A,b)\in U} [c^T x] \tag{3.6}$$

In robust optimization, the best robust value of the objective among all robust feasible solutions is searched. This results in problem (3.7) and is called the robust counterpart of the $LO_{\mathcal{U}}$ problem.

$$\max_x \left\{ \min_{(c,A,b)\in U} [c^T x] : Ax \leq b \, \forall (c, A, b) \in \mathcal{U} \right\} \tag{3.7}$$

The robust counterpart as formulated in equation (3.7) is now formulated in open form, due to the notation $(c, A, b) \in \mathcal{U}$. The uncertainty set $\mathcal{U}$ may consist of infinitely many points, resulting in infinitely many linear constraints. Solving this optimization problem is computationally difficult. For certain uncertainty sets, it is computationally tractable to obtain a deterministic equivalent formulation of the robust counterpart for linear robust problems. This is called the robust counterpart in closed form and dual theory is often used to derive this (Ben-Tal et al., 2009). It is important to mention that not all uncertainty sets can be used in equivalent deterministic formulations, and then approximations or alternative solution methods have to be used to solve the robust optimization problem.

The choice of uncertainty set in robust optimization is thus important and it influences the performance of the robust optimization model significantly. However, constructing an uncertainty set is more of a design process than a precise science, as it involves numerous design choices. The overall goal is to construct the uncertainty set with a volume as small as possible, to avoid the robust problem (3.7) being over-conservative, containing an extensive number of uncertainty realizations. On the other hand, an uncertainty set that is too small may overlook crucial uncertainties, resulting in a non-robust solution (Ben-Tal et al., 2009). One should keep in mind, that when the probability distribution of the uncertainty or historical data is known, including α percent of the uncertainties in the set, ensures robustness against more than α percent of uncertainties, as per the law of total probability (Gorissen et al., 2015). Therefore, it is typically unnecessary to include all possible uncertainty realizations in the set. When designing an uncertainty set, it is common practice to generate multiple realizations based on historical data to observe the distribution they form. Subsequently, a suitable shape for the uncertainty set is chosen that includes most of the observations. Common types of uncertainty sets include the box uncertainty set, budgeted uncertainty set, ellipsoidal uncertainty set, polyhedral uncertainty set, cone uncertainty set, and general convex uncertainty set (Ben-Tal et al., 2009).

A box uncertainty set is a straightforward approach that defines the parameter's actual value within an interval around the nominal parameter value and often yields satisfactory results in practical problems. However, the box uncertainty set assumes that all parameters can reach their worst-case values simultaneously, potentially leading to an overly conservative model (Gorissen et al., 2015). To address this issue while preserving the simplicity of the box uncertainty set, a budgeted uncertainty set can be implemented. A budgeted uncertainty set operates similarly to a box uncertainty set but imposes a constraint on the number of parameters allowed to take their worst-case values simultaneously. In this way, by effectively cutting the corners of the box, the volume of the uncertainty set is reduced, making it less conservative (Gorissen et al., 2015). Further, an ellipsoidal uncertainty set describes the uncertainty effectively when the uncertainty follows a normal distribution. It has been proven that when the uncertainty is normally distributed, it is the smallest set that can ensure that the constraint holds with at least 95 percent probability (Ben-Tal et al., 2009). The cone uncertainty set, the polyhedral uncertainty set, and the general convex uncertainty sets are all sets that try to improve the capturing of the uncertain data in the set, with smaller volumes. However, these more complicated uncertainty sets make the derivation of the robust counterparts also more comprehensive (Ben-Tal et al., 2009).

For the SBCP, the refinery prioritizes the feasibility highly and both uncertainties can be represented with the use of a connected uncertainty set. Therefore, robust optimization is a very suitable approach to consider the supply uncertainty because it aligns well with the guarantee that the problem will be feasible even in the worst case. We thus model the mass uncertainty and the mass fraction uncertainty with the use of robust optimization. A budgeted uncertainty set is chosen to describe these two supply uncertainties. A huge advantage of the budgeted uncertainty set is that it reduces the volume of the uncertainty set in comparison with the box uncertainty set, but still is a polyhedron, resulting in a robust linear programming problem. We choose to implement a one-stage robust model initially to address the two supply uncertainties. This decision is driven by the desire to balance computational efficiency and model complexity. Given the current stage of the analysis, an immediate implementation of a comprehensive multistage model may not be needed. We aim to avoid unnecessary computational effort by utilizing a simpler approach until it becomes necessary to employ a more comprehensive multistage model. For example, if the one-stage robust optimization model becomes infeasible.

4
Methodology

In this chapter, we explain the methodology. Section 4.1 introduces the created nominal linear mathematical model for the SBCP. Following this, Section 4.2 mathematically describes the supply uncertainty. In Sections 4.3 and 4.4 we describe the implementation of the chosen optimization under uncertainty method regarding the mass uncertainty and the mass fraction uncertainty, respectively. To account for these uncertainties, robust optimization has been chosen. In Section 4.5, we describe the chosen optimization under uncertainty method regarding the arrival time uncertainty of a copper concentrate. To account for this uncertainty, stochastic optimization has been chosen. Finally, Sections 5.1 and 6.1 cover the description of data generation and the evaluation method of the models with the use of simulation, respectively.

4.1. Nominal mathematical model for SBCP

To analyze the SBCP under supply uncertainty, we initially developed a nominal linear model for optimizing the SBCP. A nominal model considers no uncertainty in the parameters and instead utilizes the expected values of the parameters as deterministic inputs. Our model is constructed based on the mathematical formulation proposed in Song et al., 2018, with additional assumptions made. Firstly, we take a more generalized approach by excluding operational constraints such as feeding and unloading constraints of bins. Additionally, we simplify the blending network to exclude nonlinear constraints. By designing the blending network to eliminate multiple outgoing flows after blending copper concentrates, we can omit the nonlinear identical composition constraints for flows introduced in Song et al., 2018. Moreover, we do not directly model the transport of copper concentrates from the stockpiles to the pre-blender via a transfer ship. Instead, we apply a standard delay to the arrival time of all copper concentrates during pre-processing, effectively including the time utilization of the transportation step. In this section, we introduce the mathematical formulation of the created nominal linear model for optimizing the SBCP. Section 4.1.1 presents the notation of the mathematical model. Furthermore, Section 4.1.2 explains the mathematical model. Then, Section 4.1.3 describes an extension of the nominal linear model to better understand the problem's infeasibility. Finally, Section 4.1.4 outlines the standard reformulation of a mathematical model to adapt it for implementation of optimization under uncertainty methods.

4.1.1. Introduction notation

We begin with introducing the notation of the mathematical model. Table 4.1 introduces the indices and sets used in the mathematical formulation. Table 4.2 presents the defined decision variables, while Table 4.3 presents the used parameters. Furthermore, we describe the notation according to a schematic overview of the model.

Table 4.1: Indices and sets of the nominal SBCP model.

Sets	
$t \in \mathcal{T}$	Time periods in days, where $t = 1, ..., T$.
$c \in \mathcal{C}$	Set of concentrates, where $c = 1, ..., C$ and $C = I + CC + NC$.
$c \in \mathcal{CC} \subset \mathcal{C}$	Subset of copper concentrates, where $c = 1, ..., I, I + 1, ..., CC$. Here, I denotes the number of start-inventory.
$c \in \mathcal{NC} \subset \mathcal{C}$	Subset of non-copper concentrates which arrive daily, where $c = CC + 1, ..., CC + NC$.
$k \in \mathcal{K}$	Chemical elements, with $k = 1, ..., K$.
$m \in \mathcal{M}$	Maritime vessels, where $m = 1, ..., M$.
$j \in \mathcal{S}$	Stockpiles of copper concentrates, where $j = 1, ..., S$.
$j \in \mathcal{N}$	Stockpiles of non-copper concentrates, where $j = 1, ..., N$.
$v \in \mathcal{V}$	Set of vertices in graph $\mathcal{G}$, where $j = 1, ..., S, S + 1, ..., N + S, \lvert\mathcal{V}\rvert - 1, \lvert\mathcal{V}\rvert$. The index $\lvert\mathcal{V}\rvert - 1$ is also denoted as P and the index $\lvert\mathcal{V}\rvert$ as B.
$e \in \mathcal{E}$	Set of edges in graph $\mathcal{G}$.

Table 4.2: Decision variables of the nominal SBCP model.

Decision variables	
$f_{e,c,t}$	Flow rate on edge e of concentrate c in period t.
$F_{e,t}$	Total flow rate on edge e in period t.
$x_{j,c,t}$	Inventory at stockpile j of concentrate c in period t.
$X_{j,t}$	Total inventory of copper concentrates at stockpile j in period t.
TF_t	Total flow rate into the smelter in period t.
$E_{k,t}$	Flow rate of individual element k into the smelter in period t.
u_t	Binary variable defines the feasibility of the problem in period t (refer to Section 4.1.3 Extension).

Table 4.3: Parameters of the nominal SBCP model.

Parameters	
$g_{m,j,c,t}$	Actual mass of copper concentrate c that is shipped with maritime vessel m and unloaded at stockpile j in actual period t, with $j \in \mathcal{S}$. Both the value of the mass and the arrival period are uncertain.
$\overline{g_{m,j,c,t'}}$	Nominal mass of copper concentrate c that is shipped with maritime vessel m and unloaded at stockpile j in nominal period t', with $j \in \mathcal{S}$.
$h_{j,c,t}$	Daily arrival of non-copper concentrate c at stockpile j in period t, with $j \in \mathcal{N}$.
$\overline{F_{e,t}}$	Upper bound on the total flow rate on edge e in period t.
$\underline{F_{e,t}}$	Lower bound on the total flow rate on edge e in period t.
$\overline{ET}$	Earliest period when the smelter is fully operating.
T	Length of the scheduling time horizon.
MD	Maximum amount of non-copper concentrate material at the end of the scheduling horizon.
Q	Maximum amount of total copper concentrate at the stockpiles.
α_c	Profit for processing one ton of concentrate c.
$\theta_{k,c}$	Actual mass fraction of element k in concentrate c. The mass fraction of an element is uncertain.
$\overline{\theta_{k,c}}$	Nominal mass fraction of element k in concentrate c.
$\widehat{F}$	Full flow capacity of the smelter.
$\overline{\chi_k}$	Upper bound on the mass fraction of element k in the final blending.
U_k	Upper bound parameters for interdependency constraints of element k.
W_k	Weight parameters for interdependency constraints of element k.

We model the blending network of the SBCP using a directed graph $\mathcal{G} = (\mathcal{V}, \mathcal{E})$, where $\mathcal{V}$ represents the set of vertices and $\mathcal{E}$ represents the set of edges. Figure 4.1 illustrates this graph schematically. Each vertex is indexed as $j \in \mathcal{V}$, with $|\mathcal{V}|$ indicating the total number of vertices. The blender is represented by vertex $|\mathcal{V}|$, further in the report denoted as vertex B, while the pre-blender is represented by vertex $|\mathcal{V}|-1$, further in the report denoted as vertex P. The indices of the vertices which represent the copper concentrate stockpiles range from 1 to S, and the indices of the vertices which represent the non-copper concentrate stockpiles range from $S+1$ to $S+N$. Throughout the report, for readability, we denote these indices as $j \in \mathcal{S}$ for the copper concentrate stockpiles and $j \in \mathcal{N}$ for the non-copper concentrate stockpiles. Consequently, each edge connects then vertices j and j', denoted as $e = (j, j')$, where both $j, j' \in \mathcal{V}$.

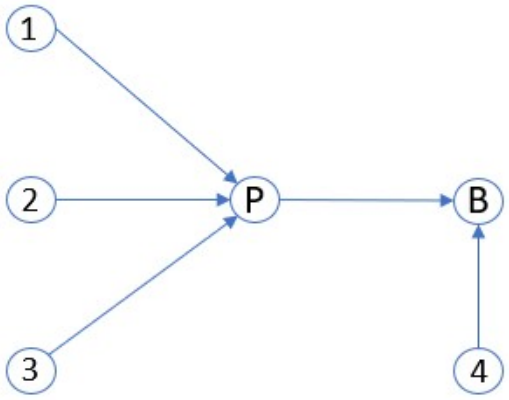

Figure 4.1: Schematic representation of directed graph $\mathcal{G} = (\mathcal{V}, \mathcal{E})$. In this example, indices $1, ..., 3$ denote the subset $\mathcal{S} \subset \mathcal{V}$ and index 4 denotes the subset $\mathcal{N} \subset \mathcal{V}$.

We define the decision variable $f_{e,c,t}$ on each edge e, denoting the flow rate of concentrate c in period t. This flow rate determines the throughput of a concentrate between two vertices in a period and is defined for every $c \in \mathcal{C}$. External flows of concentrates are the in- and output of the blending network. Figure 4.2 presents a schematic overview of the full model for the SBCP. The parameter $g_{m,j,c,t}$ represents copper concentrate c which arrived on maritime vessel m and is unloaded at stockpile j in period t. Similarly, the parameter $h_{j,c,t}$ signifies the arrival of non-copper concentrate c at stockpile j in period t, which arrive daily. These parameters serve as inputs to the blending network. The total flow rate fed into the smelter in period t is denoted as the decision variable TF_t, constituting the output of the blending network.

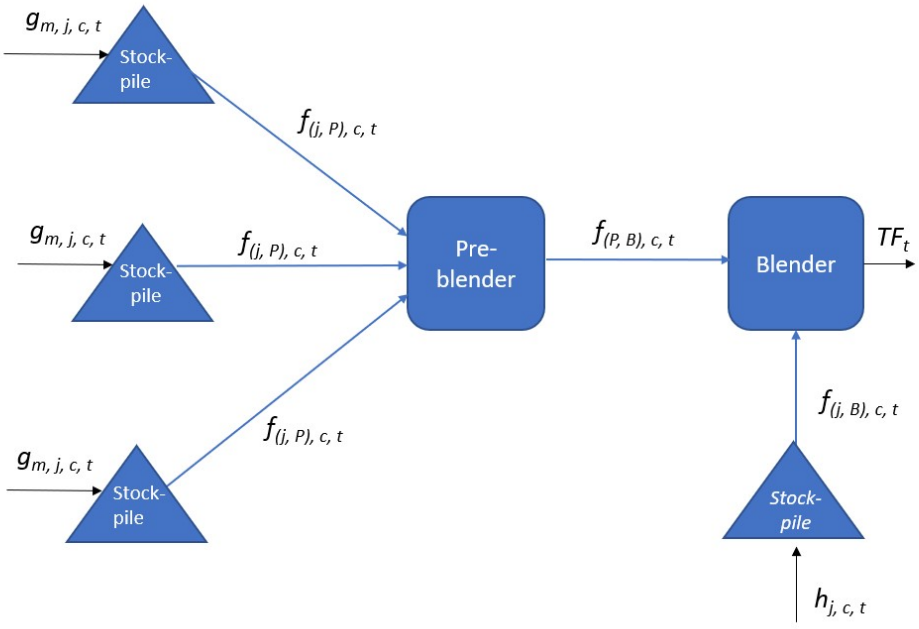

Figure 4.2: Schematic representation of the full model for the SBCP.

4.1.2. Nominal mathematical model

Objective Function. The objective is shown in equation (4.2) and maximizes the gross marginal of processing concentrates in the smelter. The profit which is earned for processing one ton of copper concentrate c, is denoted by parameter α_c. The flow rate that enters the smelter from the blender is equal to the total flow rate into the blender. To define the flow rate that enters the blender, the subset $\mathcal{E}'$ is defined as the set of all the edges that are directed towards the blender, see equation (4.1). Then, the total incoming flow rate of a concentrate into the blender B is defined as the sum over all edges in subset $\mathcal{E}'$ of the flow rate variable $f_{e,c,t}$.

$$\mathcal{E}' = \{e \in \mathcal{E} : e = (j, B), \forall j \in \{P\} \cup \mathcal{N}\} \tag{4.1}$$

The total throughput in the blender over the scheduling horizon is the sum over all concentrates $c \in \mathcal{C}$ and the sum over all periods $t \in \mathcal{T}$ of the total flow rate into the blender. This results in objective (4.2).

$$\text{max} \qquad \sum_{t\in\mathcal{T}} \sum_{c\in\mathcal{C}} \sum_{e\in\mathcal{E}'} \alpha_c f_{e,c,t} \tag{4.2}$$

Total Flow. The constraint for the total flow rate is modeled in constraint (4.3). The total flow rate for each edge e is defined as the sum over all concentrates $c \in \mathcal{C}$ of the flow rate variable $f_{e,c,t}$. Constraints (4.4) and (4.5) indicate capacity constraints on the total flow rate during the production process.

$$F_{e,t} = \sum_{c\in\mathcal{C}} f_{e,c,t} \qquad \forall e \in \mathcal{E}, \forall t \in \mathcal{T} \tag{4.3}$$

$$F_{e,t} \leq \overline{F_{e,t}} \qquad \forall e \in \mathcal{E}, \forall t \in \mathcal{T} \tag{4.4}$$

$$F_{e,t} \geq \underline{F_{e,t}} \qquad \forall e \in \mathcal{E}, \forall t \in \mathcal{T} \tag{4.5}$$

Inventory. The total inventory of concentrates at a stockpile j at a period t is defined in constraint (4.6) and constraint (4.7), for the copper concentrates stockpiles $j \in \mathcal{S}$ and the non-copper concentrates stockpiles $j \in \mathcal{N}$, respectively. The inventory of a concentrate c at a stockpile j at a period t is thus denoted as $x_{j,c,t}$, where $x_{j,c,t}$ with $j \in \mathcal{S}$ is defined for the copper concentrates and $x_{j,c,t}$ is defined with $j \in \mathcal{N}$ for the non-copper concentrates, respectively. The total inventory at a stockpile j is then defined as the sum over the corresponding concentrates at the stockpile of the inventory $x_{j,c,t}$.

$$X_{j,t} = \sum_{c\in\mathcal{CC}} x_{j,c,t} \qquad \forall j \in \mathcal{S}, \forall t \in \mathcal{T} \tag{4.6}$$

$$X_{j,t} = \sum_{c\in\mathcal{NC}} x_{j,c,t} \qquad \forall j \in \mathcal{N}, \forall t \in \mathcal{T} \tag{4.7}$$

The total inventory of each copper concentrate stockpile, $X_{j,t}$, where $j \in \mathcal{S}$, is limited. The total inventory of copper concentrates should be equal to or smaller than the capacity Q as constraint (4.8).

$$\sum_{j\in\mathcal{S}} X_{j,t} \leq Q \qquad \forall t \in \mathcal{T} \tag{4.8}$$

The total amount of a non-copper concentrate at the stockpiles j, with $j \in \mathcal{N}$, should stay below a certain upper bound at the end of the scheduling horizon to prevent accumulation as constraint (4.9).

$$\sum_{j\in\mathcal{N}} x_{j,c,t} \leq MD \qquad \forall c \in \mathcal{NC}, t = T \tag{4.9}$$

Mass Balances. Constraint (4.10) until constraint (4.12) ensure the right mass balances. Constraint (4.10) models the mass balance at the copper concentrate stockpiles. When a shipment from maritime vessel m containing copper concentrate c is unloaded at stockpile j in period t, denoted as $g_{m,j,c,t}$, it is assumed that it only can be used in period $t+1$ as a flow in the blending network. This is assumed to consider time utilization of operational actions like unloading the copper concentrates. The inventory at the start of the scheduling horizon $x_{j,c,0} = 0$ for all $c \in \mathcal{CC}$ and $j \in \mathcal{S}$. Then, the start inventory of copper concentrates is modeled as shipments $g_{m,j,c,t}$ that arrive in period $t = 0$.

$$x_{j,c,t} = x_{j,c,t-1} + \sum_{m\in\mathcal{M}} g_{m,j,c,t-1} - f_{(j,P),c,t} \qquad \forall c \in \mathcal{CC}, \forall j \in \mathcal{S}, \forall t \in \mathcal{T} \tag{4.10}$$

The mass balance for the inventory of the non-copper concentrates is defined in constraint (4.11). It is assumed that the non-copper concentrates $h_{j,c,t}$, which arrives daily at the site, can be used directly in the blending process, so in period t. There is no start inventory of the non-copper concentrates, so $x_{j,c,0} = 0$ for all $c \in \mathcal{NC}$ and $j \in \mathcal{N}$.

$$x_{j,c,t} = x_{j,c,t-1} + h_{j,c,t} - f_{(j,B),c,t} \qquad \forall c \in \mathcal{NC}, \forall j \in \mathcal{N}, \forall t \in \mathcal{T} \tag{4.11}$$

Constraint (4.12) models the flow-mass balance at the pre-blender indexed by P. The flow balance implies that for each period at the pre-blender, the incoming flow rate is equal to the outgoing flow rate.

$$\sum_{\substack{e \in \mathcal{E}: \\ e=(j,P), \forall j \in \mathcal{S}}} f_{e,c,t} = f_{(P,B),c,t} \qquad \forall c \in \mathcal{CC}, \forall t \in \mathcal{T} \tag{4.12}$$

Smelter. The smelter is working continuously. The flow rate into the smelter is denoted by the final blend of the total flow rate of copper concentrates and non-copper concentrates in period t, as defined in constraint (4.13). From the period, ET, it is ensured that the smelter works at full capacity. This is formulated in constraint (4.14).

$$\sum_{e \in \mathcal{E}'} F_{e,t} = TF_t \qquad \forall t \in \mathcal{T} \tag{4.13}$$

$$TF_t = \widehat{F} \qquad t \geq ET \tag{4.14}$$

Chemical Elements. Each copper concentrate has its own composition of elements. The mass fraction of element k in concentrate c is indicated by $\theta_{k,c}$. The total amount of individual element k which is processed by the smelter in period t is denoted by $E_{k,t}$, as formulated in constraint (4.15).

$$E_{k,t} = \sum_{c \in \mathcal{C}} \sum_{e \in \mathcal{E}'} \theta_{k,c} f_{e,c,t} \qquad \forall k \in \mathcal{K}, \forall t \in \mathcal{T} \tag{4.15}$$

The concentrations of elements in the final flow should stay below an upper bound during the blending for the right quality of the final produced copper. Additionally, these restrictions must be satisfied to control the chemical reactions in the smelter. This is modeled in constraint (4.16). The parameter $\overline{\chi_k}$ indicates the upper bound on the mass fraction of element k in the final blend.

$$E_{k,t} \leq \overline{\chi_k} \widehat{F} \qquad \forall k \in \mathcal{K}, \forall t \in \mathcal{T} \tag{4.16}$$

Interdependency. There are interdependency constraints for some specific elements. These constraints are crucial for controlling the chemical reactions in the smelter. The ratio of the individual flows of element 2 and element 7 should stay between some specific boundaries. Also, the individual flows of element 3, element 4, and element 6 have interdependency constraints with each other. These are denoted with the use of interdependency parameters W_k and U_k. The parameter W_k indicates the weighting coefficient for the element k. The parameter U_k denotes the upper bound of the weighted proportion of an element k.

$$0.64E_{2,t} \geq E_{7,t} \qquad \forall t \in \mathcal{T} \tag{4.17}$$

$$0.58E_{2,t} \leq E_{7,t} \qquad \forall t \in \mathcal{T} \tag{4.18}$$

$$U_k \sum_{k' \in \mathcal{K}} (W_{k'} E_{k',t}) \geq W_k E_{k,t} \qquad \forall k \in \mathcal{K}, \forall t \in \mathcal{T} \tag{4.19}$$

Non-negativity. The decision variables in this mathematical model are non-negative continuous variables. This is defined in constraint (4.20) until constraint (4.25).

$$f_{e,c,t} \geq 0 \qquad \forall e \in \mathcal{E}, \forall c \in \mathcal{C}, \forall t \in \mathcal{T} \tag{4.20}$$

$$F_{e,t} \geq 0 \qquad \forall e \in \mathcal{E}, \forall t \in \mathcal{T} \tag{4.21}$$

$$x_{j,c,t} \geq 0 \qquad \forall j \in \mathcal{S} \cup \mathcal{N}, \forall c \in \mathcal{C}, \forall t \in \mathcal{T} \tag{4.22}$$

$$X_{j,t} \geq 0 \qquad \forall j \in \mathcal{S} \cup \mathcal{N}, \forall t \in \mathcal{T} \tag{4.23}$$

$$E_{k,t} \geq 0 \qquad \forall k \in \mathcal{K}, \forall t \in \mathcal{T} \tag{4.24}$$

$$TF_t \geq 0 \qquad \forall t \in \mathcal{T} \tag{4.25}$$

4.1.3. Extension: introducing infeasibility variable

If the flow rate in the smelter does not match its full capacity throughput $\widehat{F}$ for a period after ET, it indicates that the smelter experienced downtime during that period. Because restarting the chemical processes in the smelter takes several days, any downtime during the period is undesirable and renders the entire schedule infeasible. Currently, this scenario is denoted as infeasible in the model. However, it is unclear in which period the flow in the smelter dropped below the full capacity throughput. To precisely identify when the full capacity flow in the smelter cannot be met, the smelter constraint (4.14) from the original linear nominal model is extended. Constraint (4.14) is replaced by constraint (4.26). In this constraint, the binary variable u_t is introduced and is multiplied to the full capacity flow $\widehat{F}$. When u_t is set to 1 it ensures a full capacity flow of the smelter in period t. Conversely, when u_t is set to 0, it indicates zero flow in the smelter during period t. This signifies that the original problem becomes infeasible during period t, given that $t \geq ET$.

$$F_t \quad = \quad u_t \widehat{F} \qquad \forall t \geq ET \tag{4.26}$$

When u_t is set to zero and the problems becomes thus infeasible, this should imply that the flow in the smelter remains zero for sequential periods. This relationship is captured in constraint (4.27).

$$u_t \quad \geq \quad u_{t+1} \qquad \forall t \geq ET \tag{4.27}$$

4.1.4. Standard reformulation of the nominal model

To implement optimization under uncertainty methods effectively, we need to reformulate the nominal linear model in the standard form for such optimization. In this form, the uncertain parameters should only appear in the constraints and not in the objective. Transforming a mathematical formulation into this standard formulation involves two steps: $i)$ the reformulation of the objective when the objective contains an uncertain parameter and additionally for robust optimization $ii)$ eliminating of equality constraints which contain an uncertain parameter.

1) Reformulation of objective

In the nominal linear mathematical formulation for the SBCP as introduced in Section 4.1.2 there are no uncertain parameters in the objective. Therefore we do not have to eliminate uncertainty in the objective for the proposed mathematical formulation for the SBCP.

2) Eliminating equality constraints

For robust optimization, it is desired that the uncertain parameters only occur in inequality constraints because when uncertain parameters appear in equality constraints, this results in ambiguity. When for instance a constraint $x = \overline{a} + b$ (1) should hold, with the nominal uncertain parameter $\overline{a}$, it should also hold for the realization of $a = \overline{a} + \epsilon$. Here, parameter $\overline{a}$ denotes the nominal value of the actual parameter a, and ϵ denotes the deviation of the parameter, resulting in the constraint $x = \overline{a} + \epsilon + b$ (2). Constraints (1) and (2) are contradicting. Therefore the equality constraints that contain uncertain parameters should be omitted. An equality constraint can be reformulated by performing the following three steps: $i)$ rewrite the equality constraint into an expression of one variable into the other variables, $ii)$ substitute this expression in all the constraints where the variable appears, $iii)$ omit the first equality constraint. This process can be repeated until all equality constraints are eliminated.

For the SBCP model, the equality constraint (4.10) contains the uncertain parameter $g_{m,j,c,t}$, and thus has to be reformulated. The constraint defines the mass balance constraints for the copper concentrates and contains the variable, $x_{j,c,t}$, which is defined as the inventory of a copper concentrate c at stockpile j in period t. As a first step, we define the variable $x_{j,c,t}$ as an expression of the other variables. This can be done by rewriting the expression recursively. It should be ensured that the inventory of the copper concentrates is always non-negative and thus the new expression should be equal or larger than zero. This results in constraint (4.28).

$$\sum_{l=1}^{t} \left(\sum_{m \in \mathcal{M}} g_{m,j,c,l-1} - f_{(j,P),c,l} \right) \geq 0 \qquad \forall j \in \mathcal{S}, \forall c \in \mathcal{CC}, \forall t \in \mathcal{T} \tag{4.28}$$

Subsequently, constraint (4.6) which defines the total inventory at a stockpile contains the variable $x_{j,c,t}$ and is an equality constraint, so, it should be eliminated. The expression (4.28) is substituted into constraint (4.6). Next, the total inventory at a stockpile $X_{j,t}$ is substituted in constraint (4.8) that describes the capacity limit on the total inventory of copper concentrates. This results in reformulated constraint (4.29). Following, equality constraint (4.6) can be omitted, and thus all equality constraints concerning the uncertain parameter $g_{m,j,c,t}$ are eliminated.

$$\sum_{l=1}^{t} \sum_{j \in \mathcal{S}} \sum_{c \in \mathcal{CC}} \left(\sum_{m \in \mathcal{M}} g_{m,j,c,l-1} - f_{(j,P),c,l} \right) \leq Q \qquad \forall t \in \mathcal{T} \tag{4.29}$$

Additionally to the equality constraints which contain the uncertain parameter $g_{m,j,c,t}$, equality constraints containing the uncertain parameter $\theta_{k,c}$, the parameter that denotes the mass fraction of an element, have to be eliminated. This applies to constraint (4.15) which defines the variable $E_{k,t}$ as the total amount of element k which is processed by the smelter in period t. We express $E_{k,t}$ in the other variables and ensure it to be non-negative, as formulated in constraint (4.30). Subsequently, equality constraint (4.15) can be omitted.

$$\sum_{c \in \mathcal{C}} \sum_{e \in \mathcal{E}'} \theta_{k,c} f_{e,c,t} \geq 0 \qquad \forall k \in \mathcal{K}, \forall t \in \mathcal{T} \tag{4.30}$$

Next, the expression for $E_{k,t}$ is substituted into the constraints containing this variable. For the upper bound on the elemental flow as described in constraint (4.16), this results in constraint (4.31).

$$\sum_{c \in \mathcal{C}} \sum_{e \in \mathcal{E}'} \theta_{k,c} f_{e,c,t} \leq \overline{\chi_k} \widehat{F} \qquad \forall k \in \mathcal{K}, \forall t \in \mathcal{T} \tag{4.31}$$

For the interdependency constraints for elemental flows as described in constraint (4.17) until constraint (4.19), this results in reformulated constraint (4.32) until constraint (4.34).

$$0.64 \sum_{c \in \mathcal{C}} \sum_{e \in \mathcal{E}'} \theta_{2,c} f_{e,c,t} \geq \sum_{c \in \mathcal{C}} \sum_{e \in \mathcal{E}'} \theta_{7,c} f_{e,c,t} \qquad \forall t \in \mathcal{T} \tag{4.32}$$

$$0.58 \sum_{c \in \mathcal{C}} \sum_{e \in \mathcal{E}'} \theta_{2,c} f_{e,c,t} \leq \sum_{c \in \mathcal{C}} \sum_{e \in \mathcal{E}'} \theta_{7,c} f_{e,c,t} \qquad \forall t \in \mathcal{T} \tag{4.33}$$

$$U_k \sum_{k' \in \mathcal{K}} (W_{k'} \sum_{c \in \mathcal{C}} \sum_{e \in \mathcal{E}'} \theta_{k',c}) f_{e,c,t} \geq W_k \sum_{c \in \mathcal{C}} \sum_{e \in \mathcal{E}'} \theta_{k,c} f_{e,c,t} \qquad \forall k \in \mathcal{K}, \forall t \in \mathcal{T} \tag{4.34}$$

So in conclusion, the nominal model for the SBCP, suitable for the implementation of optimization under uncertainty methods, is formulated by objective (4.2), constraints (4.3) until (4.5), constraint (4.6) for $j \in \mathcal{N}$, constraint (4.9), constraints (4.11) until (4.14), constraints (4.20) until (4.25) and constraints (4.28) until (4.34). In the nominal model the expected parameters are treated as the actual parameter.

4.2. Mathematical formulation of supply uncertainty

In the SBCP, supply uncertainty is a significant challenge. We define uncertainty as the variance between the expected and actual values of a parameter. Agreements with worldwide suppliers specify expected values for $i)$ the arrival time of a copper concentrate, $ii)$ the mass of a copper concentrate, and $iii)$ the mass fraction of each element $k \in \mathcal{K}$ in a copper concentrate. However, in practice, it is often observed that the actual values of these parameters differ from the expected values, leading to what we term supply uncertainty. Drawing from historical data and expert opinions, probability distributions have been derived to mathematically describe these uncertainties. This section provides a detailed mathematical description of the supply uncertainty.

4.2.1. Uncertainty in the mass

The parameter $g_{m,j,c,t}$ represents the mass of a copper concentrate. To the uncertainty in the mass of a copper concentrate a normal distribution $\mathcal{N}(0, 3.3^2)$ has been fitted, with mean $\mu = 0$ and standard deviation $\sigma = 3.3$. Figure 4.3 illustrates the probability density function of this normal distribution, showing the likelihood of the percentage deviation λ in the mass of a copper concentrate.

The actual mass $g_{m,j,c,t}$ is calculated as $g_{m,j,c,t} = \overline{g_{m,j,c,t}}(1 + \lambda)$, where $\overline{g_{m,j,c,t}}$ denotes the nominal value of the mass. The normal distribution is symmetric and bell-shaped curved. On average, there is no deviation in the mass of a copper concentrate; 99.7 percent of the probability falls between -9.9 and 9.9 percent deviation which corresponds to lambda equal to -0.099 and 0.099, respectively. The distribution of uncertainty is consistent across suppliers, and the masses of copper concentrates are independent of each other.

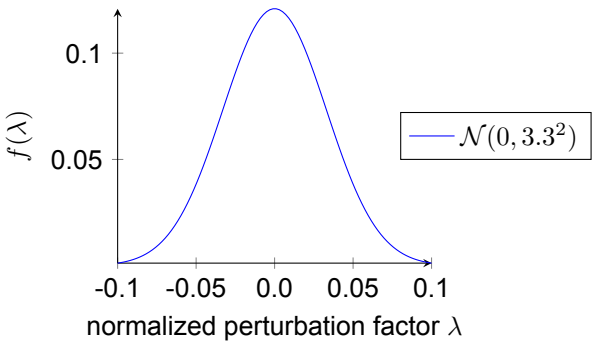

Figure 4.3: Probability density function of $\mathcal{N}(0, 3.3^2)$. This distribution describes the uncertainty in mass parameter $g_{m,j,c,t}$.

4.2.2. Uncertainty in the mass fraction of elements

The mass fraction of an element in a copper concentrate is denoted with $\theta_{k,c}$, where $k \in \mathcal{K}$ and the set $\mathcal{K}$ consists of 8 elements. Probability distributions have been fitted for each element based on historical data to describe the uncertainty. Although the best-fitted probability distributions for each element vary, the differences between them are small. For simplicity, the elements have been divided into two categories, each assumed to follow a single probability distribution.

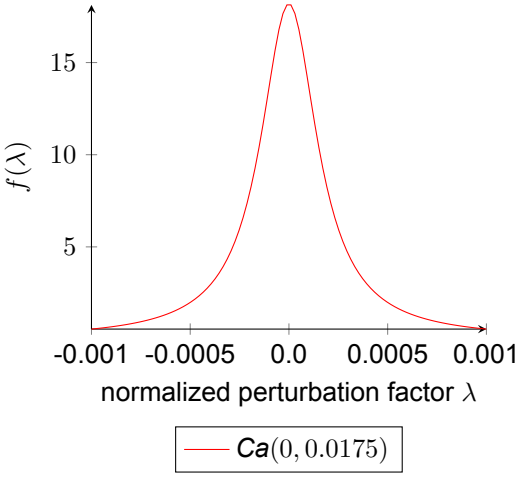

(a) Probability density function of *Cauchy*(0, 0.0175). Describes the distribution of the mass fraction uncertainty for elements 2 and 7.

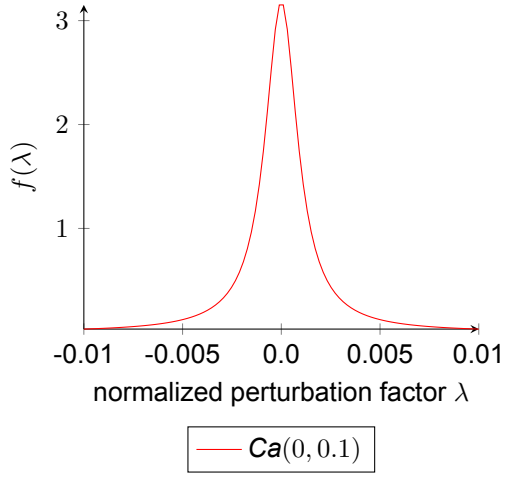

(b) Probability density function of *Cauchy*(0, 0.1). Describes the distribution of the mass fraction uncertainty for $k \in \mathcal{K} \setminus \{2, 7\}$.

The uncertainty in the mass fraction of element 2 and element 7 is described with a Cauchy distribution *Ca*$(0, 0.0175)$. Figure 4.4a illustrates the probability density function of this Cauchy distribution. The location parameter is $x_0 = 0$, denoting that the median of the distribution is zero and the scale parameter is $\gamma = 0.0175$. The distribution shows the likelihood of the percentage deviation of the mass fraction for element 2 and element 7. The actual parameter $\theta_{k,c}$ is calculated as follows: $\theta_{k,c} = \overline{\theta_{k,c}}(1 + \lambda)$, where $\overline{\theta_{k,c}}$ denotes the nominal value of the mass fraction of the element. The Cauchy distribution has a heavy tail, meaning that extreme values are possible with non-negligible probability. However, a peak in probability is observed in Figure 4.4a between -0.1 percent and +0.1 percent deviation in mass fraction, indicating relatively small deviations. This corresponds to lambda equal to -0.001 and 0.001.

The uncertainty in the mass fraction of the other elements is described with a Cauchy distribution *Ca*$(0, 0.01)$. Figure 4.4b illustrates the probability density function of this Cauchy distribution. The location parameter is again $x_0 = 0$ and the scale parameter is $\gamma = 0.01$. As before, the distribution shows the likelihood of the percentage deviation of the mass fraction, now for the remaining elements. Compared to the previous group, the uncertainty in this parameter is larger, with a peak in probability between -1 percent and +1 percent deviation in the mass fraction of the element as observed in Figure 4.4b. The observed uncertainty range corresponds to lambda from -0.01 to 0.01.

4.2.3. Uncertainty in the arrival time

The parameter $\overline{g_{m,j,c,t'}}$ reflects the uncertain arrival time, representing the nominal mass of a copper concentrate indexed by the nominal arrival period t'. The arrival period is a discrete parameter expressed in days. The actual arrival period t is calculated by adding the realization of the uncertain delay d of a copper concentrate to the expected t' as formulated in equation (4.35). The realization of the delay d lays in the set with a finite number of delays $\mathcal{D}$ and is obtained as a randomly generated variable from the corresponding probability distribution. The associated probability of a realization of the uncertain delay is denoted as p_d and is calculated using the probability distribution that describes the uncertain delay, as described later in more detail.

$$t = t' + d, \qquad \text{with probability } p_d, \quad \forall d \in \mathcal{D} \tag{4.35}$$

Ultimately, the relation between the nominal mass of a copper concentrate that arrives at period t', $\overline{g_{m,j,c,t'}}$ and the mass that arrives actually at period t, denoted as $\overline{g_{m,j,c,t}}$ can be described as shown in equation (4.36). Where the delay d is defined as $d = t - t'$.

$$\overline{g_{m,j,c,t'}} = \begin{cases} 0, & \text{with probability } 1 - p_d \\ \overline{g_{m,j,c,t}} & \text{with probability } p_d \end{cases} \tag{4.36}$$

The distribution of the uncertain delay of a copper concentrate is dependent on the location of the supplier and the location of the refinery. Generally, shipments with longer lead times tend to experience greater delays. For the studied refinery the shipments with the largest lead time originated from America and had to go through the Panama Canal to reach the refinery in Europe as illustrated in Figure 4.5a. We assume that the distribution corresponding to these shipments describes the uncertain delay of all shipments independent of their origin. This assumption is made to simplify and generalize the study.

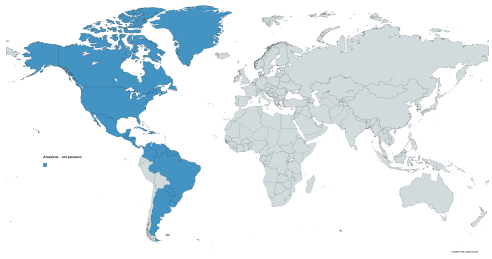

(a) Suppliers which ship their copper concentrates through the Panama Canal

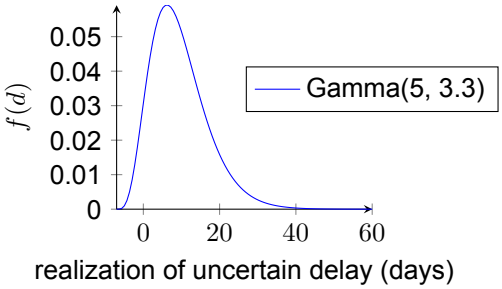

(b) Probability density function of shifted Gamma(5, 3.3)

Although the delay of a copper concentrate is a discrete parameter in days, only a fitting of continuous distributions to the historical data was available. The delay uncertainty is represented by a continuous Gamma distribution *Gamma*$(5, 3.3)$, with shape parameter $k = 5$ and scale parameter $\theta = 3.3$, as illustrated in Figure 4.5b. To make the representation of the uncertainty fit the discrete nature of the uncertainty, we sample from the continuous distribution and round it to the nearest whole number. This rounded value represents the uncertain delay. Interestingly, Figure 4.5b illustrates a shift of the gamma distribution to the left of seven days (denoted as $y = 7$), indicating the possibility of a copper concentrate being delivered earlier than expected. This results in a lower mean of the gamma distribution. The mean of the gamma distribution is calculated as $\mu = k\theta - y = 16.5 - 7 = 9.5$ days delay, and represents the expected delay of a copper concentrate. To match the discrete nature of the uncertainty, in this report the mean value is rounded to whole numbers and represents the expected delay of a copper concentrate. Additionally, experts have stipulated strict bounds on the range of possible delays for a shipment. According to experts the arrival time can range from a minimum d_{min} of one week early to a maximum d_{max} of 42 days late. To enforce these bounds, in addition to rounding the sampled values from the probability distribution, we accumulate the probability from the continuous gamma distribution that a shipment is 41.5 days late or more and assign it all to a delay of 42 days. Since the gamma distribution has no tail on the left side, the probability of a shipment arriving earlier than seven days ahead of schedule is already zero. With the introduction of the bounds, the set $\mathcal{D}$ is created which denotes the finite number of possible delays and ultimately describes the uncertainty in the arrival time.

The distribution described above is derived from data corresponding to a scheduling horizon of 90 days. However, we also need to analyze smaller instances of the SBCP. To accommodate shorter scheduling horizons without infeasibility issues due to shipments arriving frequently outside the scheduling horizon, we scale the delay distribution accordingly. For the instance with a scheduling horizon of 90 days, the shipments delay ranges from 7 days early to 42 days late, spanning thus 49 days. The finite set of possible delays can thus be expressed as a fraction of the scheduling horizon by $|\mathcal{D}| = \frac{49}{90}T$, where the set $\mathcal{D}$ ranges from d_{min} to d_{max}. (We assume that the distribution of the delay of a copper concentrate for an SBCP instance is represented by the above expression.) For SBCP instances with a scheduling horizon smaller than 90 days, for simplicity, we set the minimum delay to $d_{min} = y = 0$. Next, d_{max} is than calculated by $\frac{49}{90}T$. Ultimately, the uncertain delay of a copper concentrate is represented by sampling values from the continuous gamma distribution *Gamma*$(5, \theta)$ and rounding them to whole numbers, where θ is dependent on the scheduling horizon T. We select the shape parameter θ such that the distribution corresponds with the scaled range of possible delays $\mathcal{D}$, ranging from d_{min} to d_{max}. The bounds d_{min} and d_{max}, where $d_{min} = 0$ for instances where a scheduling horizon is smaller than 90 days and $d_{min} = -7$ for larger instances, and $d_{max} = \frac{49}{90}T - d_{min}$.

The probability of a realization of a delay d is thus calculated with the use of above described adapted gamma distribution. Let x be the random variable following above described continuous gamma distribution *Gamma*$(5, \theta)$. Then, considering that the sampled values for the delay are rounded, the probability of a realization of the uncertain delay is calculated as formulated in equation (4.37). In addition, to calculate the probability for the strict bounds of the delay interval the remaining left tail probability is added to the minimum delay d_{min} probability and the remaining right tail probability is added to the maximum delay d_{max} probability, as presented in equation (4.38) and (4.39), respectively.

$$p_d = \mathbb{P}(d - 0.5 < x \leq d + 0.5) = \mathbb{P}(x \leq d + 0.5) - \mathbb{P}(x \leq d - 0.5), d \in \mathcal{D} \tag{4.37}$$

$$p_{d_{min}} = \mathbb{P}(x \leq d_{min} + 0.5) \tag{4.38}$$

$$p_{d_{max}} = 1 - \mathbb{P}(x \leq d_{max} - 0.5) \tag{4.39}$$

4.3. Robust optimization for mass uncertainty

As formulated in the research questions in Section 1.3 it is intended to find a suitable optimization under uncertainty method to model each type of supply uncertainty. For the uncertainty in the mass of a copper concentrate, we chose robust optimization with the use of a one-stage formulation as described in Section 3.2.4. This section describes how to implement the robust approach to the corresponding uncertain parameter $g_{m,j,c,t}$, which denotes the actual mass of a copper concentrate c that is unloaded at stockpile j in period t.

4.3.1. Building box uncertainty set

As motivated in Section 3.2.4, this study prefers to model the mass fraction uncertainty with the use of a budgeted uncertainty set. For each period t, a budgeted uncertainty set $\mathcal{G}_t$ is created, indicating that not all copper concentrates arriving in period t can take their worst-case value simultaneously. The budgeted uncertainty set $\mathcal{G}_t$ involves summations over all the maritime vessels $m \in \mathcal{M}$, the stockpiles $j \in \mathcal{S}$, and the copper concentrates $c \in \mathcal{C}$. However, constraints containing the mass parameter $g_{m,j,c,t}$ do not include summations over copper concentrates and stockpiles. Given that a copper concentrate is never transported on more than one vessel in the studied instances, the summation over maritime vessels becomes also redundant, resulting in the budgeted uncertainty set $\mathcal{G}_t$ being redundant as well. That is, the budgeted set effectively reduces to a box uncertainty set. That is why, to describe the uncertainty in the mass of a copper concentrate more simply, a box uncertainty set is implemented for each copper concentrate in this study. The box uncertainty set $\mathcal{G}_{m,j,c,t}$ is formulated in equation (4.40).

$$\mathcal{G}_{m,j,c,t} = \Bigg\{ g_{m,j,c,t} \in \mathbb{R}^{mxjxcxt} : \overline{g_{m,j,c,t}}(1 - \delta p_{m,j,c,t}) \leq g_{m,j,c,t} \leq \overline{g_{m,j,c,t}}(1 + \delta p_{m,j,c,t}), \\ 0 \leq p_{m,j,c,t} \leq 1 \Bigg\} \tag{4.40}$$

Here, $\overline{g_{m,j,c,t}}$ denotes the nominal value of the mass of copper concentrate c which is unloaded from maritime vessel m at stockpile j in period t. The parameter δ denotes the maximal perturbation of the nominal parameter and $p_{m,j,c,t}$ normalizes this perturbation. The resulting normalized perturbation factor is denoted as $\lambda = \delta p_{m,j,c,t}$ and denotes the maximum perturbation of the nominal parameter expressed as a percentage. The actual value of the mass of copper concentrate c is denoted as $g_{m,j,c,t}$.

The choice of the normalized perturbation factor λ significantly impacts the performance of the box uncertainty set. We select a normalized perturbation factor of $\lambda = 0.1$ because it corresponds to the 3-standard deviation interval of the underlying normal distribution, as defined in Section 4.2.1. This ensures that 97.7 percent of the perturbations fall within the uncertainty set.

4.3.2. Derivation robust counterparts

To implement robust optimization for the mass uncertainty, the robust counterpart has to be derived for each constraint including the uncertain parameter $g_{m,j,c,t}$. A box uncertainty set $\mathcal{G}_{m,j,c,t}$ is designed for this parameter. This section explains how to derive the robust counterpart for a box uncertainty set. The constraints that contain the uncertain parameter $g_{m,j,c,t}$ are the positive copper concentrate inventory constraint (4.28) and the capacity inventory constraint (4.29). First the robust counterpart of constraint (4.28) is derived and afterward the robust counterpart for constraint (4.29) is derived.

Open Form Constraint. The robust version of the positive inventory constraint (4.28) of the copper concentrates should hold for all values of $g_{m,j,c,t} \in \mathcal{G}_{m,j,c,t}$. Equation (4.41) shows the robust constraint.

$$\sum_{l=1}^{t} \left(\sum_{m \in \mathcal{M}} g_{m,j,c,l-1} - f_{(j,P),c,l} \right) \geq 0 \qquad \forall j \in \mathcal{S}, \forall c \in \mathcal{CC}, \forall t \in \mathcal{T}, \forall g_{m,j,c,t} \in \mathcal{G}_{m,j,c,t} \tag{4.41}$$

Because the polyhedron $\mathcal{G}_{m,j,c,t}$ includes infinitely many points, the above formulation equates to an infinite set of constraints. This represents the open form of a constraint. Achieving a closed-form solution is preferable for problem-solving. By reformulating the robust constraint into a deterministic robust counterpart, which is called the robust counterpart, we can express the constraint as a finite set of linear constraints. Often duality theorem is needed to reformulate the constraints, however, the box uncertainty set enables us to derive the robust counterparts quite straightforwardly.

Worst-Case Constraint. To begin deriving the closed-form deterministic constraint, we formulate worst-case constraint (4.42). Because the uncertainty set is a box, the upper or lower bound from the box uncertainty set can directly be substituted as the worst-case value in the constraints. For constraint (4.41), the lower bound of the box uncertainty set restricts most of the inequality. By substituting the worst-case, the robust counterpart as shown in equation (4.43) is directly obtained.

$$\sum_{l=1}^{t} \min_{g \in \mathcal{G}} \left(\sum_{m \in \mathcal{M}} g_{m,j,c,l-1} \right) \geq \sum_{l=1}^{t} f_{(j,P),c,l} \qquad \forall j \in \mathcal{S}, \forall c \in \mathcal{CC}, \forall t \in \mathcal{T} \tag{4.42}$$

$$\equiv \sum_{l=1}^{t} \sum_{m \in \mathcal{M}} (\overline{g_{m,j,c,l-1}} - \delta p_{m,j,c,t}) \geq \sum_{l=1}^{t} f_{(j,P),c,l} \qquad \forall j \in \mathcal{S}, \forall c \in \mathcal{CC}, \forall t \in \mathcal{T} \tag{4.43}$$

The above steps are also applied to the copper concentrate capacity constraint (4.29). For this constraint, the upper bound from the box uncertainty set restricts the inequality the most. So, this bound can substituted in the worst-case constraint, and immediately the closed-form deterministic, called robust counterpart, is derived. Equation (4.44) presents the resulting robust counterpart.

$$\sum_{l=1}^{t} \sum_{j \in \mathcal{S}} \sum_{c \in \mathcal{CC}} \left(\sum_{m \in \mathcal{M}} (\overline{g_{m,j,c,l-1}} + \delta p_{m,j,c,t}) - f_{(j,P),c,l} \right) \leq Q \qquad \forall t \in \mathcal{T} \tag{4.44}$$

4.4. Robust optimization for mass fraction uncertainty

As formulated in the research questions in Section 1.3 it is intended to find a suitable optimization under uncertainty method to model each type of supply uncertainty. For the uncertainty in the mass fraction

of the elements in a copper concentrate, we chose robust optimization as described in Section 3.2.4 with the use of a one-stage formulation. This section describes the implementation of robust approach to the uncertain parameter $\theta_{k,c}$, which denotes the mass fraction of element k in concentrate c.

4.4.1. Building budgeted uncertainty set

As motivated in Section 3.2.4 in this study it is chosen to model the mass fraction uncertainty with the use of a budgeted uncertainty set. For the uncertain parameter, $\theta_{k,c}$, the budgeted uncertainty set is formulated as follows.

$$\Theta_k = \left\{ \theta_{k,c} \in \mathbb{R}^{kxc} : \overline{\theta_{k,c}}(1-\delta p_{k,c}) \leq \theta_{k,c} \leq \overline{\theta_{k,c}}(1+\delta p_{k,c}), 0 \leq p_{k,c} \leq 1, 0 \leq \sum_{c \in \mathcal{C}} p_{k,c} \leq \Gamma \right\} \quad (4.45)$$

Here, $\overline{\theta_{k,c}}$ represents the nominal mass fraction of element k in copper concentrate c. The parameter δ denotes the maximal perturbation of this parameter, while $p_{k,c}$ normalizes the perturbation factor. The parameter $\lambda = \delta p_{k,c}$ represents the resulting normalized perturbation factor. The actual mass fraction of element k in copper concentrate c is denoted by $\theta_{k,c}$. The budget parameter Γ denotes the total budget on the normalized perturbations of $\overline{\theta_{k,c}}$. This means that only an amount of Γ expected copper concentrates can take their worst-case value for an element k simultaneously.

Choosing the parameters δ and Γ significantly influences the performance of the uncertainty set. For the budgeted uncertainty Θ_k, we select a normalized perturbation factor $\lambda = 0.001$ for elements 2 and 7, and $\lambda = 0.01$ for the other elements. These numbers have been chosen based on the observed peak in the probability distributions of the uncertainty as described in Section 4.2.2. This approach ensures that the majority of the possible perturbations are included in the uncertainty set, but the volume is not too large. To analyze the influence of the budget parameter Γ, we perform experiments with a budget parameter varying from one to the maximum number of expected copper concentrates CC.

4.4.2. Derivation of robust counterpart

To implement robust optimization for the mass fraction uncertainty, the robust counterpart has to be derived for each constraint including the uncertain parameter $\theta_{k,c}$. The designed budgeted uncertainty set Θ_k is used for this. This section shows how to derive a robust counterpart for a constraint with holds for a budgeted uncertainty set using the duality theorem. The derivation of the robust counterpart for upper bound constraint (4.31) on the elemental final flow is used as an illustration. Appendix A presents the derivations of the robust counterparts for the other constraints containing parameter $\theta_{k,c}$.

Open Form Constraint. The robust version of the upper bound constraint (4.31) on the elemental flow should hold for all values of $\theta_{k,c} \in \Theta_k$. The robust constraint is shown in equation (4.46).

$$\sum_{c \in \mathcal{C}} \sum_{e \in \mathcal{E}'} \theta_{k,c} f_{e,c,t} \leq \overline{\chi_k} \widehat{F} \qquad \forall k \in \mathcal{K}, \forall t \in \mathcal{T}, \forall \theta_{k,c} \in \Theta_k \quad (4.46)$$

Because the polyhedron Θ_k includes infinitely many points, the above formulation equates to an infinite set of constraints. This represents the open form of a constraint. Achieving a closed-form solution is preferable for problem-solving. By reformulating the robust constraint into a deterministic robust counterpart using the duality theorem, we can express the constraint as a finite set of linear constraints. Introducing additional dual variables is necessary for this reformulation. This does not form a problem for smaller problems, it may lead to longer computational times for larger problems.

Worst-Case Constraint. To begin deriving the robust counterpart, the first step involves formulating the worst-case constraint. The problem's objective is to maximize the gross margin of the process, which is a linear function of the variables $f_{e,c,t}$. Consequently, the worst case occurs when the variables in the objective function are most constrained by the uncertain parameters, resulting in a lower objective value. The worst-case of constraint (4.46) can be found by maximizing the terms on the left side of the inequality. The corresponding worst case constraint is presented in constraint (4.47).

$$\max_{\theta \in \Theta_k} \left(\sum_{c \in \mathcal{C}} \sum_{e \in \mathcal{E}'} \theta_{k,c} f_{e,c,t} \right) \leq \overline{\chi_k} \widehat{F} \qquad \forall k \in \mathcal{K}, \forall t \in \mathcal{T} \quad (4.47)$$

To make the derivation more tractable, we reformulate the worst-case constraint (4.47) and build an auxiliary optimization problem (4.48). First, we focus on the left maximization term of $\theta \in \Theta_k$ of the worst-case constraint. This term is equivalent to the maximization of the term where the uncertain $\theta_{k,c}$ is substituted with the upper bound of the uncertainty set. Because the variables $f_{e,c,t}$ are non-negative and the upper bounds of the uncertainty set would always be feasible, this upper bound should hold tightly in the maximum. The resulting reformulation for every individual inequality ($k \in \mathcal{K}, t \in \mathcal{T}$) is then given by problem (4.48).

$$\max_{\theta \in \Theta_k} \left(\sum_{c \in \mathcal{C}} \sum_{e \in \mathcal{E}'} \theta_{k,c} f_{e,c,t} \right)$$

$$\equiv \max_{\theta \in \Theta_k} \left(\sum_{c \in \mathcal{C}} \sum_{e \in \mathcal{E}'} \overline{\theta_{k,c}} f_{e,c,t} (1 + \delta p_{k,c}) \right)$$

Auxiliary Optimization Problem.

$$\iff \max_{p} \left(\sum_{c \in \mathcal{C}} \sum_{e \in \mathcal{E}'} \overline{\theta_{k,c}} f_{e,c,t} p_{k,c} \right) \tag{4.48}$$

$$\text{s.t.} \quad 0 \leq p_{k,c} \leq 1 \qquad \forall c \in C$$

$$\sum_{c \in C} p_{k,c} \leq \Gamma$$

Dual optimization problem. By duality theory for Linear Program (LP) problems, it is known that if the primal problem is feasible and bounded, strong duality holds. Given that optimization problem (4.48) is feasible and bounded, it implies that the corresponding dual problem is also feasible and bounded. Consequently, the optimal values of the two optimization problems coincide. Thus, we can formulate the dual auxiliary optimization problem. This formulation begins with constructing the Lagrangian relaxation of the problem, as shown in equation (4.49). Maximizing this function is illustrated in equation (4.50). We introduce the dual variables $s_{k,c}$ and q_k for the first and second constraint of the optimization problem (4.48), respectively. From these equations the dual problem results.

$$L(s_{k,c}, q_k, \theta_{k,c}) = \sum_{c \in \mathcal{C}} \sum_{e \in \mathcal{E}'} \overline{\theta_{k,c}} f_{e,c,t} p_{k,c} + \sum_{c \in \mathcal{C}} s_{k,c}(1 - p_{k,c}) + q_k \left(\Gamma - \sum_{c \in C} p_{k,c} \right) \tag{4.49}$$

$$g(s_{k,c}, q_k) = \max_{p_{k,c} \geq 0} L(s_{k,c}, q_k, \theta_{k,c})$$

$$= \sum_{c \in C} s_{k,c} + q_k \Gamma + \max_{p_{k,c} \geq 0} \sum_{c \in \mathcal{C}} \sum_{e \in \mathcal{E}'} \overline{\theta_{k,c}} f_{e,c,t} p_{k,c} + p_{k,c} \left(\sum_{c \in \mathcal{C}} (-s_{k,c} - q_k) \right) \tag{4.50}$$

Problem (4.51) presents the dual auxiliary optimization problem for each inequality ($k \in \mathcal{K}, t \in \mathcal{T}$).

$$\min_{q_k, s_{k,c}} \quad \Gamma q_k + \sum_{c \in \mathcal{C}} s_{k,c} \tag{4.51}$$

$$\text{s.t.} \quad s_{k,c} + q_k \geq \sum_{e \in \mathcal{E}'} \overline{\theta_{k,c}} f_{e,c,t} \qquad \forall c \in \mathcal{C}$$

$$s_{k,c} \geq 0 \qquad \forall c \in \mathcal{C}$$

$$q_k \geq 0$$

By strong duality optimization problem (4.48) is equivalent to optimization problem (4.51), and the optimal solution of the dual is attained. So, we can substitute the optimal solution of the primal problem with the optimal solution of the dual problem in the worst-case constraint resulting in equation (4.52).

$$\sum_{c \in \mathcal{C}} \sum_{e \in \mathcal{E}'} \overline{\theta_{k,c}} f_{e,c,t} + \delta \min_{q_k, s_{k,c}} (\Gamma q_k + \sum_{c \in \mathcal{C}} s_{k,c}) \leq \overline{\chi_k} \widehat{F} \qquad \forall k \in \mathcal{K}, \forall t \in \mathcal{T} \tag{4.52}$$

Robust Counterpart. Because the primal problem and dual problem are equivalent, constraint (4.52) will hold for some value of the dual variable. Therefore, it will definitely hold for the optimal value and

thus the minimum sign can be dropped. This results in the closed form deterministic version of the constraint, which is denoted as the final robust constraint, as shown in problem (4.53).

$$\begin{aligned}
&\sum_{c\in\mathcal{C}}\sum_{e\in\mathcal{E}'}\overline{\theta_{k,c}}f_{e,c,t}+\delta(\Gamma q_k+\sum_{c\in\mathcal{C}}s_{k,c})\leq\overline{\chi_k}\widehat{F} && \forall k\in\mathcal{K},\forall t\in\mathcal{T} \qquad (4.53)\\
&\text{s.t. } s_{k,c}+q_k\geq\sum_{e\in\mathcal{E}'}\overline{\theta_{k,c}}f_{e,c,t} && \forall c\in\mathcal{C},\forall k\in\mathcal{K}\\
&\quad s_{k,c}\geq 0 && \forall c\in\mathcal{C},\forall k\in\mathcal{K}\\
&\quad q_k\geq 0 && \forall k\in\mathcal{K}
\end{aligned}$$

The derivations of the robust counterparts for the other constraints containing uncertain parameter $\theta_{k,c}$ are presented in Appendix A. These derivations follow the same steps as the derivation described above.

4.5. Stochastic optimization for the uncertainty in arrival time

As formulated in the research questions in Section 1.3 it is intended to find a suitable optimization under uncertainty method to model each type of supply uncertainty. For the uncertainty in the arrival time of a copper concentrate, as described in Section 3.2.3, we chose stochastic optimization with the representation of the discrete uncertainty with a finite set of scenarios. Both a one-stage and multistage formulation are implemented as motivated in Section 3.2.3. This section describes how to implement this approach to the corresponding uncertain parameter $\overline{g_{m,j,c,t'}}$, denoting the nominal mass of a copper concentrate c transported on maritime vessel m unloaded at stockpile j in nominal period t'.

4.5.1. Scenario-based stochastic optimization

In this study, we model the uncertainty in the arrival time of a copper concentrate as a finite set of realizations. As discussed in Section 4.2.3, each copper concentrate is subject to a finite number of potential delays denoted as the set $\mathcal{D}$, ranging from the minimum delay d_{min} to the maximum delay d_{max}. Then the actual arrival time of a copper concentrate is determined by the realization of the delay added to the expected arrival time. For the SBCP we define a scenario as a schedule detailing the actual arrival times of the expected copper concentrates within a scheduling horizon. The total set of possible scenarios is denoted as $\mathcal{Z}$. The total number of scenarios, denoted as $|\mathcal{Z}|$, are then all possible combinations of the realizations of the delays for the expected copper concentrates. The number of possible scenarios can be calculated as the number of possible delays $|\mathcal{D}|$ raised to the power of the number of expected copper concentrates CC, yielding $|\mathcal{Z}| = |\mathcal{D}|^{CC}$. Ideally, we want to include all possible scenarios in the formulations of the stochastic models. However, for the SBCP it is computationally hard to solve these models because the number of constraints becomes quickly too large. Therefore, we implement a reduced set of scenarios $\overline{\mathcal{Z}}$. For the one-stage stochastic model, we both explore a sampling approach and a selecting approach to define the reduced set of scenarios $\overline{\mathcal{Z}}$. For the stochastic multistage model the selecting approach is used to define the reduced set of scenarios $\overline{\mathcal{Z}}$.

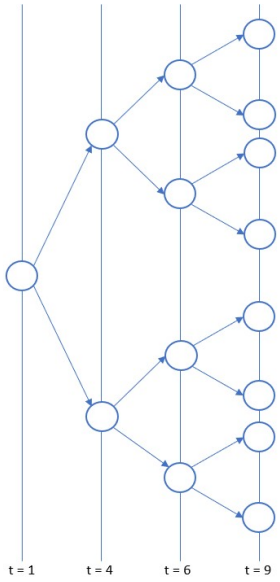

Figure 4.6: Schematic example of a scenario tree with three arriving copper concentrates whose corresponding expected arrival times are t = 4, t = 6, and t = 9. Either the copper concentrate is actually on time or has the maximum possible delay.

The set of scenarios can be effectively represented using a scenario tree, which captures the possible outcomes of uncertain parameters over time in a structured manner. Figure 4.6 illustrates an example of such a scenario tree for the SBCP problem considering arrival time uncertainty. In this example, we anticipate the arrival of three copper concentrates whose expected arrival times are 4, 6, and 9. In the example, it is assumed that the copper concentrate is either on time ($d_1 = 0$) or is maximum delayed

($d_2 = d_{max}$), respectively. The scenario tree branches accordingly with each new expected copper concentrate, capturing the potential delay realizations. Consequently, each path from the initial node to a terminal node of the scenario tree represents a unique scenario. Thus, the number of terminal nodes equals the number of scenarios. In this example, the reduced set of scenarios $\overline{\mathcal{Z}}$ consists of $|\overline{\mathcal{Z}}| = |\mathcal{D}'|^C C = 2^3 = 8$ scenarios. In the formulations, we assume non-anticipativity constraints but do not model them explicitly for brevity. These constraints ensure that decisions are only dependent on information from the past and are not dependent on information from the future. In addition, they ensure that when in different scenarios z the same uncertainties have realized before period t, the decision variables $f^z_{e,c,t}$ of period t are the same.

In the stochastic approach, the expected objective is maximized. As presented in equation (4.2) the objective of the SBCP maximizes the profit of processing concentrates. Because the arrival times of each copper concentrate are independent of each other, the probability of a scenario p_z can be calculated by multiplying the probabilities of the individual delays p_d of the copper concentrates as introduced in Section 4.2.3. The objective of a scenario q_z is denoted by the profit which is generated from the flow variables that correspond with this scenario. For a one-stage model, one set of decision variables is used for all scenarios, so for each scenario, the optimal solution is the same, and since the objective does not contain uncertain parameters, the same optimal expected objective is obtained. For a multistage model, there are different variables defined for each stage, so the optimal solution and thus optimal objective varies for each scenario. The total expected objective is calculated by summing over all possible scenarios the probability of a scenario multiplied by the objective of that scenario, which is denoted as the function $O^z(f)$. The total expected objective is linear and is presented in equation (4.55).

$$\text{max} \quad \mathbb{E}\left[\sum_{t\in\mathcal{T}}\sum_{e\in\mathcal{E}'}\sum_{c\in\mathcal{C}} \alpha_c f_{e,c,t}\right] \equiv \text{max} \quad \sum_{z=1}^{|\mathcal{Z}|} p_z \sum_{t\in\mathcal{T}}\sum_{e\in\mathcal{E}'}\sum_{c\in\mathcal{C}} \alpha_c f^z_{e,c,t} \tag{4.54}$$

$$\equiv \text{max} \quad \sum_{z=1}^{|\mathcal{Z}|} p_z O^z(f) \tag{4.55}$$

4.5.2. One-stage stochastic model

We implement a one-stage model with a reduced set of scenarios $\overline{\mathcal{Z}} \subset \mathcal{Z}$ to reduce the computation time as motivated in Section 3.2.3. We implement two ways of reducing the scenario set; including only scenarios based on some selection rule and by sampling a set from the probability distribution of the arrival times uncertainty.

First, we define the reduced set $\overline{\mathcal{Z}}_{worst}$ by reducing the number of possible delays. Namely, only the delays $\{d_1, d_2\} = \{0, d_{max}\}$ are included. With these possible delays all the corresponding scenarios for the arrival times of the copper concentrates are constructed. This set is considered because the number of scenarios is strongly reduced, but still, the worst-case delay is considered, matching the priority of feasibility of the refinery. The second set of reduced scenarios $\overline{\mathcal{Z}}_{mean}$ is defined by including the possible delays $\{d_1, d_2\} = \{0, d_{mean}\}$, where we consider no delay and the mean delay. In this way, the number of scenarios is reduced, but still, the average delay is considered. The probability of each scenario is calculated by multiplying the probabilities of the individual delays of the copper concentrates. The probability of the two assumed delays is calculated by dividing the probability space in two. In the first case, when $\{d_1, d_2\} = \{0, d_{max}\}$, the probability volume left of the mean of the defined probability distribution of the uncertainty as described in Section 4.2.3 is assumed for d_1 and is denoted as $p_1 = 0.56$. For the possibility that the copper concentrate has a maximum delay, the probability volume of the right of the mean of this probability distribution is assumed, which is $p_2 = 0.44$, since those delays are assumed to be independent. The same probabilities for the delays are assumed for the set of possible delays $\{d_1, d_2\} = \{0, d_{mean}\}$.

Then, a sampling approach is used to define the third set of reduced scenarios $\overline{\mathcal{Z}}_{sampled}$. A sample of N is randomly generated by drawing a delay for a copper concentrate from the probability distribution of the uncertainty as defined in Section 4.2.3. The drawn values are rounded to obtain a discrete delay in days. When the number of samples is large enough, the sample will give a good representation of

the possible scenarios, while the corresponding model will be less computationally hard to solve. The probability corresponding to the randomly drawn delay of each copper concentrate is used to calculate the probability of a scenario. Again, the probability of each scenario is calculated by multiplying the probabilities of the individual delays of the copper concentrates. To implement the one-stage stochastic model with the reduced set of scenarios $\overline{\mathcal{Z}}$ the constraints containing the uncertain arrival time should hold for all the scenarios $z \in \overline{\mathcal{Z}}$. The positive copper concentrate inventory constraint (4.28) and the capacity constraint (4.29) both contain the uncertain parameter $\overline{g_{m,j,c,t'}}$. In equation (4.56) the resulting constraints for the one-stage models are shown. These are thus three different models of which the performance can be compared, each for the defined sets $\overline{\mathcal{Z}}_{worst}$, $\overline{\mathcal{Z}}_{mean}$ and $\overline{\mathcal{Z}}_{sampled}$.

$$\sum_{l=1}^{t}\Big(\sum_{m\in\mathcal{M}}\overline{g^{z}_{m,j,c,l-1}} - f_{(j,P),c,l}\Big) \geq 0 \qquad \forall j\in\mathcal{S},\forall c\in\mathcal{CC},\forall t\in\mathcal{T},\forall z\in\overline{\mathcal{Z}},$$
$$\overline{\mathcal{Z}} = \big(\overline{\mathcal{Z}}_{worst}\vee\overline{\mathcal{Z}}_{mean}\vee\overline{\mathcal{Z}}_{sampled}\big) \tag{4.56}$$

$$\sum_{l=1}^{t}\sum_{j\in\mathcal{S}}\sum_{c\in\mathcal{CC}}\Big(\sum_{m\in\mathcal{M}}\overline{g^{z}_{m,j,c,l-1}} - f_{(j,P),c,l}\Big) \leq Q \qquad \forall t\in\mathcal{T},\forall z\in\overline{\mathcal{Z}},$$
$$\overline{\mathcal{Z}} = \big(\overline{\mathcal{Z}}_{worst}\vee\overline{\mathcal{Z}}_{mean}\vee\overline{\mathcal{Z}}_{sampled}\big) \tag{4.57}$$

4.5.3. Multistage stochastic model

To add flexibility to the stochastic model, we apply the multistage approach next to the one-stage approach. In a multistage model, at some nodes in the scenario tree, new sets of decision variables are introduced. Through this, different decisions can be made, based on what has happened in the past resulting in a more flexible model. The tree which shows at which nodes new decision variables are introduced is called the decision tree. Two examples of a decision tree for a multistage model, corresponding to the scenario tree as shown in Figure 4.6 are presented. Figure 4.7 shows at the top a decision tree where at every new period, there is the possibility to make new decisions using the observed uncertainty realizations. Therefore at every node, a new set of decision variables is introduced. This results in a very flexible model. Due to the newly introduced set of decision variables, the decisions can differ depending on the realization of the uncertainty in earlier periods. However, it has to be made certain that the solution is feasible for the actual parameters from the corresponding scenario. In Figure 4.7 at the bottom the decision tree for the formulated multistage model for the SBCP is shown. At the refinery, it is common to re-optimize the schedule every seven days. In alignment a new stage is defined every seven days and thus after seven days new sets of decision variables are created. The scenario tree branches after the seven days according to the number of possible scenarios in the last time frame. When for example three copper concentrates were expected to arrive in the last seven days, denoted as CC_7 and two possible delays are considered in the set $\mathcal{D}$, the tree branches $|\mathcal{D}|^{CC_7} = 2^3 = 8$ times. For the multistage model, we reduce the set of scenarios to stay within reasonable computational time limits. We implement the multistage models with the defined reduced set of scenarios $\overline{\mathcal{Z}}_{worst}$ and $\overline{\mathcal{Z}}_{mean}$ as introduced above, with $\{d_1, d_2\} = \{0, d_{max}\}$ and $\{d_1, d_2\} = \{0, d_{mean}\}$, respectively. The corresponding probabilities are defined by dividing the probability space under the gamma distribution by the mean, resulting in $p_1 = 0.56$ and $p_2 = 0.44$ as described in Section 4.5.2.

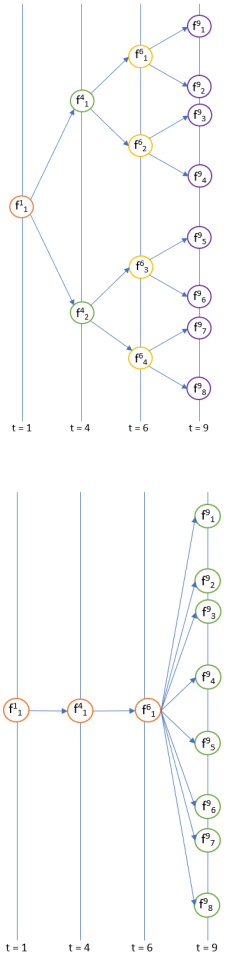

Figure 4.7: Decision trees corresponding to scenario tree from Figure 4.6 with (top) every period a new stage and (bottom) a new stage every seven periods.

5 Data

This chapter describes the data instances that are used to study the optimization models for the SBCP. First, Section 5.1 describes how these data instances are obtained and then Section 5.2 presents the characteristics of these SBCP instances.

5.1. Data generation

Although the thesis is done in cooperation with an actual refinery, as a benchmark for the models' performance the company preferred to use the artificial instances from Song et al., 2018. These artificial instances are used because the real data would be too time-consuming to clean and anonymize. Also, the interdependency parameters are clearly specified in this paper. Five data instances have been created. Data instance A aligns with the motivational example of the paper, while instance B mirrors the industrial example outlined in the paper. The only deviation lies in the scheduling horizon and smelter capacity used in data instance A, which have been adjusted to suit the characteristics of the studied refinery. The paper originally employed a scheduling horizon of 13 days and a smelter capacity of 1500 ton/day, whereas our research adopts a 10-day horizon and a 3000 ton/day smelter capacity. Data instances C through E are generated randomly, with the distribution based on parameters from the paper. These parameters represent the nominal values. The mass fraction of an element in a copper concentrate is randomly generated from the uniform distribution $\mathcal{U}_k(a, b)$, where a and b denote the minimum and maximum bounds of this distribution, respectively. These bounds are determined by the minimum and maximum observed mass fractions of elements in the data samples from the paper Song et al., 2018. Through trial and error, adjustments were made to ensure feasibility. Table 5.1 shows the final bounds.

Table 5.1: Bounds of uniform distribution to generate randomly the mass fraction of an element in a copper concentrate during data generation for instance C until instance E.

Parameter	**1**	**2**	**3**	**4**	**5**	6	**7**	**8**
Upper bound b	0.7	0.4	0.002	0.0006	0.000184	0.0015	0.3	0.5680
Lower bound a	0.00219	0.005	0.0000706	0.000000075	0.0	0.0000135	0.0	0.1997

We randomly generate the mass of the copper concentrate from the uniform distribution $\mathcal{U}(100, 16000)$, representing a range between 100 and 16000 tons. Similarly, the mass of the non-copper concentrate arriving daily is randomly generated from the uniform distribution $\mathcal{U}(30, 40)$. The profit for the copper concentrate is also randomly generated from the uniform distribution $\mathcal{U}(0, 1500)$, while the profit for all non-copper concentrates is assumed to be zero. We ensure that within the set of non-copper concentrates, there is always a concentrate present consisting solely of element 7, namely sand, as it is indispensable for blending. For the generated instances, we assume that approximately five copper concentrates are expected to arrive every fifteen days. We randomly generate the arrival period of each copper concentrate following a uniform distribution. However, to guarantee the arrival of copper concentrates over the entire scheduling horizon, we divide the scheduling horizon and the set of copper concentrates into three parts. Each third of the expected copper concentrates is uniformly distributed over one-third of the scheduling horizon.

5.2. SBCP instances

We utilized five data instances to analyze the optimization models. Table 5.2 presents the data characteristics for each instance. The scheduling horizon is measured in days, with each day denoted as a single period. The parameter ET signifies the earliest period when the total flow rate into the smelter matches the full capacity rate of the smelter. Furthermore, the table indicates the number of elements subject to mass fraction constraints in the final blend, the number of copper concentrates that is the initial start inventory, the number of expected copper concentrates denoted as CC, and the number of daily arriving non-copper concentrates. In addition, Table 5.3 presents the characteristics of the blending system, which remain consistent across all instances.

Table 5.2: Data characteristics SBCP instances. The table presents the earliest time of full capacity flow rate ET, the number of elements K, the number of start-inventory I, the number of expected copper concentrates and the number of on-copper concentrates that arrive daily NC.

	ET	T	K	I	CC	NC
Instance A	2	10	4	3	2	1
Instance B	5	15	8	6	4	4
Instance C	5	15	8	5	5	4
Instance D	5	30	8	5	10	4
Instance E	5	90	8	10	35	4

Table 5.3: Characteristics blending system.

System parameters	
Upper bound total flow rate $\overline{F_{e,t}}$	3000 ton/day
Lower bound total flow rate $\underline{F_{e,t}}$	0 ton/day
Copper concentrates capacity stockpiles Q	unlimited
Non-copper concentrates capacity MD	unlimited

Table 5.4: Characteristics for the distribution of the uncertainty in arrival time of the copper concentrates for each instance which is dependent on the size of the scheduling horizon T.

	Scale parameter θ	d_{min} (days)	d_{max} (days)	d_{mean} (days)
Instance A	0.4125	0	5	2
Instance B	0.55	0	8	3
Instance C	0.55	0	8	3
Instance D	1.1	0	16	6
Instance E	3.3	-7	42	10

Table 5.5 and Table 5.6 present the parameters concerning constraints on the mass fraction of an element in the final blend. These tables present the upper bounds on the mass fraction of an element in the final blend for instances A through E. Additionally, they provide the interdependency parameters U_k and W_k for instances B through E. In instance A, we omitted the interdependency constraints to expand the solution space.

Table 5.5: Elemental flow parameters for each element $k = 1, \ldots, 4$ in instance A.

Parameter	1	2	3	4
Upper bound mass fraction of element in final blend $\overline{\chi}_k$	0.4	0.285	0.31	1

Table 5.6: Elemental flow parameters for each element $k = 1, \ldots, 8$ in instance B till instance E.

Parameter	1	2	3	4	5	6	7	8
Upper bound mass fraction of element in final blend $\overline{\chi}_k$	1	0.285	0.0011	0.00005	1	0.001	1	1
Upper bound interdependency parameter U_k	1	1	0.001	0.0001	1	0.0033	1	1
Weight interdependency parameter W_k	0.8680	0	0.1888	0.9078	0	0.4319	0	0.00016

As described in Section 4.2.3, the distribution of the arrival time uncertainty is dependent on the size of the scheduling horizon. The probability distribution that describes the uncertainty is a gamma distribution with shape parameter $k = 5$, and scale parameter θ, which is dependent on the time horizon. The scale parameter θ is chosen such that the tail corresponds with the upper bound $d_{\text{max}} = \frac{49}{90}T - y$. The realizations of the uncertain arrival time drawn from the gamma distribution are rounded to correspond to the discrete nature of the uncertain parameter. Additionally, a minimum delay $d_{min} = 0$ is applied for instances with a scheduling horizon smaller than 90 days and $d_{min} = -7$ for larger instances. The mean values for the delay d_{mean} of the probability distribution are rounded. Table 5.4 displays the resulting characteristics of the uncertainty in arrival time for the studied instances.

6

Numerical experiments

This chapter presents the numerical results of the optimization models developed for the SBCP. Both optimization and simulation results are provided for each model. Optimization results include the sum of modeling and solving time, along with the optimal objective value obtained. Simulation results evaluate model performance, presenting the feasibility ratio and average objective ratio based on N simulated realizations of the uncertain parameters, along with the total simulation time. First, Section 6.1 describes the simulation procedure to evaluate model performance. Then, Section 6.2 presents results for the nominal model, evaluating its performance under different types of supply uncertainty individually and collectively. Subsequent Sections 6.3 to 6.6 detail results for each optimization method considering uncertainty separately, assessing performance under the corresponding type of uncertainty. Finally, Section 6.7 discusses results for combinations of different optimization under uncertainty models and their performance under supply uncertainty.

6.1. Evaluation simulation

To evaluate the performance of each model, the models are tested in a simulation for different realizations of the supply uncertainty. Each optimization under uncertainty model is tested for the type of uncertainty for which it is designed. Additionally, the nominal model has been tested for all three types of supply uncertainty individually. During the evaluation, the performance of the solution of a model is tested on N randomly drawn realizations of the corresponding uncertainty. This means that we generate random values by drawing from the probability distributions as described in Section 4.2, for either the mass of the copper concentrates, the mass fraction of the elements in the copper concentrates or the arrival times of the copper concentrates for all copper concentrates in the scheduling horizon or a combination of above uncertainties. When the simulation is repeated, the same randomly generated realizations will be drawn from the probability distribution.

At the end of the simulation, two performance measures, namely the feasibility ratio and the average objective, are calculated. Equations (6.1) and (6.2) present the calculation of these performance measures. In the simulation, a solution is defined as feasible when the solution remains feasible for the realization of the uncertain parameters over the entire scheduling horizon. The feasibility ratio denotes for what part of the realizations the solution of the model remained feasible.

$$\text{Feasibility ratio} = \frac{\text{total number of feasible solutions with realized parameters}}{N} \tag{6.1}$$

The average objective denotes the objective value which on average is earned over the number of feasible solutions with the optimal solution from the model.

$$\text{Average objective} = \frac{\text{sum of objectives of all feasible solutions}}{\text{total number of feasible solutions}} \tag{6.2}$$

During the evaluation, we implement a rolling horizon principle. A rolling horizon means that a time-dependent model is solved repeatedly, and the planning interval is moved forward in time during each solution step. In our case, we can solve the model for the entire scheduling horizon, so, we do not

need to move the planning interval forward, however, we fix decisions for some periods and remove corresponding uncertainty, and re-solve the problem. Figure 6.1 illustrates the working of the rolling horizon for the simulation used to evaluate the SBCP. For the simulation a re-optimization period of seven days is used, corresponding to the re-optimization period of the refinery. Initially, we solve the instance for the entire scheduling horizon using expected parameters and evaluate the studied model (Figure 6.1, a). Subsequently, we insert the realized uncertain parameters for the first seven days, denoted by A in the plot, and assess the feasibility of the solution using the resulting model (Figure 6.1, b). If the solution proves feasible with the actual parameters, we save it for the initial seven days and fix the decision variables, which is marked by F in the plot (Figure 6.1, c). We then re-optimize the instance using the evaluated model, incorporating the fixed variables for the first seven days. Introducing the parameter t_{start} enables us to model the evaluated model from this period onward while utilizing the nominal model for earlier periods. In this way, we avoid being over-conservative during evaluation. This process continues until reaching the end of the scheduling horizon, ensuring that for each rolling-horizon window, we find a feasible solution accommodating the realized uncertain parameters (Figure 6.1, d until f).

Essentially, when we thus denote the solution infeasible during simulation, this can be caused by two reasons. Either with the model only an infeasible solution could be found for the next seven days denoted as a double star (**), or the found solution of seven days by the model is not feasible with the realized parameters denoted as a triple star(***). These notations will be used in the following tables presenting the simulation results. In the optimization results a star (*) indicates that the solution is infeasible for the entire scheduling horizon. Important to note is that such a solution sometimes leads to a feasible solution during simulation, due to the re-optimization of the model every seven days.

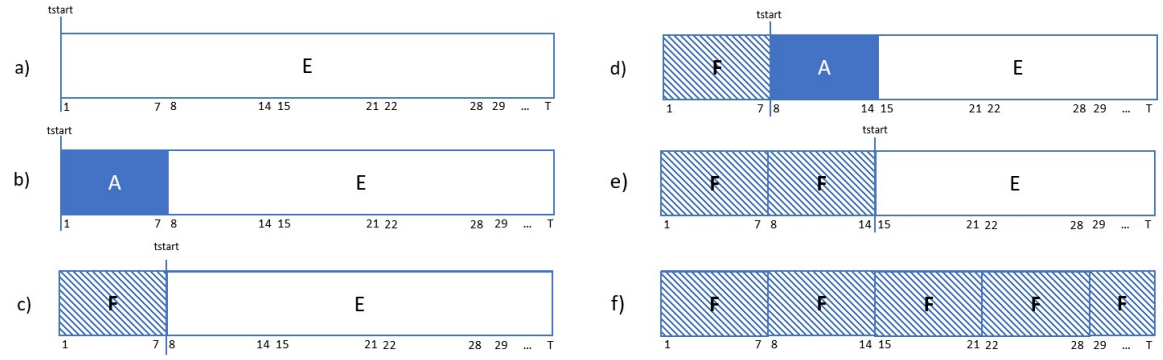

Figure 6.1: Rolling horizon principle for simulation evaluation of SBCP. A re-optimization period of seven days is applied. A denotes the use of actual parameters. E denotes the use of expected parameters. F denotes that the decision variables are fixed. The parameter t_{start} denotes the period from which the evaluated model is applied.

When the simulation is applied to evaluate the model's performance on arrival time uncertainty, during re-optimization it is important to consider that the realizations of the actual parameters can lay outside the current optimized time frame because deviations between the actual and expected arrival period are applied. In this study, when a copper concentrate was expected during a time frame, but in the realization it becomes apparent that the copper concentrate has not arrived yet, we assume a maximum delay for the copper concentrate and this new assumed arrival time is included as deterministic input during the re-optimization of the stochastic model, so no new scenarios are generated for the newly assumed arrival period of the copper concentrate.

6.2. Nominal model

This section presents the results for the nominal model, which does not directly consider parameter uncertainty. Section 6.2.1 presents the optimization results of the model and Section 6.2.2 presents the performance of the model across different simulations.

6.2.1. Optimization results

Table 6.1 presents the optimization results of the nominal model for all five instances. These results include the computation time, which comprises both the construction and solving phases of the CPLEX model, measured in seconds, as well as the objective value representing the profit generated by the optimal solution, expressed in millions of euros.

Table 6.1: Optimization results of the nominal model.

	Objective value (million euros)	Computation time (s)
Instance A	9.5	0.33
Instance B	17.5	0.30
Instance C	36.9	0.25
Instance D	63.2	0.38
Instance E	199.0	16.18

All five instances are feasible for the nominal model within remarkably short computation times, with almost every instance solvable in under one second. Even instance E, representative of the refinery case study, is quickly modeled and solved in a couple of seconds. This efficiency stands in contrast to the current linear optimization model employed for the SBCP of the refinery, which involves additional complexities such as optimizing sequential batch processes alongside the smelter's feeding schedule, resulting in significantly longer computation times. An important advantage of the created nominal model for the SBCP is thus the ability to gain quick insights into the feasibility of the blending schedule considering the current procurement agreements of copper concentrates.

6.2.2. Performance of nominal model

We evaluate the performance of the nominal model using four different simulations. Each simulation assesses the optimal solution found by the model across N randomly generated realizations of uncertainty. The first three simulations generate random realizations for one type of supply uncertainty, specifically $a)$ mass uncertainty, $b)$ mass fraction uncertainty, and $c)$ arrival time uncertainty. Finally, simulation $d)$ generates random realizations for all three types of supply uncertainty together. Table 6.2 presents the results of these simulations for the nominal model (NM) across all instances. The number of simulations is varied between $N = \{10, 100, 1000\}$. For instance E the simulation results with $N = \{100, 1000\}$ are excluded due to extended computation times. The performance measures, namely the feasibility ratio and the average objective ratio, are presented. In addition, the simulation time is presented, denoting the entire running time of the simulation encompassing the solving of the models and the re-optimization over the time horizon.

In the simulation, the rolling horizon principle, as described in Section 6.1, is applied with a re-optimization period of seven days. This approach allows for the adaptation of forthcoming decision variables to the realization of revealed uncertain parameters after each re-optimization period. Consequently, the objective value of the solution found with re-optimization may exceed the optimal nominal objective value obtained without re-optimization. This scenario is indicated by an average objective ratio greater than 100 percent.

Simulation $a)$ evaluates the performance of the nominal model concerning uncertainty in the mass of a copper concentrate. For the first four instances, the nominal solution for the SBCP remains feasible for the majority of the realizations, with feasibility ratios ranging from 70 (Instance C) to 100 (Instance B). This can be explained due to the nature of the SBCP and the nature of the mass uncertainty. The uncertainty in the mass of copper concentrates follows a normal distribution with a mean of $\mu = 0.0$ and a standard deviation of $\sigma = 3.3$. This indicates potential deviations of the actual mass of a copper concentrate with the nominal value in both directions, however, these variations do not always directly lead to an infeasible solution. While an excess delivery of copper concentrates could theoretically exceed capacity constraints, we observed that the capacity constraint in the SBCP is typically not quickly binding and this is particularly true for the instances with unlimited capacity. Conversely, instances where the actual mass of a copper concentrate is lower than expected may compromise solution feasibility. Feasibility in this context necessitates the smelter operating continuously at full capacity, supported by an appropriate blend of copper concentrates to satisfy throughput and element constraints. If there is

Table 6.2: Performance of the nominal model for simulated uncertainty in $a)$ the mass of a copper concentrate, $b)$ the mass fraction of elements in a copper concentrate, $c)$ the arrival time of a copper concentrate, and $d)$ general supply uncertainty. The re-optimization period of the rolling horizon is seven days. (***) denotes that the average objective ratio is undefined because the solution does not remain feasible for the realizations of the uncertainty. (**) denotes that the model could only find an infeasible solution during re-optimization.

	Number of simulations	Performance measures	NM for a)	NM for b)	NM for c)	NM for d)
Instance A	10	Feasibility ratio	100.0	20.0	0.0	0.0
		Average objective ratio	100.3	100.0	***	***
		Simulation time (s)	2.11	2.22	1.42	0.84
	100	Feasibility ratio	95.0	26.0	0.0	0.0
		Average objective ratio	100.3	100.8	***	***
		Simulation time (s)	16.01	14.53	5.58	5.66
	1000	Feasibility ratio	94.7	24.9	0.3	0.2
		Average objective ratio	100.3	100.8	100.2	100.0
		Simulation time (s)	200.24	52.83	41.94	52.92
Instance B	10	Feasibility ratio	100.0	10.0	0.0	0.0
		Average objective ratio	100.0	101.0	***	***
		Simulation time (s)	17.17	1.97	2.13	2.82
	100	Feasibility ratio	100.0	9.0	0.0	0.0
		Average objective ratio	100.0	100.0	***	***
		Simulation time (s)	154.11	17.28	15.10	15.87
	1000	Feasibility ratio	100.0	8.1	0.0	0.0
		Average objective ratio	100.0	100.0	*	*
		Simulation time (s)	1407.56	158.02	127.93	154.75
Instance C	10	Feasibility ratio	70.0	0.0	0.0	0.0
		Average objective ratio	100.4	***	***	***
		Simulation time (s)	5.05	1.32	1.36	2.12
	100	Feasibility ratio	70.0	0.0	0.0	0.0
		Average objective ratio	100.3	***	***	***
		Simulation time (s)	84.68	13.35	13.25	12.83
	1000	Feasibility ratio	70.1	0.0	0.0	0.0
		Average objective ratio	100.3	***	***	***
		Simulation time (s)	790.77	123.56	127.93	148.85
Instance D	10	Feasibility ratio	80.0	0.0	0.0	0.0
		Average objective ratio	100.6	***	***	***
		Simulation time (s)	46.05	3.74	3.58	3.85
	100	Feasibility ratio	78.0	0.0	0.0	0.0
		Average objective ratio	100.5	***	***	***
		Simulation time (s)	381.98	27.77	28.34	32.60
	1000	Feasibility ratio	78.3	0.0	0.0	0.0
		Average objective ratio	100.4	***	***	***
		Simulation time (s)	1225.15	257.79	285.88	283.58
Instance E	10	Feasibility ratio	30.0	0.0	** / 0.0	** / 0.0
		Average objective ratio	99.7	***	** / ***	** / ***
		Simulation time (s)	4520.01	311.10	392.68	306.88

insufficient mass of a copper concentrate available to follow the model's solution, the feasibility of the solution is compromised. However, due to re-optimization over the scheduling horizon, the solution can adjust every seven days based on the realized uncertain mass of the delivered copper concentrates. Additionally, the copper concentrate whose actual mass is lower than expected should be used in the solution. to create an infeasible solution. Therefore, even a lower mass of a copper concentrate than expected does not always immediately lead to infeasibility of the solution. Instance E has a lower feasibility ratio of 30.0 ($N = 10$). This indicates that instance E is more sensitive to mass uncertainty than the other instances. This can be explained by having more arrivals of copper concentrates in the scheduling horizon, which all can have a lower mass than expected. Therefore, the total probability that the actual mass of a copper concentrate is lower than the expected mass and will be used in the solution in the next seven days is larger. We conclude that the SBCP is moderately sensitive to the mass uncertainty of a copper concentrate, and the sensitivity increases with the size of the scheduling horizon and decreases with the number of expected copper concentrates and start inventory.

Simulation $b)$ evaluates the performance of the nominal model concerning uncertainty in the mass fraction of elements in a copper concentrate. The feasibility ratio for the nominal model is low, varying from 26.0 (instance A, $N = 100$) to 0.0 (instance C, D, and E). Based on the low feasibility ratios we conclude that the SBCP is sensitive to fluctuations in the mass fraction of the elements. The elemental upper bound constraints ensure that the ratio of an element in the final flow stays below a certain upper bound. When the nominal solution is used, but the mass fractions (of multiple) copper concentrates are higher than expected the upper bound may be exceeded, resulting in an infeasible solution. The low feasibility ratios reflect that this is often the case for the SBCP. Furthermore, interdependency constraints are enforced to instance B till instance E. For element 2 and element 7, the interdependency constraints impose both a lower bound and upper bound on the ratio of these elements in the final flow. Complementary for element 1, element 3, element 4, and element 6 the interdependency constraints impose upper bounds on the interdependent ratios of these elements. Both lower and higher actual mass fractions than expected can thus lead to exceeding the interdependency bounds. The presence of these additional constraints intensifies the challenge for the solution to remain feasible under mass fraction uncertainty, which is reflected in low feasibility ratios of 10.0 (instance B) and 0.0 (instances C, D, and E). To assess the sensitivity of the SBCP to fluctuations in element mass fractions, we varied the re-optimization period. Despite shorter re-optimization periods providing more flexibility for solutions to adapt to uncertainty, instances C, D, and E still had zero feasibility ratios even with a re-optimization period of two periods. This underscores the high sensitivity of the SBCP to fluctuations in element mass fractions, leading to (near-)zero feasibility ratios. We observe that instance A is less sensitive to mass fraction uncertainty because for this instance the interdependency constraints are not required and additionally for a lower number of elements upper bound constraints are required.

Simulation $c)$ evaluates the performance of the nominal model concerning uncertainty in the arrival time of a copper concentrate. Across all instances, the feasibility ratio is zero, rendering the average objective ratio undefined. This may be explained by the nature of the arrival time uncertainty. As described in Section 4.2.3, the uncertain delay of the arrival of a copper concentrate follows a gamma distribution. For instance E this distribution describes possible delays varying from seven days early to forty-two days late for the scheduling horizon of 90 days. For the smaller instances, this range of possible delays is scaled corresponding to the size of the scheduling horizon. Early arrivals of copper concentrate do not affect solution feasibility because there is unlimited inventory capacity. On the other hand, when one copper concentrate arrives later than the period it is used originally in the solution, the solution becomes infeasible immediately. For all instances, there is a significantly large probability that a minimum of one copper concentrate arrives late. This results in low feasibility ratios as shown in the table. We thus conclude that the SBCP is very sensitive to uncertainty in the arrival time of a copper concentrate. For instance E it is sometimes even not possible to find a feasible solution with the nominal model during re-optimization denoted as (**).

Simulation $d)$ evaluates the performance of the nominal model under supply uncertainty, considering uncertainty in the mass, mass fraction of elements, and arrival time of a copper concentrate simultaneously. The table reveals feasibility ratios of zero. The results show that the combined uncertainty results in feasibility ratios that are the same as the lowest feasibility ratio for an individual type of supply uncertainty or worse. For most instances the feasibility ratio was already zero for the arrival time uncertainty, resulting in also zero feasibility ratios for the total supply uncertainty. In addition, the feasibility ratios for mass fraction uncertainty for most instances were also already low. We conclude that SBCP is very sensitive to supply uncertainty primarily due to mass fraction uncertainty and arrival time uncertainty. Essentially, the nominal model is strictly not able to provide a robust solution that remains feasible for realizations of supply uncertainty.

Further, the table illustrates how the number of simulation iterations N influences performance measures. Generally, a larger N leads to more realistic feasibility and average objective ratios since the solution is tested against a greater number of randomly generated realizations of uncertainty. However, this comes at the expense of longer simulation times. Interestingly, there is only a small difference in results between simulations with $N = 100$ and $N = 1000$. This suggests that using $N = 100$ simulations is sufficient to evaluate the models effectively. This finding holds promise for evaluating larger instances, in future research, as it indicates shorter computation times without significant loss in accuracy.

6.3. Robust mass model

This section presents the results of the robust mass model, which utilizes a box uncertainty set for the mass of the copper concentrate parameter as introduced in Section 4.3. Section 6.3.1 presents the optimization results of the model and Section 6.3.2 presents the performance of the model evaluated by the simulation for uncertainty in the mass of a copper concentrate.

6.3.1. Optimization results

Table 6.3 presents the optimization results of the robust mass model for different normalized perturbation parameters λ. This parameter denotes the maximum deviation of the uncertain mass parameter as a percentage of the nominal parameter within the box uncertainty set and is varied between 0.0 (equivalent to a deterministic model) and 0.5. The results include the feasibility status of the solution, computation time in seconds, and objective value in million euros for each instance. The feasibility status indicates whether the solution is feasible or infeasible. In cases of infeasibility, it specifies the period at which the smelter throughput constraint could no longer be satisfied. A star in the table (*) denotes that the solution is infeasible for the entire scheduling horizon leaving the remaining output irrelevant.

Table 6.3: Optimization results of the robust model for uncertainty in the mass of the copper concentrates with the use of a box uncertainty set with varying normalized perturbation factor λ for instance A till instance E. A star (*) denotes that the solution is infeasible for the entire scheduling horizon and thus that the output is irrelevant.

	\Output	$\lambda = 0.0$ (deterministic)	$\lambda = 0.1$	$\lambda = 0.2$	$\lambda = 0.3$	$\lambda = 0.4$	$\lambda = 0.5$
Instance A	Feasibility status	feasible	feasible	feasible	infeasible at p10	infeasible at p10	infeasible at p8
	Computational time (s)	0.30	0.21	0.21	*	*	*
	Objective value (million euros)	9.5	9.4	9.2	*	*	*
Instance B	Feasibility status	feasible	feasible	feasible	feasible	feasible	feasible
	Computational time (s)	0.26	0.37	0.47	0.30	0.51	0.29
	Objective value (million euros)	17.5	17.5	17.5	17.5	17.5	16.0
Instance C	Feasibility status	feasible	feasible	feasible	feasible	feasible	infeasible at p14
	Computational time (s)	0.31	0.50	0.40	0.45	0.842	*
	Objective value (million euros)	36.9	35.8	34.4	33.0	31.5	*
Instance D	Feasibility status	feasible	feasible	feasible	infeasible at p29	infeasible at p26	infeasible at p26
	Computational time (s)	0.80	0.45	0.53	*	*	*
	Objective value (million euros)	63.2	60.0	56.7	*	*	*
Instance E	Feasibility status	feasible	feasible	infeasible at p89	infeasible at p73	infeasible at p61	infeasible at p47
	Computational time (s)	3.88	3.10	*	*	*	*
	Objective value (million euros)	199.0	187.0	*	*	*	*

The table illustrates that the robust mass model for the SBCP becomes infeasible for higher values of the normalized perturbation factor λ. A higher normalized perturbation factor λ, indicates that a lower amount of copper concentrate can be used in the robust solution. In instances where an infeasible solution is found, the model is too conservative, indicating that the perturbation factor is too large. Specifically, the results demonstrate that for this normalized perturbation factor λ, there is insufficient copper concentrate available to satisfy the smelter throughput and element constraints in the worst case, resulting in infeasibility. Furthermore, we observe that for larger values of λ, the problem becomes earlier in the scheduling horizon infeasible because, at an earlier period, there is not enough copper concentrate available to meet the smelter constraints in the worst case. For different values of λ the instances become infeasible, indicating that each instance has its sensitivity to the mass uncertainty. This can be explained by different amounts of start inventory and the total amount of copper concentrate present in each instance. The objective values of the robust mass model are lower than the deterministic objective value. Increasing the perturbation factor results in a lower objective value, denoting a more conservative solution. The computation times of the robust mass model are small, not varying much from the computation times of the nominal model.

For further analysis of the robust mass model, we choose a normalized perturbation factor $\lambda = 0.1$ because for this value the robust solution is feasible across all instances. When the refinery desires a model that provides a solution that is robust against larger perturbations than 10 percent different than the nominal value, a multistage model should be defined. A multistage model with for instance two stages may already provide feasible solutions for a higher perturbation factor during simulation.

6.3.2. Performance of robust mass model

Table 6.4 presents the simulation results on the performance of the robust mass model, which utilizes a box uncertainty set for the mass of a copper concentrate with a normalized perturbation factor $\lambda = 0.1$. The model is evaluated for uncertainty in the mass of a copper concentrate. For the rolling horizon in the simulation re-optimization period of seven days is used. We exclude the simulation results for instance E with $N = \{100, 1000\}$ due to extended computation times.

Table 6.4: Performance of robust mass model and nominal model for simulated uncertainty in the mass of a copper concentrate. The robust model has implemented a box uncertainty set with normalized perturbation parameter $\lambda = 0.1$ for the mass parameter of a copper concentrate. The number of iterations is N and the re-optimization period is seven days. Results are presented for instance A till instance E.

	Number of simulations	Performance measures	Nominal Model	Robust mass model
Instance A	10	Feasibility ratio	100.0	100.0
		Average objective ratio	100.3	98.7
		Simulation time (s)	2.11	1.35
	100	Feasibility ratio	95.0	100.0
		Average objective ratio	100.3	98.7
		Simulation time (s)	16.01	14.23
	1000	Feasibility ratio	94.7	100.0
		Average objective ratio	100.3	98.7
		Simulation time (s)	200.24	140.22
Instance B	10	Feasibility ratio	100.0	100.0
		Average objective ratio	100.0	100.0
		Simulation time (s)	17.17	11.34
	100	Feasibility ratio	100.0	100.0
		Average objective ratio	100.0	100.0
		Simulation time (s)	154.11	106.45
	1000	Feasibility ratio	100.0	100.0
		Average objective ratio	100.0	100.0
		Simulation time (s)	1407.56	1738.40
Instance C	10	Feasibility ratio	70.0	100.0
		Average objective ratio	100.4	97.5
		Simulation time (s)	5.05	16.18
	100	Feasibility ratio	70.0	100.0
		Average objective ratio	100.3	97.5
		Simulation time (s)	84.68	105.3
	1000	Feasibility ratio	70.1	100.0
		Average objective ratio	100.3	97.5
		Simulation time (s)	790.77	1595.69
Instance D	10	Feasibility ratio	80.0	100.0
		Average objective ratio	100.6	99.4
		Simulation time (s)	46.05	42.83
	100	Feasibility ratio	78.0	100.0
		Average objective ratio	100.5	99.4
		Simulation time (s)	381.98	344.55
	1000	Feasibility ratio	78.3	100.0
		Average objective ratio	100.4	99.3
		Simulation time (s)	1225.15	3468.52
Instance E	10	Feasibility ratio	30.0	100.0
		Average objective ratio	99.7	97.4
		Simulation time (s)	4520.01	4135.01

The table illustrates that the robust mass model performs very well regarding the feasibility ratio and it has improved in comparison with the nominal model. The feasibility ratio is for all instances 100 denoting that the robust solution is feasible for all simulated realizations of the uncertain mass parameter when a re-optimization period of seven days is applied. Realizations of the mass uncertainty that have not been captured by the box uncertainty set can thus perfectly be adapted by the rolling-horizon window of seven days. The average objective ratio is lower than 100, which is explained by the robust mass model having a lower optimal objective due to the conservative approach. However, the

decrease in objective value is minor, indicated by an average objective ratio ranging from 97.4 to 100. Notably, this conservative approach leads thus to perfect robust results in the evaluation. It can be concluded that the used uncertainty set captures the uncertainty in the mass well and is suitable to create a robust solution while requiring only minor profit reductions.

6.4. Robust mass fraction model

This section presents the results for the robust mass fraction model, which utilizes a budgeted uncertainty set for each element for the corresponding uncertain mass fraction parameter as described in Section 4.4. Section 6.4.1 presents the optimization results and Section 6.4.2 presents the performance of the robust mass fraction model evaluated by the simulation for uncertainty in the mass fraction of elements in a copper concentrate.

6.4.1. Optimization results

Table 6.5 presents the optimization results of the robust mass fraction model, which incorporates budgeted uncertainty sets for the mass fraction parameters of the elements. We tested different settings for the normalized perturbation factor λ_k, which denotes the maximum percentage deviation of the nominal mass fraction of an element, in the corresponding budgeted uncertainty set. A summary of these experiments is presented in Appendix B.1. We conclude that for values from $\lambda_k = 0.01$ applied to all the budgeted uncertainty sets, the model can not find feasible solutions across all instances. Specifically, we observe that the SBCP reacts more sensitively to uncertainty in the mass fraction of elements 2 and 7. When we choose $\lambda_2 = \lambda_7 = 0.001$, for values from $\lambda_k = 0.03$ for the remaining elements the model finds infeasible solutions for some instances. After multiple experiments, we chose to model the robust mass fraction model with a normalized perturbation factor $\lambda_2 = \lambda_7 = 0.001$ for element 2 and element 7, while we applied a normalized perturbation factor of $\lambda_k = 0.01$ to the remaining elements. These settings are chosen because they provide feasible solutions for the model across all the instances and correspond with the observed peaks in the probability distributions of the mass fraction uncertainty as described in Section 4.2.3.

When not stated differently, these parameter settings are used in the rest of the analysis for the robust mass fraction model. Insights into the impact of the budget parameter Γ for all the budgeted uncertainty sets were obtained by varying its value. Initially, we implemented $\Gamma = 0$ for each budgeted uncertainty set, representing a deterministic model. Subsequently, the values $\Gamma = \{1, \frac{1}{2}CC, CC\}$ were implemented, where CC signifies the expected number of copper concentrates. For the budget parameter $\Gamma = CC$, all the expected copper concentrates can take their worst-case value simultaneously, effectively forming a box uncertainty set.

Table 6.5: Optimization results of the robust model for uncertainty in the mass fraction of elements in a copper concentrate. A budgeted uncertainty set has been implemented with normalized perturbation factor $\lambda = 0.001$ for element 2 and element 7, and $\lambda = 0.01$ for the other elements. The budget parameter Γ has been varied between 0, 1, $\frac{1}{2}CC$ and CC. The results are shown for instance A till instance E.

	Output	$\Gamma = 0$ (deterministic)	$\Gamma = 1$	$\Gamma = 1/2\|CC\|$	$\Gamma = \|CC\|$
Instance A	Feasibility status	feasible	feasible	feasible	feasible
	Computational time (s)	0.23	0.21	0.21	0.36
	Objective value (million euros)	9.5	9.4	9.4	9.3
Instance B	Feasibility status	feasible	feasible	feasible	feasible
	Computational time (s)	0.76	0.91	0.95	1.30
	Objective value (million euros)	17.5	17.4	17.3	17.2
Instance C	Feasibility status	feasible	feasible	feasible	feasible
	Computational time (s)	0.32	0.70	0.74	0.70
	Objective value (million euros)	36.9	36.8	36.7	36.6
Instance D	Feasibility status	feasible	feasible	feasible	feasible
	Computational time (s)	0.53	18.56	5.60	12.85
	Objective value (million euros)	63.2	63.2	62.9	62.6
Instance E	Feasibility status	feasible	feasible	feasible	feasible
	Computational time (s)	3.16	264.64	590.05	554.64
	Objective value (million euros)	199.0	197.7	189.8	187.9

We observe that the objective value of the robust models tends to be lower than that of the deterministic model. This trend becomes more pronounced with larger values of the budget parameter, allowing more mass fractions of an element in the copper concentrates to take their worst-case value simultaneously, resulting in more conservative solutions with lower objective values. Computation times for the robust model are generally higher than those for the deterministic model, particularly for larger instances (e.g., instance E 590.05 seconds or 0.04 seconds). For further analysis, we choose the model with a budget parameter of $\Gamma = \frac{1}{2}CC$, to consider that it is unlikely that in all copper concentrates the mass fraction of an element takes the worst-case value simultaneously, but at the same time not be over conservative.

We further study the sensitivity of the SBCP to mass fraction uncertainty by creating different robust models, each incorporating a budgeted uncertainty set implemented for an individual element k as opposed to an uncertainty set applied to all elements simultaneously. The normalized perturbation factor λ_k is varied between 0 and 0.1 with steps of 0.01. This allows us to analyze how sensitive the optimal solution reacts to the size of the uncertainty set for an individual element. For this analysis, the budget parameter $\Gamma = \frac{1}{2}CC$ is used, and the study is performed on instance A till instance C. Figure 6.2 shows these results for element 1, element 2 and element 7, respectively, where the objective value of each instance is scaled between 0.0 and 1.0. These results illustrate similar trends as observed in the robust models for the other elements. For completeness, the results for the other elements are included in Appendix B.2.

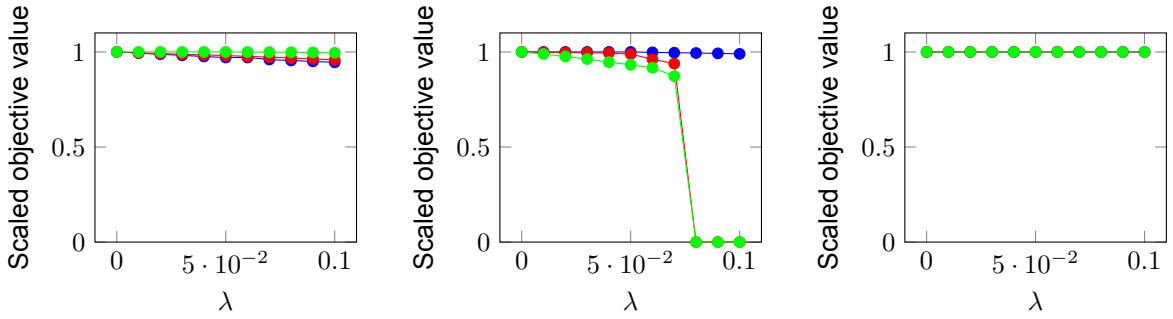

(a) Robust mass fraction model with budgeted uncertainty set for mass fraction of element 1.

(b) Robust mass fraction model with budgeted uncertainty set for mass fraction of element 2.

(c) Robust mass fraction model with budgeted uncertainty set for mass fraction of element 5.

Figure 6.2: Robust mass fraction model with budgeted uncertainty set for an individual element. Showing the relation between λ and the scaled objective value between zero and 1.0, where 1.0 represents the optimal objective value obtained with the nominal model and 0.0 denotes the infeasibility of the solution. The blue line represents instance A, the red line represents instance B and the green line represents instance C.

Graph 6.2a illustrates the model with a budgeted uncertainty set for element 1, presenting the general trend occurring for most elements. It shows that as the normalized perturbation parameter λ increases, the objective value of the robust solutions decreases. A higher λ implies a greater potential deviation of the actual mass fraction from the expected value, leading to quicker violations of the element upper bound constraints. It is crucial for a robust solution that, even in the worst-case scenario, the element upper bound constraints remain feasible. This necessitates incorporating a lower amount of each copper concentrate in the blend to ensure the upper bound element constraint is met under worst-case conditions. To compensate for this, additional copper concentrate with a lower profit parameter is added to the blend to satisfy the throughput constraint of the smelter. Consequently, the robust solution achieves a lower objective value in comparison with the nominal model.

Graph 6.2c presents the results for the model formulated robust against uncertainty in the mass fraction of element 5. The graph for element 8 illustrates the same relation. Contradictory, for these elements we observe no decrease in objective value for a larger value of the normalized perturbation factor δ. As described in Section 5, the upper bound on the mass fraction of these elements in the final flow is 1. According to this constraint, the final blend is thus allowed to completely consist of element 5 or element 8, which is never the case for the SBCP. Therefore these upper bound constraints are never binding and ensuring that the upper bound element constraints hold for the budgeted uncertainty sets

does thus not affect the (nominal) solution. Additionally, for element 5 there are no interdependency constraints because the weight interdependency parameter is $W_5 = 0$. For element 8 the weight interdependency is $W_8 = 0.00016$, but from the graph, it can be concluded that ensuring that the constraints hold for the budgeted uncertainty set does not influence the objective value. Essentially, the SBCP is not sensitive to uncertainty in the mass fraction of element 5 and element 8.

Furthermore, Graph 6.2b shows the results for the robust model with a budgeted uncertainty set for element 2. The graph for element 7 shows the same relation. For these two models, a drop to zero is observed in the objective value when the normalized perturbation factor λ is increased for instance B and instance C. In these graphs, a scaled objective value of 0.0 denotes an infeasible solution. The infeasibility of these solutions can be explained by the interdependency constraints that are required for these instances. These interdependency constraints define that the ratio of element 2 and element 7 in the final blend should stay between a strict lower and upper bound. However, when in the robust model the constraints have to hold for all the values of the budgeted uncertainty set, and thus for the worst case of each constraint, for large values of λ, this becomes contradictory for the upper and lower bound constraints. We demonstrate this with the use of an example. The mass fraction ratio between element 7 and element 2 in the final blend is bounded by $[0.58, 0.64]$ as described in equations (4.32) and (4.33). If the uncertainty set for an element is too large, the worst cases of the defined uncertainty set will always violate the lower- and upper bound. Let the amount of element 7 be represented by Q' and the amount of element 2 be represented by Q. Let the ratio be for instance $\frac{Q'}{Q} = 0.60$. If we look at the uncertainty for only element 7, a budgeted uncertainty set of 0.10 percent results thus in always violating the bounds. Therefore the robust model will always be infeasible. It can be concluded that when in the SBCP the interdependency constraints are required the SBCP is very sensitive to uncertainty in the mass fraction of element 2 and element 7 and there are strict bounds on the uncertainty set for which the model can be designed robust against.

The robust solution for instance A becomes not infeasible in the graphs for element 2 and element 7. This is because for instance A the interdependency constraints are not required. Further, instance A becomes infeasible for element 3 for values from $\lambda = 0.3$ and higher. This is instance-specific because there are no copper concentrates available at the beginning of the scheduling horizon with a low enough nominal mass fraction of element 3, to not exceed the robust upper bound constraint. Overall, we conclude that for a smaller instance, the feasibility of the solution is more dependent on the specifics of the present copper concentrates in the instance. because there is limited choice.

6.4.2. Performance of robust mass fraction model

Table 6.6 presents the results of the performance of the robust mass fraction model, in comparison with the nominal model. In the robust mass fraction model a budgeted uncertainty set with a normalized perturbation parameter $\lambda_2 = \lambda_7 = 0.001$ for element 2 and element 7 and a normalized perturbation parameter $\lambda_k = 0.01$ for the other elements are applied. The budget parameter $\Gamma = \frac{1}{2}CC$ is implemented, denoting half the number of expected copper concentrates in the instance. The model is evaluated for uncertainty in the mass fraction of elements in a copper concentrate. For the rolling horizon, a re-optimization period of seven days is applied. We excluded the results for instance D with $N = 1000$ and instance E with $N = \{100, 1000\}$ due to extended computation times.
The results show that the robust mass fraction model has a higher feasibility ratio than the nominal model. The feasibility ratio is high for instance B until instance E, varying from 80.0 (Instance E) to 100.0 (Instance C, $N = 10$). The feasibility of the robust solution is highly increased in comparison with the feasibility of the nominal solution, which was infeasible with the actual parameters for (nearly) all realizations. The average objective ratio is for any instance not lower than 95.5, indicating a minor profit reduction in comparison with the nominal objective value. We conclude that the defined budgeted uncertainty set captures the uncertainty sufficient for instance B till instance D and is sufficient to provide a robust solution that remains feasible for realizations of the mass fraction uncertainty at the cost of minor profit reductions.

Nevertheless, instance A has a feasibility ratio of 40 percent. Although for this instance the interdependency constraints are not required, the results show that instance A is more sensitive to deviations in the mass fractions of the elements in comparison with the other instances. The current budgeted uncer-

Table 6.6: Performance of robust mass fraction model (RMFM) and nominal model for simulated uncertainty in mass fraction of the elements in the copper concentrates. The robust model has implemented a budgeted uncertainty set with normalized budget parameters $\lambda = 0.001$ for element 2 and element 7 and $\lambda = 0.01$ for the other elements. The budget parameter is $\Gamma = \frac{1}{2}CC$ and the re-optimization period is seven days.

	Number of simulations	Performance measures	Nominal Model	RMFM : $\Gamma = \frac{1}{2}CC$
Instance A	10	Feasibility ratio	20.0	40.0
		Average objective ratio	100.0	99.0
		Simulation time (s)	2.22	1.69
	100	Feasibility ratio	26.0	46.0
		Average objective ratio	100.8	99.3
		Simulation time (s)	14.53	10.73
	1000	Feasibility ratio	24.9	45.4
		Average objective ratio	100.8	99.3
		Simulation time (s)	52.83	89.18
Instance B	10	Feasibility ratio	10.0	90.0
		Average objective ratio	101.0	99.0
		Simulation time (s)	1.97	16.40
	100	Feasibility ratio	9.0	96.0
		Average objective ratio	100.0	98.9
		Simulation time (s)	17.28	128.58
	1000	Feasibility ratio	8.1	94.7
		Average objective ratio	100.0	99.0
		Simulation time (s)	158.02	1371.71
Instance C	10	Feasibility ratio	0.0	100.0
		Average objective ratio	***	99.5
		Simulation time (s)	1.32	11.62
	100	Feasibility ratio	0.0	81.0
		Average objective ratio	***	99.4
		Simulation time (s)	13.35	90.00
	1000	Feasibility ratio	0.0	81.5
		Average objective ratio	***	99.4
		Simulation time (s)	123.56	888.73
Instance D	10	Feasibility ratio	0.0	90.0
		Average objective ratio	*	99.6
		Simulation time (s)	3.74	91.214
	100	Feasibility ratio	0.0	86.0
		Average objective ratio	*	99.5
		Simulation time (s)	27.77	898.81
Instance E	10	Feasibility ratio	0.0	80.0
		Average objective ratio	***	95.5
		Simulation time (s)	311.10	27539.18

tainty set is thus insufficient to provide a robust solution for instance A. Instance A only has four copper concentrates which are expected in the scheduling horizon. This means that during re-optimization not many other copper concentrates can be used to adapt the solution. Therefore we may conclude that instances with a smaller time horizon and lower number of copper concentrates, such as instance A, are more sensitive to uncertainty in the mass fraction of elements than instances B till E.

To obtain a robust solution for instance A with a higher feasibility ratio we model the robust mass fraction model again but choose the budget parameter $\Gamma = CC$ and define the normalized perturbation parameters λ the same as previously. The performance of this robust mass fraction across all instances is evaluated with the simulation for uncertainty in the mass fraction of elements of a copper concentrate. Table 6.7 presents the simulation results of this model. The table illustrates that the feasibility ratio for all instances stayed the same or increased in comparison with the robust mass fraction with a budget parameter $\Gamma = \frac{1}{2}CC$, varying between 80 (instance E) to 100 (instance C, $N = 100$) and specifically instance A has now also a high feasibility ratio of 96.3 for $N = 1000$. The robust mass fraction model which utilizes a box uncertainty set is thus sufficient to capture the uncertainty across all instances. The average objective ratio of the robust mass fraction model with $\Gamma = CC$ is lower than that of the robust

Table 6.7: Performance of robust mass fraction model (RMFM) and nominal model for simulated uncertainty in mass fraction of the elements in the copper concentrates. The robust model has implemented a budgeted uncertainty set with normalized budget parameters $\lambda = 0.001$ for element 2 and element 7 and $\lambda = 0.01$ for the other elements. The budget parameter is $\Gamma = CC$ and the re-optimization period is seven days.

	Number of simulations	Performance measures	Nominal Model	RMFM: $\Gamma = CC$
Instance A	10	Feasibility ratio	20.0	100.0
		Average objective ratio	100.0	97.6
		Simulation time (s)	2.22	2.11
	100	Feasibility ratio	26.0	96.0
		Average objective ratio	100.8	97.9
		Simulation time (s)	14.53	19.36
	1000	Feasibility ratio	24.9	96.3
		Average objective ratio	100.8	97.8
		Simulation time (s)	52.83	89.96
Instance B	10	Feasibility ratio	10.0	90.0
		Average objective ratio	101.0	98.6
		Simulation time (s)	1.97	21.3
	100	Feasibility ratio	9.0	97.0
		Average objective ratio	100.0	98.5
		Simulation time (s)	17.28	170.83
	1000	Feasibility ratio	8.1	95.40
		Average objective ratio	100.0	98.6
		Simulation time (s)	158.02	1548.46
Instance C	10	Feasibility ratio	0.0	100.0
		Average objective ratio	***	97.9
		Simulation time (s)	1.32	15.3
	100	Feasibility ratio	0.0	89.0
		Average objective ratio	***	97.9
		Simulation time (s)	13.35	128.29
	1000	Feasibility ratio	0.0	90.6
		Average objective ratio	***	97.9
		Simulation time (s)	123.56	1147.64
Instance D	10	Feasibility ratio	0.0	90.0
		Average objective ratio	***	98.5
		Simulation time (s)	3.74	213.08
	100	Feasibility ratio	0.0	89.0
		Average objective ratio	***	99.0
		Simulation time (s)	27.77	1043.55
Instance E	10	Feasibility ratio	0.0	80.0
		Average objective ratio	***	94.5
		Simulation time (s)	311.10	15422.17

model with $\Gamma = \frac{1}{2}CC$. This is expected because the box uncertainty set provides a more conservative solution in comparison with the budgeted uncertainty set, however, the profit reduction is still minor, indicated by a lowest average objective ratio of 94.5. Selecting the value of Γ carefully is thus of high importance for the refinery. For very small instances a higher value of the budget parameter should be chosen to find a robust solution with a sufficient feasibility ratio against a small profit reduction. For the rest of the analysis, we choose to model the robust mass fraction model with a budget parameter $\Gamma = CC$ for instance A and with a budget parameter $\Gamma = \frac{1}{2}CC$ for instances B till E.

6.5. One-stage stochastic arrival time model

This section presents the results of the one-stage stochastic model created to capture the arrival time uncertainty of a copper concentrate with the reduced set $\overline{\mathcal{Z}}$. The results of the one-stage model with the reduced scenario tree $\overline{\mathcal{Z}}_{mean}$ or $\overline{\mathcal{Z}}_{worst}$, respectively, are discussed, which are created by selecting a decreased number of delays for each copper concentrate. Section 6.5.1 presents the optimization results and Section 6.5.2 presents the performance of the one-stage stochastic model evaluated by the simulation for arrival time uncertainty. Further, the conclusions drawn from the results of the one-stage

model using the reduced scenario set $\overline{\mathcal{Z}}_{sampled}$, generated by random sampling from the probability distribution representing the uncertain delay, are discussed. These conclusions align closely with those drawn from the one-stage stochastic model with scenario trees $\overline{\mathcal{Z}}_{mean}$ or $\overline{\mathcal{Z}}_{worst}$. For completeness, the optimization results and performance results obtained by this one-stage stochastic model, are presented in Appendix B.3.

6.5.1. Optimization results

Table 6.8 shows the optimization results for the one-stage stochastic model with the reduced scenario trees $\overline{\mathcal{Z}}_{mean}$ and $\overline{\mathcal{Z}}_{worst}$. These trees are constructed by considering two possible delays for each copper concentrate, denoted as d_1 and d_2, that form the branches in the scenario tree. For the pair of delays we chose to implement first the zero delay together with the mean delay, denoted as $\{d_1, d_2\} = \{0, d_{mean}\}$ and secondly, the zero delay together with the worst case delay, denoted as $\{d_1, d_2\} = \{0, d_{max}\}$, resulting in the reduced scenario trees $\overline{\mathcal{Z}}_{mean}$ and $\overline{\mathcal{Z}}_{worst}$, respectively. For comparison, the deterministic results reflecting zero delay are also presented, denoted as $\overline{\mathcal{Z}}_0$, across all instances.

Table 6.8: Optimization results of the one-stage stochastic model where the branches of the reduced scenario tree consist of two selected delays for each copper concentrate denoted as $\{d_1, d_2\}$. The reduced scenario sets $\overline{\mathcal{Z}}_{mean}$ which is constructed by $\{d_1, d_2\} = \{0, d_{mean}\}$ and $\overline{\mathcal{Z}}_{worst}$ which is constructed by $\{d_1, d_2\} = \{0, d_{max}\}$ are implemented. Further, $\overline{\mathcal{Z}}_0$ denotes the scenario tree where each copper concentrate is considered on time. A star (*) denotes that the solution of the model is infeasible for the entire scheduling horizon and thus that the output is irrelevant.

	Output	$\overline{\mathcal{Z}} = \overline{\mathcal{Z}}_0$ (deterministic)	$\overline{\mathcal{Z}} = \overline{\mathcal{Z}}_{mean}$	$\overline{\mathcal{Z}} = \overline{\mathcal{Z}}_{worst}$
Instance A	Feasible status	feasible	infeasible at p9	infeasible at p6
	Computational time (s)	0.23	*	*
	Objective value (million euros)	9.5	*	*
Instance B	Feasible status	feasible	feasible	infeasible at p15
	Computational time (s)	0.21	0.30	*
	Objective value (million euros)	17.5	14.2	*
Instance C	Feasible status	feasible	feasible	feasible
	Computational time (s)	0.39	0.49	0.27
	Objective value (million euros)	36.9	32.7	23.6
Instance D	Feasible status	feasible	feasible	infeasible at p15
	Computational time (s)	0.25	25.34	*
	Objective value (million euros)	63.2	55.6	*
Instance E	Feasible status	feasible	feasible	infeasible at p21
	Computational time (s)	17.10	1.75	*
	Objective value (million euros)	199.0	172.8	*

The table above illustrates that the one-stage stochastic model with the reduced scenario set $\overline{\mathcal{Z}}_{mean}$, which considers zero delay and average delay for each copper concentrate, successfully identifies feasible solutions for instances B, C, D, and E. This indicates that when the average delay is considered for each copper concentrate, still a feasible blending schedule can be found for these instances. For instance A this is not the case, denoted by the infeasibility of the solution. Conversely, the one-stage stochastic model with the reduced scenario set $\overline{\mathcal{Z}}_{worst}$, which considers the zero delay and the maximum delay for each copper concentrate, finds only a feasible solution for instance C, and infeasible solutions are obtained for instances A, B, D and E. This indicates that considering a worst-case delay for each copper concentrate is over-conservative because the model can not find a feasible solution for the entire scheduling horizon. Especially, when we additionally consider that the probability of a maximum delay for a copper concentrate is not major based on the distribution as described in Section 4.2.3, the model which is robust against the scenario that all copper concentrates are maximum delayed may be over-conservative. The solutions for instances B, D, and E however become infeasible only after period seven in the scheduling horizon. This offers the possibility to find a feasible blending schedule for the entire scheduling horizon when applying a re-optimization period of seven days. Overall, the infeasibilities from the above table denote that the SBCP is very sensitive to arrival time uncertainty, and not across all instances a feasible solution can be found when considering a maximum or mean delay of each copper concentrate. Ultimately, the formulated one-stage stochastic models are thus not sufficient in capturing the arrival time uncertainty and providing a feasible solution.

Remarkably, we observe in the solutions of the above one-stage stochastic model that from the generated scenarios, the largest included delay for each copper concentrate is prominent for feasibility. Essentially, this suggests that instead of employing the predefined scenario sets $\overline{\mathcal{Z}}_{mean}$ and $\overline{\mathcal{Z}}_{worst}$ for the one-stage stochastic models, we could utilize a single scenario where all copper concentrates experience either their mean or maximum delay, respectively, and still achieve identical results. This is noteworthy because it enhances computational efficiency. In addition, the results suggest that the sensitivity of the SBCP to arrival time uncertainty is instance-specific. Instance A specifically shows sensitivity to arrival time uncertainty indicated by the infeasibility of the solutions of both stochastic models. This instance has a lower number of copper concentrates expected over the scheduling horizon and less start inventory present in comparison with the other instances. We conclude that the sensitivity of the SBCP to arrival time uncertainty appears to be instance-specific and is influenced by factors such as the availability of start inventory, the number of expected copper concentrates, and the scheduling horizon's length.

The robust solutions of both one-stage models come at the cost of a lower objective value. Because the robust solution is feasible for the scenario that the copper concentrates are averagely delayed, or maximum delayed, respectively, the solution considers that copper concentrates are at a later period in the scheduling horizon available. Therefore, for the robust solutions at the beginning of the scheduling horizons, there is a reduced selection of (profitable) copper concentrates, leading to a lower objective value of the solution compared to the nominal solution. Because the one-stage model with the reduced scenario set $\overline{\mathcal{Z}}_{worst}$ is more conservative than the one-stage model with the reduced scenario set $\overline{\mathcal{Z}}_{mean}$ the corresponding objective value is lower. Because the one-stage stochastic models have one set of decision variables, and there is no uncertainty in the objective, the expected objective is the same for each scenario. The objective values however show a large decrease in objective value. This indicates that implementing a multistage model may be more suitable.

The optimization and performance results of the one-stage stochastic model with a scenario set $\overline{\mathcal{Z}}_{sampled}$ are presented in Appendix B.3. This reduced scenario set is generated by randomly sampling from the probability distribution representing the uncertain delay. We can draw similar conclusions from these results as the results drawn from the above one-stage stochastic models. Namely, in the scenario set the largest delay for an individual copper concentrate is most important, resulting effectively in that the model protects us from the scenario where each copper concentrate is delayed most, within the delays occurring in the sample. The model could only be evaluated within computationally tractable times for rather a small scenario set consisting of $N = 10$ scenarios. These performance results show that the SBCP reacts sensitively to arrival time uncertainty and the sensitivity is instance-specific. We conclude that the one-stage stochastic model with a scenario set $\overline{\mathcal{Z}}_{sampled}$ is insufficient in considering the arrival time uncertainty sufficiently.

6.5.2. Performance of one-stage stochastic arrival time model

Table 6.9 presents the simulation results for the one-stage stochastic model utilizing the reduced scenario trees $\overline{\mathcal{Z}}_{mean}$ and $\overline{\mathcal{Z}}_{worst}$, where the scenarios are generated by including a reduced number of delays. The model is evaluated with the simulation for uncertainty in the arrival time of a copper concentrate. In the simulation, a rolling horizon is applied with a re-optimization period of seven days.
The one-stage stochastic model, utilizing the reduced scenario set $\overline{\mathcal{Z}}_{worst}$, which includes scenarios reflecting the worst-case delay and no delay of a copper concentrate, could find solutions that remained feasible across the majority of the realizations of the arrival time uncertainty for instances B, C, and D, indicated by feasibility ratios ranging from (instance D, $N = 100$) to 100.0 (instance C). This indicates that the model is sufficient for most instances in providing a solution that remains feasible during re-optimization and captures the arrival time uncertainty sufficiently. However, it is important to note that the one-stage stochastic model with scenario tree $\overline{\mathcal{Z}}_{worst}$ was not able to find feasible solutions for most instances without re-optimization, as presented in Table 6.8 and therefore we suggested that the model is over-conservative. However, with the use of a re-optimization period of seven days during simulation, we observe that for instance B, C, and D, it is possible to find a feasible solution for the majority of the realizations of the arrival time uncertainty.

For instance A the solution is always infeasible, because the one-stage stochastic model finds a so-

Table 6.9: Performance of one-stage stochastic model and nominal model for simulated uncertainty in arrival time of a copper concentrate. For the one-stage stochastic model the reduced scenario trees $\overline{\mathcal{Z}}_{mean}$ and $\overline{\mathcal{Z}}_{worst}$, that are constructed by $\{d_1, d_2\} = \{0, d_{mean}\}$ and $\{d_1, d_2\} = \{0, d_{max}\}$, respectively, are implemented. A re-optimization period of seven days is applied. A star (*) denotes that the initial solution was infeasible for the first seven days. A double star (**) denotes that during re-optimization the solution could only find an infeasible solution for the next seven days. A triple star (***) denotes that the solution did not remain feasible with the realized parameters.

	Number of simulations	Performance measure	Nominal Model	OSM: $\overline{\mathcal{Z}} = \overline{\mathcal{Z}}_{mean}$	OSM: $\overline{\mathcal{Z}} = \overline{\mathcal{Z}}_{worst}$
Instance A	10	Feasibility ratio	0.0	** / ***	*
		Average objective ratio	***	** / ***	*
		Simulation time (s)	1.42	2.59	1.27
	100	Feasibility ratio	0.0	5.0	*
		Average objective ratio	*	96.0	*
		Simulation time (s)	5.58	28.85	18.02
Instance B	10	Feasibility ratio	0.0	** / ***	90.0
		Average objective ratio	***	** / ***	65.6
		Simulation time (s)	2.13	12.89	21.15
	100	Feasibility ratio	0.0	1.0	96.0
		Average objective ratio	***	83.0	65.6
		Simulation time (s)	15.10	130.35	195.80
Instance C	10	Feasibility ratio	0.0	10.0	100.0
		Average objective ratio	***	89.6	64.39
		Simulation time (s)	1.36	11.62	16.14
	100	Feasibility ratio	0.0	7.0	100.0
		Average objective ratio	*	89.6	65.73
		Simulation time (s)	13.25	18.29	141.91
Instance D	10	Feasibility ratio	0.0	30.0	60.0
		Average objective ratio	***	90.7	87.5
		Simulation time (s)	3.58	13.36	48.12
	100	Feasibility ratio	0.0	26.0	40.0
		Average objective ratio	*	90.8	87.0
		Simulation time (s)	285.88	130.32	446.72
Instance E	10	Feasibility ratio	**/ ***	**	**
		Average objective ratio	** / ***	**	**
		Simulation time (s)	392.68	946.63	1027.62

lution that becomes infeasible before the re-optimization period. For instance E the feasibility ratio is also not defined. The one-stage stochastic model finds a solution that becomes infeasible in period 21. We observe that with the use of re-optimization every seven days, the model still finds infeasible solutions somewhere during the scheduling horizon. In contrary, the one-stage stochastic model found a feasible solution for the entire scheduling horizon. This results in a feasibility ratio of 100.0 during simulation. This outcome aligns with expectations, considering that the scenario set $\overline{\mathcal{Z}}_{worst}$ includes the scenario with the worst-case delay of each copper concentrate and the probability distribution of the delay has strict bounds. Therefore, it is impossible that a realization of the uncertain arrival time of a copper concentrate is larger than the defined worst case highlighting the potential of this model.

Nevertheless, for the instances where the model found an infeasible solution, but infeasibility occurs after the first re-optimization period, this leaves room during re-optimization that the model does find a feasible solution for the next seven days based on the realization of the arrival time uncertainty, resulting ultimately in a feasible solution for the entire scheduling horizon. The results show that this is often the case for instance B (feasibility ratio 90.0 and 96.0) and also frequently the case for instance D (feasibility ratio of 60.0 and 40.0). For the instances where feasible solutions could be found in the simulation, the average objective ratio is significantly lower than 100.0 because the solution is conservative. Ultimately, because the one-stage stochastic model with scenario tree $\overline{\mathcal{Z}}_{worst}$ includes the worst-case delay of each copper concentrate when a feasible solution is found with the model, it remains feasible across all realizations of the arrival time uncertainty, resulting in absolute being robust against a significant profit reduction. However, due to its conservatism, it is also possible that the model can not find a feasible solution at all.

6.6. Multistage stochastic arrival time model

This section presents the results for the multistage stochastic model which considers the uncertainty in the arrival time of a copper concentrate. The reduced scenario trees $\overline{\mathcal{Z}}_{mean}$ and $\overline{\mathcal{Z}}_{worst}$ are applied. Additionally, the multistage nature of the problem is considered by introducing a new stage every seven days as described in Section 4.5.3. Section 6.6.1 presents the optimization results and Section 6.6.2 presents the simulation results.

6.6.1. Optimization results

Table 6.10 presents the optimization result of the multistage stochastic model, for which the scenario tree is constructed with two possible delays for each copper concentrate; $d_1 = 0$, representing zero delay, and d_2 is either the rounded mean of the underlying gamma distribution d_{mean} or the maximum possible delay of a copper concentrate d_{max}. These delays are associated with probabilities $p_1 = 0.56$ and $p_2 = 0.44$, respectively, obtained by dividing the probability space into two based on the mean. The multistage model defines a new stage every seven days, introducing new sets of decisions for different nodes in the scenario tree. This flexibility allows the model to adapt its decision variables based on the revealed uncertainty every seven days. We omit the results of instance E, due to memory constraints. The table illustrates that the one-stage stochastic model with the reduced scenario tree $\overline{\mathcal{Z}}_{worst}$ performs better than both the nominal model and the one-stage stochastic model with the reduced scenario tree $\overline{\mathcal{Z}}_{mean}$. The feasibility ratio for the nominal model is zero across all instances because the solution becomes immediately infeasible when one copper concentrate arrives later than the scheduled period for blending, indicating the sensitivity of the SBCP to arrival time uncertainty. While the one-stage stochastic model with the scenario tree $\overline{\mathcal{Z}}_{mean}$ finds feasible solutions for most instances in the optimization results, the simulation outcomes reveal its poor performance. The feasibility ratio never exceeds 30.0, indicating significant difficulty in finding a solution that remains feasible across realizations of the uncertain arrival time. For instances A and B with $N = 10$ specifically, the feasibility ratio does not exist because for half the realizations of the arrival time uncertainty the solution does not remain feasible (***), and for the other half the model could only find an infeasible solution during re-optimization (**). Although initially promising, it is evident that the reduced scenario set $\overline{\mathcal{Z}}_{mean}$ is inadequate for providing a robust solution capable of remaining feasible across various realizations of the arrival time uncertainty.

Table 6.10: Optimization results of the multistage stochastic model. The reduced scenario trees $\overline{\mathcal{Z}}_{mean}$ which is constructed by the branches $\{d_1, d_2\} = \{0, d_{mean}\}$ and $\overline{\mathcal{Z}}_{worst}$ which is constructed by the branches $\{d_1, d_2\} = \{0, d_{max}\}$ are implemented. Further, $\overline{\mathcal{Z}}_0$ denotes the scenario tree where each copper concentrate is considered on time. A star (*) denotes that the model is infeasible for the entire scheduling horizon, so the remaining output is irrelevant.

	Output	$\overline{\mathcal{Z}} = \overline{\mathcal{Z}}_0$ (deterministic)	$\overline{\mathcal{Z}} = \overline{\mathcal{Z}}_{mean}$	$\overline{\mathcal{Z}} = \overline{\mathcal{Z}}_{worst}$
Instance A	Feasibility status	feasible	infeasible at p9	infeasible at p6
	Computational time (s)	0.05	*	*
	Objective value (million euros)	9.5	*	*
Instance B	Feasibility status	feasible	feasible	infeasible at p15
	Computational time (s)	0.16	0.18	*
	Objective value (million euros)	17.5	14.2	*
Instance C	Feasibility status	feasible	feasible	feasible
	Computational time (s)	0.25	0.20	0.38
	Objective value (million euros)	36.9	32.7	26.9
Instance D	Feasibility status	feasible	feasible	infeasible at p15
	Computational time (s)	13.22	239.99	*
	Objective value (million euros)	63.2	55.6	*

The table illustrates that the multistage stochastic model that utilizes scenario tree $\overline{\mathcal{Z}}_{mean}$ finds a feasible solution for instances B, C, and D. For the scenario tree $\overline{\mathcal{Z}}_{worst}$ that includes scenarios with the worst-case delay of a copper concentrate a feasible solution is found for instance C. The solutions for the other instances become infeasible after multiple periods. These results indicate again the strong sensitivity of the feasibility of the solution of the SBCP to the delay of copper concentrates. We conclude that for most instances a feasible solution can be found when an average delay is considered for each copper concentrate, however, considering the worst-case delays is too conservative to find a

feasible solution directly for the entire scheduling horizon.

We observe that the feasibility results of the multistage stochastic model are identical to the optimization results of the one-stage stochastic models with the same defined scenario trees as presented in Table 6.8. This is because we observe that ultimately in both stochastic models, the solution should be feasible for the same scenario set, including both the same worst-case scenario. Because in the SBCP it is not possible to purchase extra concentrate during the scheduling horizon, we conclude that the feasibility of the solution for an instance over the entire scheduling horizon is similar for the one-stage and multistage model with the same defined scenario tree. However, the objective value generated by the first seven days from the solution of the one-stage model and the multistage model, corresponding with the first stage of the multistage model, is different, indicating that the solution of the first seven days of both models is different. Because the multistage model results in a solution for the first seven days generating a higher profit, the solution is less conservative in the first seven days compared to the solution obtained with the one-stage model. This can be explained for example by the multistage model scheduling more profitable inventory concentrates earlier in the scheduling horizon, than the one-stage stochastic model.

Notably, the expected objective value of the multistage stochastic is higher in comparison with the one-stage model. This is an advantage of the multistage model, it provides a more realistic expected objective because it considers different solutions for each scenario and takes into account the probability of each scenario instead of generating one fixed solution for the entire scheduling horizon. However, the increase in expected objective when considering scenario tree $\overline{\mathcal{Z}}_{worst}$ is not very large in comparison with the one-stage model utilizing the same scenario tree. When even a more realistic expected objective value is desired to be obtained, more scenarios should be included in the scenario tree, improving the representation of the probability space. The computation times of the multistage stochastic model are not significantly larger in comparison with the other optimization models, however, they do increase significantly for the number of scenarios included.

6.6.2. Performance of multistage stochastic model

Table 6.11 presents the results of the performance of the multistage stochastic model in comparison with the nominal model for simulated uncertainty in the arrival time of a copper concentrate. The models utilizing the scenario trees $\overline{\mathcal{Z}}_{mean}$ and $\overline{\mathcal{Z}}_{worst}$ are evaluated. A rolling horizon is applied with a re-optimization period of seven days.

The table illustrates that in comparison with the nominal model, the multistage stochastic model performs better for arrival time uncertainty. The multistage model with scenario tree $\overline{\mathcal{Z}}_{mean}$ for instances B and C finds for the majority of the realizations a feasible solution, indicated by feasibility ratios between 50.0 (instance B, $N = 10$) and 64.0 (instance B, $N = 100$). For the other realizations, the solution did not remain feasible. This denotes that the reduced scenario tree $\overline{\mathcal{Z}}_{mean}$ does not span the whole probability space of the arrival time uncertainty, resulting in solutions that do not remain feasible across all realizations of the uncertain arrival time. In addition, for instance A and D, the feasibility ratio is low, varying between 0.0 (instance D) and 5.0 (instance A, $N = 100$). This leads to the conclusion that the multistage stochastic model with the reduced scenario tree $\overline{\mathcal{Z}}_{mean}$ is not sufficient to capture the arrival time uncertainty and provide a robust solution that remains feasible for the arrival time uncertainty realizations.

The multistage model with scenario tree $\overline{\mathcal{Z}}_{worst}$ has for instances B, C, and D feasibility ratios varying from 50.0 (instance B, $N = 10$) to 100.0 (instance C, $N = 100$). This indicates that the multistage model considering the worst-case delay of a copper concentrate can provide a solution that remains feasible in the majority of the realizations of the arrival time uncertainty. However, the model finds only infeasible solutions for the next seven days somewhere during re-optimization for the other realizations of the uncertainty. In addition, the model immediately finds only infeasible solutions for instance A because the solution became already infeasible before the first re-optimization period. These results indicate that the solution may be (over-)conservative, however when with the use of re-optimization of the model for the realized parameters a feasible solution is found, even worst-case delays of a copper concentrate remain feasible.

Table 6.11: Performance of the multistage stochastic model and nominal model for simulated arrival time uncertainty. A re-optimization of 7 days is applied. The model utilizes the reduced scenario tree $\overline{\mathcal{Z}}_{mean}$ or $\overline{\mathcal{Z}}_{worst}$, that are constructed by $\{d_1, d_2\} = \{0, d_{mean}\}$ and $\{d_1, d_2\} = \{0, d_{max}\}$, respectively. A star (*) denotes here that the initial solution is not feasible for the first seven days. A double star (**) denotes that during re-optimization the model could only find an infeasible solution for the next seven days. A triple star (***) denotes that the solution does not remain feasible for the realized parameters.

	Number of simulations	Performance measures	Nominal Model	MSM: $\overline{\mathcal{Z}} = \overline{\mathcal{Z}}_{mean}$	MSM: $\overline{\mathcal{Z}} = \overline{\mathcal{Z}}_{worst}$
Instance A	10	Feasibility ratio	0.0	0.0	*
		Average objective ratio	***	***	*
		Simulation time (s)	1.42	1.07	*
	100	Feasibility ratio	0.0	5.0	*
		Average objective ratio	***	96.0	*
		Simulation time (S)	5.58	10.59	*
Instance B	10	Feasibility ratio	0.0	50.0	50.0
		Average objective ratio	***	81.2	65.8
		Simulation time (s)	2.13	19.82	20.99
	100	Feasibility ratio	0.0	64.0	77.0
		Average objective ratio	***	81.3	66.0
		Simulation time (s)	15.10	179.98	175.03
Instance C	10	Feasibility ratio	0.0	60.0	100.0
		Average objective ratio	****	89.5	67.1
		Simulation time (s)	1.36	16.51	17.12
	100	Feasibility ratio	0.0	54.0	100.0
		Average objective ratio	***	89.4	68.7
		Simulation time (s)	13.25	157.11	153.62
Instance D	10	Feasibility ratio	0.0	0.0	80.0
		Average objective ratio	***	***	83.9
		Simulation time (s)	3.58	3121.03	2535.98

We observe that the expected objective of the multistage solutions is slightly higher than the objective obtained by the one-stage solutions. However, the feasibility ratios of the multistage stochastic models are different than the feasibility ratios obtained by the one-stage stochastic models. For the scenario tree $\overline{\mathcal{Z}}_{worst}$ the feasibility ratio of instance B is lower, being 50.0 ($N = 10$) and 77.0 ($N = 100$), instead of 90.0 ($N = 10$) and 96.0 ($N = 100$). For instance D, we see a contrary relation, the multistage model results in higher feasibility ratio of 80.0 compared to the feasibility ratio of the one-stage model which is 60.0. We expect that these differences can be explained by the differences in solutions the models obtained for the first seven days. The one-stage model provided a more conservative result for these first seven days, denoted by a slightly lower objective value generated by the first seven days solution, compared to the solution obtained for the first seven days with the multistage model. The results illustrate that the more conservative solution at the beginning of the scheduling horizon for some instances leads to a better performance and for instances leads to a lower performance, compared to the more risky solution obtained by the multistage model.

6.7. Robust supply uncertainty model

The refinery aims to find a blending schedule that is robust against all three types of uncertainty; mass uncertainty, mass fraction of elements uncertainty, and arrival time uncertainty. The three uncertainties together are denoted as supply uncertainty. In an attempt to find a solution that is robust against supply uncertainty the created models for each type of uncertainty are combined. First, the robust mass model and robust mass fraction model are combined in a model denoted as the double robust model (DRM) to study how sufficient the model is in capturing both mass uncertainty and mass fraction uncertainty and provide a robust solution that remains feasible for realizations of mass uncertainty and mass fraction uncertainty simultaneously. Afterward, the robust mass model, robust mass fraction model, and multistage stochastic arrival time model are implemented together in a model denoted as the robust supply model (RSM) in an attempt to create a model that provides a solution that is robust against supply uncertainty. Table 6.7.1 presents the optimization results of the models and Section 6.7.2 presents the performance of the models under supply uncertainty.

6.7.1. Optimization results

This section presents the optimization results of the above-defined combinations of optimization models to consider multiple types of supply uncertainty simultaneously. To analyze these results properly, Table 6.12 provides an overview of the optimization results of all developed optimization models considering uncertainty in this study. The table presents the feasibility status, the computation time, and the objective value across the instances. We excluded the results for instance E due to extended computation times. For the model parameters, we implement the values as motivated in previous sections. Next, we provide an overview of the presented models with specified model parameters.

First, the table presents the results for the robust mass model (RMM), utilizing a box uncertainty set with normalized perturbation factor $\lambda = 0.1$ for the mass parameter. Then the table shows the results for the robust mass fraction model (RMFM). The model employs a budgeted uncertainty for all the elements with the normalized perturbation factor $\lambda_2 = \lambda_7 = 0.001$ for the budget uncertainty set for elements 2 and 7 and normalized perturbation factor $\lambda = 0.01$ for the budgeted uncertainty set applied to the other elements. The implemented budget parameter Γ is instance specific and is set to $\Gamma = CC$ for instance A, and is set to $\Gamma = \frac{1}{2}CC$ for instance B till instance E. Next, the table presents the results of the double robust model (DRM) combining the previously specified robust mass model and robust mass fraction model. Following, the table presents the results for the multistage stochastic model (MSM), employing a new defined stage every seven days. The scenario tree $\overline{\mathcal{Z}}_{worst}$ is implemented, which is constructed as the scenario set with two branches, zero delay and maximum delay, for each copper concentrate with corresponding probabilities $p_1 = 0.56$ and $p_2 = 0.44$. Afterward, the table presents the results for the model where the multistage stochastic model is added to the double robust model denotes as the robust supply model (RSM).

Table 6.12: Optimization results models of the defined optimization models for the SBCP under supply uncertainty. Results are presented for the robust mass model (RMM), the robust mass fraction model (RMFM), the multistage stochastic arrival time model (MSM), the double robust model (DRM), and the multistage robust supply model (RSM)

	Output	RMM	RMFM	DRM	MSM	RSM
Instance A	Feasibility status	feasible	feasible	feasible	infeasible at p6	infeasible at p6
	Computational time (s)	0.26	0.16	0.24	*	*
	Objective value (million euros)	9.4	9.3	9.2	*	*
Instance B	Feasibility status	feasible	feasible	feasible	infeasible at p15	infeasible at p11
	Computational time (s)	0.31	1.05	1.24	*	*
	Objective value (million euros)	17.5	17.4	17.3	*	*
Instance C	Feasibility status	feasible	feasible	feasible	feasible	feasible
	Computational time (s)	0.29	0.79	0.60	0.38	7.68
	Objective value (million euros)	35.8	36.7	35.6	26.9	25.9
Instance D	Feasibility status	feasible	feasible	feasible	infeasible at p17	infeasible at p5
	Computational time (s)	0.25	10.43	5.357	*	*
	Objective value (million euros)	60.0	62.9	59.5	*	*

The optimization results of the robust mass model, robust mass fraction model, and stochastic arrival time models have been previously discussed in this chapter and will not be discussed in detail here. However, these results are compared to the optimization results of the defined combinations of the models. The double robust model (DRM) finds feasible solutions for all four instances. The optimal objective value of the DRM is slightly lower than the objective value found by the RMM or the RMFM. This is expected because the model is designed robust against two types of uncertainty instead of one and therefore is more conservative than the individual models. The robust supply model (RSM) finds only a feasible solution for instance C. This is expected because it combines the three optimization models and the MSM also only found feasible solutions for instance C. Notably, the solutions for instance A and instance D become infeasible before a potential re-optimization period of seven days, indicating that these solutions will stay infeasible during simulation when re-optimization is applied. Possibly for instance B a feasible solution can be found for realized parameters when a re-optimization period of seven days is applied because the solution becomes infeasible after period 7. The objective value of the RSM is slightly lower than the solution of the MSM and the instances become earlier in the scheduling horizon infeasible. Essentially, the RSM is more conservative than the MSM because besides considering arrival time uncertainty, it also captures the mass and mass fraction uncertainty.

6.7.2. Performance of robust supply model

This section describes the performance of the double robust model and robust supply model. Appendix B.4 presents the simulation results of the double robust model. The model has high feasibility ratios, varying between 80.0 and 100.0, when evaluated for combined mass and mass fraction uncertainty. This is as expected, because both defined robust models performed well in providing a robust solution that remained feasible for realizations of the uncertainty they were designed for. The objective ratio of the double robust model is slightly lower than the individual models because it is more conservative. Essentially, the model provides a solution with high feasibility ratios for combined mass and mass fraction uncertainty, under a small profit reduction, indicated by an average objective ratio of 96.9 or higher. Next, the performance of the robust supply model is evaluated with a simulation where all three types of supply uncertainty are simulated simultaneously. Table 6.13 presents these results. To compare the performance of the nominal model and the performance of the double robust model (DRM) under supply uncertainty are also presented. The results of instances D and E are excluded due to extended computation times.

Table 6.13: Performance of robust supply model (RSM), nominal model (NM), multistage stochastic model (MSM), and double robust model (DRM) for simulated supply uncertainty. The RSM is a combination of the robust mass model, robust mass fraction model, and multistage stochastic model. The double robust model combines the robust mass model and the robust mass fraction model. The performance results are presented for instance A till instance C.

	Number of simulations	Performance measures	Nominal Model	DRM	MSM	RSM
Instance A	10	Feasibility ratio	0.0	0.0	*	*
		Average objective ratio	***	***	*	*
		Simulation time (s)	0.83	1.14	1.15	2.38
	100	Feasibility ratio	0.0	** / ***	*	*
		Average objective ratio	***	** / ***	*	*
		Simulation time (s)	6.02	7.37	18.21	17.18
Instance B	10	Feasibility ratio	0.0	0.0	50.0	50.0
		Average objective ratio	***	***	66.2	65.2
		Simulation time (s)	2.08	12.89	28.34	339.46
	100	Feasibility ratio	0.0	0.0	77.0	77.0
		Average objective ratio	***	***	66.1	65.2
		Simulation time (s)	14.11	86.90	197.12	3680.05
Instance C	10	Feasibility ratio	0.0	0.0	100.0	100.0
		Average objective ratio	***	***	67.2	64.0
		Simulation time (s)	1.52	7.80	19.23	125.56
	100	Feasibility ratio	0.0	0.0	100.0	98.0
		Average objective ratio	***	***	68.8	66.1
		Simulation time (s)	11.31	88.16	161.42	1178.41

The above table illustrates that the feasibility ratio of the nominal model under supply uncertainty is zero across all instances because no solution remains feasible for the realized uncertain parameters. As earlier stated, this is primarily due to the sensitivity of the SBCP to arrival time uncertainty. The double robust model (DRM) performs also poorly when evaluated for supply uncertainty indicated by feasibility ratios of zero. In addition, the performance of the DRM is evaluated for a combination of mass and mass fraction uncertainty as presented in Appendix B.4. Contrarily, these results illustrate a high performance of the DRM indicated by feasibility ratios ranging from 80.0 to 100.0 across the instances combined with a minor profit reduction. We conclude that the DRM captures well the mass and mass fraction, but performs poorly evaluated for supply uncertainty because the model fails in capturing the arrival time uncertainty. The solution of the DRM does not result in a robust solution that remains feasible across realizations of the supply uncertainty.

The table presents the performance of the multistage stochastic model under supply uncertainty. Important for the MSM was that for most instances the model could not find a feasible solution for the entire scheduling horizon, however for some realizations with the use of re-optimization still a feasible blending schedule is obtained at the end of the simulation. We observe that the feasibility ratios are identical to the feasibility ratios obtained when evaluated for only arrival time uncertainty. The results show that when the MSM can find a feasible solution with re-optimization every seven days, the model is also effective against mass and mass fraction uncertainty, because there is no decrease in feasibility ratio.

The robust supply model (RSM) illustrates similar results for the feasibility ratios as obtained by the MSM. The uncertainty in arrival time is leading for the performance of the model. For instance A only infeasible solutions could be found because the solution becomes infeasible before the first re-optimization period. This instance is small and has a lower number of expected copper concentrates and start-inventory present. For instance B and instance C the robust supply model finds feasible solutions. For instance B the model finds for the majority of the realizations a feasible solution in the simulation indicated by feasibility ratios of 50.0 and 77.0. The model finds an infeasible solution for the entire scheduling horizon, however, with the use of re-optimization for the majority of the realizations of supply uncertainty a feasible solution is obtained. For instance C the RSM provides solution that effectively capture all three components of the supply uncertainty. For instance C the multistage stochastic model was able to find a feasible solution. Due to its conservatism of the MSM, by including the maximum delay of each copper concentrate, the RSM is robust against all realizations of the arrival time uncertainty. The feasibility ratio for ($N = 100$) is lower than 100, because for some realizations including mass and mass fraction uncertainty, the RSM that combines the three previous models was too conservative and could only find an infeasible solution. We observe that the robust solution is obtained against a profit decrease, denoted by average objective ratios between 64.0 (instance C, $N = 10$) and 66.1 (instance C, $N = 100$).

Ultimately, we conclude that capturing the arrival time uncertainty is the primarily bottleneck to find a solution that remains feasible across all the supply uncertainty realizations. Notably, with the created models a large improvement is made in feasibility of the solution against supply uncertainty compared to the performance of the nominal model under supply uncertainty. The feasibility of the SBCP is very sensitive to supply uncertainty. With the created models a solution is obtained which is robust against uncertainties in the mass and mass fraction and has improved a lot for the robustness against arrival time uncertainty.

7
Conclusion

In this research, the SBCP under supply uncertainty has been studied. This section addresses the formulated sub-questions and consequently formulates an answer to the main research question.

Research question (a)
How can the SBCP be modeled as a linear nominal optimization problem?

The SBCP is a problem that in an industrial context increases quickly in size. It consists of many operational and logistic constraints, resulting in the need to introduce binary variables into mathematical optimization formulation. Additionally, industrial refineries often have multiple blender units working simultaneously on the site, imposing the need for nonlinear blending constraints. This is because in such a large blending network, there are multiple outgoing flows after a blender, and it is essential to ensure that the composition of each outgoing flow is equal. Optimization models that try to capture the whole SBCP in detail result in comprehensive nonlinear mixed integer models where approximation methods are needed to solve the model in reasonable computation time.

As opposed to formulating a comprehensive model that models every part of the SBCP in detail we made an effort to capture the essence of the SBCP with a nominal linear optimization model. This model allows us to study the effects of supply uncertainty on the SBCP, due to reasonable computational effort and easy interpretation of the model, and additionally can easily be extended by optimization under uncertainty methods. We base the created model for the SBCP on the discrete-time MILP-NLP formulation as presented in Song et al., 2018. To be able to describe the SBCP with a linear model, the following two simplifications have been made. $i)$ It is assumed that there is only one blender and one pre-blender at the site. There are thus no multiple outgoing flows in the blending network, making it possible to omit the nonlinear constraints. $ii)$ Operational and logistics constraints are omitted from the formulation and are addressed through the preprocessing of data to incorporate time delays caused by operations. Furthermore, the model is formulated with a discrete-time formulation to consider that not at every moment in time new blends can be made. By following the above-designed blending network, the SBCP can be modeled linearly. The model includes element constraints, flow (mass-balance) constraints, inventory constraints, smelter capacity constraints, and the objective function that maximizes the profit earned by processing concentrates.

Research question (b)
Which optimization under uncertainty methods can best be applied to consider supply uncertainty for the SBCP? What are the drawbacks and benefits of the different optimization methods?

The supply uncertainty consists of three sources, uncertainty in the mass of a copper concentrate, the uncertainty in the mass fraction of elements of a copper concentrate, and the uncertainty of the arrival time of a copper concentrate. The first two sources of uncertainty have a continuous nature and the latter has a discrete nature. This is an important difference, making other optimization under uncertainty methods suitable.

The refinery prioritizes the feasibility of the SBCP, indicating that the smelter can work continuously throughout the entire scheduling horizon. Furthermore, the mass uncertainty and the mass fraction uncertainty can be described using a connected set. This leads to the conclusion that robust optimization is a suitable method to model the mass and mass fraction uncertainty because it is a method that aligns very well with these characteristics. An advantage of robust optimization is that the probability distribution of the uncertainty does not need to be known and thus can be applied to any generally distributed uncertainty. First, a budgeted uncertainty set is implemented for the uncertain mass fraction parameter of each element. The main reason is that the budgeted uncertainty set reduces the volume of the uncertainty set in comparison with the box, but still is a polyhedron, resulting in a robust linear programming problem, which is a main advantage due to computational efficiency. Secondly, following the same reasoning, a budgeted uncertainty set is chosen to represent the uncertain mass parameter, however, due to the constraints in which the uncertain mass parameter appears, it becomes apparent that the budgeted uncertainty set becomes redundant and can be effectively described using a box uncertainty set for this formulation of the SBCP. So, a box uncertainty set is implemented for the uncertain mass parameter of each expected copper concentrate.

To represent the arrival time uncertainty robust optimization is a less suitable approach, mainly because we expect that by only considering the worst-case delay of each copper concentrate, the solution becomes (over-)conservative. In addition, the arrival time uncertainty can not be described with a connected set. A natural approach to describe the discrete uncertainty is as a finite set of scenarios $\mathcal{Z}$ where each scenario has a corresponding probability. Therefore a stochastic approach utilizing the representation with a finite number of scenarios is a very suitable method to consider the arrival time uncertainty. Stochastic optimization optimizes the expected objective, by considering the probability of uncertainty realizations. Considering the expected objective aligns well with the fact that for the refinery the SBCP is a repetitive problem. In addition, an advantage of stochastic optimization is that it considers the available probability information of the uncertainty. Therefore, the arrival time uncertainty is considered by using stochastic optimization.

We implement a one-stage formulation in the robust models considering mass and mass fraction uncertainty. We aim to avoid unnecessary implementation of multi-stage formulations which is accompanied by more computational effort by utilizing the simpler approach until it becomes necessary to employ a more comprehensive multistage formulation, for instance when the one-stage formulation becomes infeasible. For the stochastic model, we implemented both a one-stage and multi-stage formulation. The models provided different solutions for the first seven days, where the solution by the multistage model was less conservative.

The above-described approaches are suitable to describe the supply uncertainty as motivated above, however, the selection of the parameters of the uncertainty sets and the selection of the scenario set are very important for the performance of the models. The models were evaluated for five instances named A through E. The most fitting parameters for these instances are now discussed. The optimization results illustrate that for the robust mass model, utilizing the box uncertainty set a normalized perturbation factor $\lambda = 0.1$, which denotes the maximum perturbation of the uncertain parameter described as a percentage of the nominal value, results in feasible solutions across all instances. The performance of the robust mass model indicates that this defined box uncertainty is sufficient to capture the majority of the mass uncertainty. If the refinery desires to consider larger perturbations in the robust mass model, a multistage model should be considered.

The optimization results for the robust mass fraction model illustrate that a budgeted uncertainty set with $\lambda_2 = \lambda_7 = 0.001$ and $\lambda_k = 0.01$ for the remaining elements results in feasible solutions across all instances. Notably, the mass fraction parameters for element 2 and element 7 are more sensitive to mass fraction uncertainty than the other elements, due to upper and lower bound constraints on the ratio of these two elements. The use of these budgeted uncertainty sets for the elements, results in a robust mass fraction model that provides robust solutions that remain feasible across realizations of mass fraction uncertainty for the elements. However, additionally, the choice of the budget parameter is important and instance-specific. For instance A a box uncertainty set resulted in a model that performed sufficiently. Where for the larger instances the volume of the uncertainty set can be reduced

by implementing a budgeted uncertainty with a budget parameter of $\Gamma = \frac{1}{2}CC$. This results in a robust mass fraction model that sufficiently captures the mass fraction uncertainty.

For the stochastic model, we implemented a reduced scenario set. Namely, when for the SBCP all delays are considered for each copper concentrate, this results quickly in a very large scenario tree, resulting in a computationally hard model to solve. Therefore, for each copper concentrate only the zero delay and the mean delay, or the zero delay and the maximum delay, are considered. In this way, an approximation of the original problem is solved. The optimization results show that considering the mean delay for each copper concentrate, this results in feasible solutions, however, considering the worst-case delay for each copper concentrate, this results in finding infeasible solutions for the entire scheduling horizon for most instances, indicating that the model is over-conservative. Nevertheless, the simulation results illustrate that including maximum delays of copper concentrates results in higher feasibility ratios than including the mean delay. Considering the worst-case of a copper concentrate is thus more sufficient to create a solution that remains feasible for all realizations of the arrival time uncertainty. The results suggest however that there is still room for improvement in the representation of the uncertain arrival time in the optimization model for the SBCP. Ultimately, to consider supply uncertainty for the SBCP in the optimization model, the above three optimization models are combined. This model is denoted as the robust supply model.

Research question (c)
How does the SBCP react to supply uncertainty? How can we quantify the risks associated with different uncertainty types, and what is the quantified risk of the infeasibility of the nominal solution due to supply uncertainty for the SBCP?

An optimal solution to the SBCP is a feasible schedule that describes which blend should be created at which period to earn maximum profit over a certain scheduling horizon, also denoted as an optimal blending schedule. We quantify the risks associated with the different uncertainty types, by simulating N random generated realizations of the studied uncertainty type. To evaluate if the obtained optimal solution of the model remains feasible for the realized uncertain parameters a rolling horizon is applied with a re-optimization period of seven days. Afterward, the feasibility ratio and average objective ratio are calculated as performance measures. The risk of infeasibility of the nominal solution due to each type of supply uncertainty is presented in Table 6.2 in Chapter 6. The optimal solution of the nominal model for the SBCP becomes infeasible for simulated mass uncertainty in the minority of the realizations. The feasibility ratio ranges from 100 (instance B) to 30 (instance E). The feasibility ratio decreases when the scheduling horizon grows. We conclude that in general, the nominal model can handle to some extent uncertainty in the mass of copper concentrates because having a larger mass than expected is not a problem for feasibility when the capacity constraints are not binding, and a lower amount of copper concentrate only results in infeasibility when the copper concentrate is used before the solution is re-optimized or there is not enough copper concentrate available at the site that meets the smelter throughput and element constraints. Concluding, the SBCP is moderately sensitive to mass uncertainty of copper concentrates, increasing by an increasing scheduling horizon.

We observe that the SBCP is sensitive to mass fraction uncertainty in the elements with feasibility ratios ranging from 26.0 (instance A, $N = 100$) to 0.0 (instances C, D, E). This is due to the strict upper bound constraints for the mass fraction of elements in the final flow. In addition, for the larger instances, interdependency constraints on the ratios of elements in the final flow are required for the SBCP. When the actual mass fraction deviates, both higher and lower, this can quickly result in exceeding these element constraints, which results in an infeasible solution. Specifically, the SBCP reacts very sensitively to uncertainty in the mass fractions of element 2 and element 7. Furthermore, we conclude that the SBCP is very sensitive to arrival time uncertainty. The solution of the nominal model does not remain feasible for any of the arrival time uncertainty realizations indicated by feasibility ratios of zero across all instances. This is because when one copper concentrate arrives later than expected but is used in the current re-optimization period, the solution becomes infeasible immediately. The feasibility of the nominal solution to the SBCP is thus very sensitive to arrival time uncertainty.

For general supply uncertainty, where the above uncertainties are combined, the risk of infeasibility of

the nominal solution is 100 percent, denoted by the feasibility ratios of zero for all instances. This is primarily due to the mass fraction uncertainty and arrival time uncertainty for which the SBCP is very sensitive. We conclude that the feasibility of the nominal solutions to the SBCP is very sensitive to supply uncertainty.

Research question (d)
We call a solution to the SBCP obtained via optimization under uncertainty a robust solution. The final sub-question is, what is the quantified risk of the infeasibility of the robust solution due to supply uncertainty for the SBCP? How much has the performance improved in comparison with the nominal solution?

The performance of each designed optimization under uncertainty model is evaluated with a simulation that generates N realizations of the corresponding uncertainty type. The performances of the designed optimization models are much better than the performance of the nominal model. However, they still are not 100 percent robust against supply uncertainty, denoting that the optimal blending schedule should remain feasible across all realizations of the supply uncertainty. The feasibility ratios of the robust mass model are 100.0, 100.0, 97.5, 100.0, and 100.0 for instances A through D with $N = 1000$, and instance E with $N = 100$, respectively. These feasibility ratios have either remained the same or increased compared to the nominal model, which has feasibility ratios of 94.7, 100.0, 70.3, 78.3, and 30.0 for instances A through E, respectively. The risk of infeasibility due to mass uncertainty is thus small with the robust solution obtained from the robust mass model. The model effectively captures mass uncertainty and, with weekly re-optimization, can effectively adapt to changes in the mass of copper concentrates. Overall, it can be concluded that the feasibility ratio of the robust mass model is high, nearly reaching 100 for all instances at the cost of minor profit reduction.

The feasibility ratios of the solution of the robust mass fraction model are also increased compared to those of the nominal model. The feasibility ratios of the nominal model for mass fraction uncertainty are low, with feasibility ratios of 20.0, 10.0, 0.0, 0.0, and 0.0 for instances A through E, respectively. The feasibility ratios of the designed robust mass fraction models are 96.3 (instance A, $\Gamma = CC$, $N = 1000$), 94.7, 81.5, 86.0 (instances B, C, D, $\Gamma = \frac{1}{2}CC, N = 1000$), and 80.0 (instance E, $N = 10$). This indicates that the provided robust solution is more feasible against realizations of mass fraction uncertainty. However, as the scheduling horizon increases, there is a higher probability that at some point in the scheduling horizon, the mass fractions of the copper concentrates deviate too much, resulting in an infeasible solution. This suggests that the defined budgeted uncertainty sets do not completely cover the probability space of mass fraction uncertainty. The robust model results in a minor profit reduction.

The feasibility of the nominal solution for the SBCP reacted very sensitively to arrival time uncertainty, resulting in feasibility ratios of zero across all instances. The feasibility ratios are increased for the multistage stochastic arrival time model with scenario tree $\overline{\mathcal{Z}}_{worst}$. The feasibility ratio of instance A is zero because the solution becomes infeasible before the re-optimization period; however, feasibility ratios of 77.0, 98.0, and 80.0 are obtained for instances B through D, respectively, with $N = 100$. The multistage stochastic model is conservative, resulting that for not all realizations with the use of re-optimization feasible solutions can be found. However, when a feasible solution is found it is robust against worst-case delays of the expected copper concentrates. The conservative solution results in significant profit reduction. The SBCP still experiences a risk of infeasibility due to arrival time uncertainty; however, the risk is significantly decreased compared to the performance of the nominal model.

The quantified risk of the infeasibility of the robust solution for all supply uncertainty is obtained by combining the three above models. The feasibility ratios are similar to the feasibility ratios obtained by the multistage stochastic model evaluated only on arrival time uncertainty. This indicates that we can create solutions that remain robust against realizations of the mass and mass fraction uncertainty, by either using the double robust model or considering that all copper concentrates experience their maximum delay, as in the multistage stochastic model. Concluding, the quantified risk of the infeasibility obtained by the robust supply model is very instance dependent. The robust supply model finds often infeasible solutions because including the worst-case delay for each copper concentrate is over-conservative. However, the robust supply model illustrates that with the use of optimization under uncertainty meth-

ods the mass and mass fraction uncertainty can be effectively captured and the risk of infeasibility due to these uncertainties is decreased significantly. Capturing the complete arrival time uncertainty and creating a model that finds feasible solutions for the entire scheduling proved to be more difficult. However, when a feasible solution is obtained it shows promising effects for the robustness of the solution across realizations of the supply uncertainty.

Main research question

" What is the influence of supply uncertainty on the feasibility of the SBCP and how can we find a robust solution to the SBCP, indicating a feasible blending schedule for the entire scheduling horizon after the uncertainty realization, with the use of optimization for a mid-term scheduling time horizon?"

Due to the supply uncertainty, the nominal solution to the SBCP becomes infeasible across all uncertainty realizations even when a re-optimization period of the model of seven days is applied. Primarily, mass fraction uncertainty and arrival time uncertainty have the largest negative impact on the feasibility of the solution. The SBCP has strict elemental and smelter throughput constraints, which makes it a difficult problem to solve, in particular under supply uncertainty. The feasibility of the SBCP is thus very sensitive to supply uncertainty. Currently, many last-minute adjustments are made to obtain feasible blends that can be fed into the smelter to let the smelter continuously work to avoid the interruptions costs of a million euros per day the smelter does not work.

An effort is made to create a robust blending schedule that remains feasible across different realizations of the supply uncertainty can by considering the supply uncertainty directly in the optimization model for the SBCP. The defined optimization model can be applied to any general probability distribution. We observed that mass uncertainty can be sufficiently modeled with the use of a box uncertainty set with a normalized perturbation factor of $\lambda = 0.1$. This results in solutions with a feasibility ratio of 100, indicating that the solution remains feasible for all the simulated realizations of the mass uncertainty with a re-optimization period of seven days. The model captures thus mass uncertainty effectively against a minor profit reduction. The mass fraction uncertainty for an element can be sufficiently modeled with the use of a budgeted uncertainty set. The normalized perturbation factors $\lambda = 0.001$ for element 2 and element 7 and $\lambda = 0.01$ for the other elements are chosen. The SBCP reacts very sensitively to mass fraction uncertainty, especially for the uncertainty in the mass fraction of element 2 and element 7, and therefore the included budgeted uncertainty sets can not be very large. The robust mass fraction model provides feasibility ratios ranging from 70 to 100, indicating that they effectively capture mass fraction uncertainty, however less efficient for larger scheduling horizons. The arrival time uncertainty is modeled with the use of a multistage stochastic model. However, the lower average objective ratio may indicate that the current scenario tree considering no delay or the maximum delay for each copper concentrate does not span the whole probability space for the arrival time uncertainty. The multistage stochastic model with the scenario tree defined by $\overline{\mathcal{Z}}_{worst}$ provides feasibility ratios between 50 percent and 100 percent, for the instances where a feasible solution could be found with the model. Considering the worst-case delay for each copper concentrate results thus in a solution that remains feasible during arrival time uncertainty, however, is denoted as over-conservative, because for most instances only infeasible solutions can be obtained with the model.

The models combined result in a robust supply optimization model which provides results of 50 percent feasibility ratio to 100 percent, dependent on the SBCP instance. In comparison with the performance of the nominal model, an increase in feasibility ratio is obtained by the robust supply model performances has increased. The model has difficulty in capturing effectively the arrival time uncertainty, because the conservative model leads not to feasible solutions for each instance. However, when a feasible solution is found it will remain feasible across all realizations of arrival time uncertainty. The conservative model leads to a significant decrease in profit. The double robust model effectively captures the mass uncertainty and the mass fraction uncertainty and finds feasible solutions that remain feasible across most realizations of these uncertainties. The feasibility ratio is thus increased with the use of the robust supply model. Especially, when the fee for downtime of the smelter is considered, the use of the robust solutions provided by the robust supply model will be profitable for the refinery. The results illustrate that using robust blending schedules that consider supply uncertainty improves the feasibility ratios of the solution.

8

Discussion

While this study contributes significantly to the literature on the optimization of the SBCP, particularly in the context of supply uncertainty, it is essential to acknowledge its inherent limitations. Section 8.1 describes these limitations. Furthermore, Section 8.2 provides recommendations for further research.

8.1. Limitations

The linear nominal model developed serves as a foundational framework for understanding the refinery blending operations. However, its simplifications are notable, designed to render it a quickly solvable linear model. While these simplifications aid in comprehending the impact of supply uncertainty on the SBCP and lay the groundwork for implementing optimization under uncertainty methods, they introduce several limitations. Firstly, the nominal model overlooks detailed operational constraints. Therefore, any solution derived from it must align with additional operational constraints before implementation. Moreover, the current discrete-time model assumes daily periods for blending operations. However, in reality, operational shifts are often changed at multiple periods in a day. Therefore, the possibility of changing a blend during the day is overlooked. Furthermore, the nominal model assumes a singular outgoing flow, utilizing a blending network consisting of one pre-blender and one blender because in this way the nonlinear constraints needed to ensure identical concentrations of multiple outgoing flows can be omitted. While the model can be adapted for refineries with multiple units by running it separately for each unit, this approach overlooks the interactions between different blending units. Additionally, the linear nominal model optimizes the profit generated solely by throughput in the smelter. However, recent research indicates that optimizing the duration of one blend could lead to enhanced throughput for the entire refinery and less accumulation of materials. This aspect is not accounted for in the current model, highlighting a potential avenue for further improvement.

The optimization models that consider the supply uncertainty offer a more realistic optimization approach for the SBCP. The robust models considering mass uncertainty and mass fraction uncertainty both provided promising results for creating solutions that remain feasible under mass and mass fraction uncertainty. However, the one-stage robust mass fraction model could not find feasible solutions for the entire scheduling horizon for values of the normalized perturbation factor larger than $\lambda = 0.1$. Similarly, the one-stage robust mass fraction model could not find feasible solutions for larger values than $\lambda = 0.3$ for all the budgeted uncertainty sets for the elements together. If the refinery desires to include larger perturbations of the uncertain parameters into the uncertainty set, a multistage model should be employed. These bounds on the size of the uncertainty sets are thus limitations of the current robust one-stage models. Additionally, the upper and lower bound constraint on the ratio between the mass fraction of element 7 and element 2 results in a maximum range of uncertainty that can be included in an uncertainty set for these parameters, without creating a contradiction. This is a limitation of the robust approach. If the refinery desires to include perturbations outside the range of the maximum uncertainty set, for example, a violating model can be formulated with a penalty in the objective for the size of the violation term. However, the model becomes than less interpretive but could result in robust solutions with a higher feasibility ratio. The stochastic model with reduced scenario tree $\overline{\mathcal{Z}}_{worst}$ was for most instances not capable of finding a feasible solution for the entire scheduling horizon. This denotes that the model is too conservative. Although copper concentrates may experience their maxi-

mum delay, by including this possibility in the scenario tree, the resulting stochastic model should hold for the scenario that all copper concentrates are maximum delayed. The results illustrate that this is (over-)conservative for most instances. However, by including the mean delay as possible realization for each copper concentrate, the model found feasible solution, but the simulation results showed that these solutions did not remain feasible for the majority of the arrival time uncertainties. Therefore, a limitation of the current stochastic model where for each copper concentrate two possible delays are selected to generate the scenario tree, is that is does not result in a feasible solution for the entire scheduling horizon that remains feasible across different arrival time uncertainty realizations.

An additional limitation of the multistage stochastic model, is that for larger instances with more expected copper concentrates, the scenario tree expands quickly in size. When more delays for a copper concentrate are considered, the scenario tree grows even more quickly. This results in computational hard models to solve. The current models could not be solved for instance E, denoting that the number of scenarios and instances size is a severe limitation of the multistage stochastic model due to extended computation times. A similar limitation is denoted for the simulation algorithm which is used to evaluate the models. For larger instances it takes longer to compute the simulation, due to more re-optimizations over the scheduling horizon. Currently, the re-optimization of the larger instances leads to memory issues. It should be looked into how the potential memory leak can be eliminated in the simulation algorithm.

8.2. Further Research

Finally, we provide a couple of recommendations for further research. First, we observed that for the simulation results the performance measures for $N = 100$ and $N = 1000$ did not differ largely. We would recommend further analyzing how much the results change for larger numbers of simulation iterations. If $N = 100$ turns out to be a sufficient number of iterations, this is promising for the option to evaluate larger instances in reasonable computation time. It is in the refinery's interest to evaluate how the solutions change for a long-term scheduling horizon. Therefore we recommend extending the scheduling horizons of the studied SBCP instances, and adjust the programming of the models accordingly so they stay computationally efficient. Further, we highly recommend validating the results on a case study with actual data from a refinery. In this way, the performance of the optimization models and the results of this study can be validated.

Next, the construction of the scenarios for the multistage stochastic model can be further studied. The current results show that the scenario tree including the worst-case delay or the scenario tree including the mean delay both lead to insufficient solutions. We recommend further studying which delays of a copper concentrate should be selected in the generation of the scenario tree. For instance, the construction of a scenario tree where a delay in between the average delay and worst-case delay could be studied. Another possibility is to include only the worst-case delay for the most important copper concentrates, necessary for feasibility of the SBCP, and to be less conservative for the other copper concentrates. It could be studied to add scenarios to the model following an sequential approach in such a way that not only the worst-case scenarios are included.

By creating both a nominal optimization model and optimization models that consider uncertainty, different mathematical formulations have been obtained for the SBCP. When a robust formulation is used with an uncertainty set containing only the zero element, this revealed that different solutions are obtained for the optimal objective value with the different formulations of the model. This is of interest, because this indicates that multiple feasible blending schedules are generating the same optimal objective value. It is of interest to study the differences of the solutions and if they influence the robustness of the model under supply uncertainty.

Further, it is of interest to perform a sensitivity analysis on the capacity and the start-inventory in the SBCP and how these parameters influence the sensitivity of the SBCP to supply uncertainty. Including a limited capacity increased the difficulty of remaining feasible for the SBCP considering supply uncertainty. The results show that the feasibility of the SBCP is very dependent on the agreements

made with the suppliers about when and which copper concentrates are deliver over the scheduling horizon. Therefore, performing experiments with different frequencies of averring copper concentrates and studying the effect on the feasibility ratio of the solution under supply uncertainty is recommended. In addition, sensitivity analysis on how much start-inventory is included in comparison with how much copper concentrate is ordered is of interest. Lastly, it is suggested to classify copper concentrates using a categorisation system based on how easy they are to blend and the profitability. This could help to gain insights in how to obtain a robust blending schedule under supply uncertainty.

References

Bakker, H., Dunke, F., & Nickel, S. (2020). A structuring review on multi-stage optimization under uncertainty: Aligning concepts from theory and practice. *Omega*, *96*.

Barros, K. S., Vielmo, V. S., Moreno, B. G., Riveros, G., Cifuentes, G., & Bernardes, A. M. (2022). Chemical composition data of the main stages of copper production from sulfide minerals in chile: A review to assist circular economy studies. *Minerals*, *12*(250).

Ben-Tal, A., Ghaoui, L. E., & Nemirovski, A. (2009). *Robust optimization* (1th ed.). Princeton University Press.

Birge, J. R., & Louveaux, F. (2011). *Introduction to stochastic programming* (2th ed.). Springer.

Bundschuh, M., Klabjan, D., & Thurston, D. L. (2003). Modeling robust and reliable supply chains. *Optimization online*.

Cox, J., & Blackstone, J. (2002). *Apics dictionary - the educational society for resource management* (10th ed.). APICS.

Derpich, I., Munoz, N., & Espinoza1, A. (2019). Improving the productivity of the copper mining process in the chilean copper industry. *Croatian Operational Research Review*, *10*, 227–240.

Flores, G. A., Risopatron, C., & Pease, J. (2020). Processing of complex materials in the copper industry: Challenges and oppurtunities ahead. *The Minerals, Metals and Materials Society*, *72*(10).

Goodfellow, R. C., & Dimitrakopoulos, R. (2016). Global optimization of open pit mining complexes with uncertainty. *Applied Soft Computing*, *40*.

Gorissen, B. L., Yanikogly, I., & den Hartog, D. (2015). A practical guide to robust optimization. *Omega*, *53*, 124–137.

https://copperalliance.org/. (2023). *Copper recycling*. https://copperalliance.org/resource/copper-recycling/

Imanbekova, U., Hotra, O., Koshimbayev, S., Popiel, P., & Tanaś, J. (2015). Optimal control of blending and melting of copper concentrates. *PROCEEDINGS OF SPIE*.

investopedia. (2024). *Supply chain management: How it works and why it's important*. https://www.investopedia.com/terms/s/scm.asp

Kucukyavyz, S., & Jiang, R. (2022). Chance-constrained optimization under limited distributional information: A review of reformulations based on sampling and distributional robustness. *Journal on Computational Optimization*, *10*.

Langner, B. E. (2011). *Understanding copper*. Publisher.

liro Harjunkoski, Borchers, H. W., & Fahl, M. (2006). Simultaneous scheduling and optimization of a copper plant. *European Symposium on Computer Aided Process Engineering*.

Muthumariappan, S., & David, S. A. (2019). A study of the chemical composition of copper concentrate and granulated slag. *International Journal of Scientific Research and Review*, *7*(3).

Pan Pacific Copper. (2024). *Copper smelting and refining process*. https://www.ppcu.co.jp/eng/about_ppc/processes.html

Pengfei Chenga, b., Garcia-Herrerosc, P., Lalpuriac, M., & Grossmannb, I. E. (2020). Optimal scheduling of copper concentrate operations under uncertainty. *Computers and Chemical Engineering*, *140*(106919).

Pflug, G. C., & lois Pichler. (2014). *Multistage stochastic optimization* (1th ed.). Springer.

Sahinidis, N. V. (2004). Optimization under uncertainty: State-of-the-art and oppurtunities. *Computers and Chemical Engineering*, *28*, 971–983.

Savi, I. J. M., Zivkovi, Z., Boyanov, B. S., & Peltekov, A. (2016). An linear programming model for batch optimization in the ecological zinc production. *Environ Model Assess*, 455–465.

Song, Y., Menezes, B., Garcia-Herreros, P., & Grossmann, I. E. (2018). Scheduling and feed quality optimization of concentrate raw materials in the copper refining industry. *Industrial & Engineering Chemistry Research*, *57*(2), 11686–11701.

Statista.com. (2023). *Copper mine production worldwide 2010-2022*. https://www.statista.com/statistics/254839/copper-production-by-country/

Suominen, O., Björkqvist, T., Vilkko, M., & Korpi, M. (n.d.). Copper production as an application of optimization and scheduling. *Automation Science and Engineering*.

Suominen, O., Mörsky, V., Ritala, R., & Vilkkoa, M. (2016). Framework for optimization and scheduling of a copper production plant. *Computer Aided Process Engineering*.

Suryawanshi, P., & Dutta, P. (2022). Optimization models for supply chains under risk, uncertainty, and resilience: A state-of-the-art review and future research directions. *Transportation Research*, *157*.

Torabi, S., Baghersad, M., & Mansouri, S. (2015). Resilient supplier selection and order allocation under operational and disruption risks. *Transportation Research*, *59*(22-48).

USGS science for a changing world. (2016). *Global copper map*. https://www.usgs.gov/media/images/global-copper-map-0

worldatlas.com. (2023). *What was the first metal used by humans?* https://www.worldatlas.com/articles/what-was-the-first-metal-used-by-man.html

Zhang, H., Zhao, J., Leung, H., Fellow, & Wang, W. (2022). Adaptive weighted optimization framework for multiobjective long-term planning of concentrate ingredients in copper industry. *IEEE transactions on instrumentation and measurement*, *71*.

A

Derivation of robust counterparts

This chapter presents the derivation of the robust counterparts for the constraints including the uncertain mass fraction parameter $\theta_{k,c}$. For the uncertain parameter, $\theta_{k,c}$, the implemented budgeted uncertainty set is formulated as follows.

$$\Theta_k = \left\{ \theta_{k,c} \in \mathbb{R}^{kxc} : \overline{\theta_{k,c}}(1-\delta p_{k,c}) \leq \theta_{k,c} \leq \overline{\theta_{k,c}}(1+\delta p_{k,c}), 0 \leq p_{k,c} \leq 1, 0 \leq \sum_{c\in\mathcal{C}} p_{k,c} \leq \Gamma \right\} \tag{A.1}$$

Upperbound element 7/2 ratio constraint

Open Form Robust Constraint. The steps of the derivation of the robust counterpart are applied for the interdependency ratio constraint for element 2 and element 7.

$$0.64 \sum_{c\in\mathcal{C}} \sum_{e\in\mathcal{E}'} \theta_{2,c} f_{e,c,t} \quad \geq \quad \sum_{c\in\mathcal{C}} \sum_{e\in\mathcal{E}'} \theta_{7,c} f_{e,c,t} \qquad \forall t \in \mathcal{T}, \forall \theta_{2,c} \in \Theta_2, \forall \theta_{7,c} \in \Theta_7 \tag{A.2}$$

Worst-Case Constraint. The worst case of this constraint is when the left side of the inequality is minimized and the right side is maximized over the uncertain parameter $\theta_{k,c}$. The uncertainty sets of element 2 and element 7 are independent of each other.

$$0.64 \min_{\theta_{2,c}\in\Theta_2} \sum_{c\in\mathcal{C}} \sum_{e\in\mathcal{E}'} \theta_{2,c} f_{e,c,t} \quad \geq \quad \max_{\theta_{7,c}\in\Theta_7} \sum_{c\in\mathcal{C}} \sum_{e\in\mathcal{E}'} \theta_{7,c} f_{e,c,t} \qquad \forall t \in \mathcal{T} \tag{A.3}$$

Auxiliary Problem. This constraint can be split into two auxiliary optimization problems. These are a minimization optimization problem and a maximization optimization problem. The minimization problem can as follows be transformed into a maximization problem. In this way, the same dual auxiliary problem can be used. Than the reformulation for every individual inequality $(t \in \mathcal{T})$ is given by:

$$\begin{aligned}
&\min_{\theta_{2,c}\in\Theta_2} \left(\sum_{c\in\mathcal{C}} \sum_{e\in\mathcal{E}'} \theta_{2,c} f_{e,c,t} \right) \\
&\equiv \min_{\theta_{2,c}\in\Theta_2} \left(\sum_{c\in\mathcal{C}} \sum_{e\in\mathcal{E}'} \overline{\theta_{2,c}} f_{e,c,t}(1-\delta p_{2,c}) \right) \\
&\iff \min \left(-\sum_{c\in\mathcal{C}} \sum_{e\in\mathcal{E}'} \overline{\theta_{2,c}} f_{e,c,t} p_{2,c} \right) && \text{(A.4)} \\
&\equiv -\max \left(\sum_{c\in\mathcal{C}} \sum_{e\in\mathcal{E}'} \overline{\theta_{2,c}} f_{e,c,t} p_{2,c} \right) && \text{(A.5)} \\
&\text{s.t.} \quad 0 \leq p_{2,c} \leq 1 && \forall c \in \mathcal{C} \\
&\qquad \sum_{c\in\mathcal{C}} p_{2,c} \leq \Gamma
\end{aligned}$$

Robust Counterpart. Now we can use the already derived dual auxiliary problem for both maximization problems and substitute it into the constraint. This provides the robust counterpart as shown in equation (A.6).

$$0.64 \sum_{c\in\mathcal{C}} \sum_{e\in\mathcal{E}'} \overline{\theta_{2,c}} f_{e,c,t} - \delta(\Gamma q_2 + \sum_{c\in\mathcal{C}} s_{2,c}) \geq \quad \sum_{c\in\mathcal{C}} \sum_{e\in\mathcal{E}'} f_{e,c,t}\overline{\theta_{7,c}} + \delta(\Gamma q_7 + \sum_{c\in\mathcal{C}} s_{7,c}) \quad \forall t \in \mathcal{T} \tag{A.6}$$

Lowerbound element 7/2 ratio constraint

Open Form Robust Constraint. The open form of the robust constraint for the lower bound of the ratio of element 7 and element 2 is formulated as follows.

$$0.58 \sum_{c\in\mathcal{C}} \sum_{e\in\mathcal{E}'} \theta_{2,c} f_{e,c,t} \quad \leq \quad \sum_{c\in\mathcal{C}} \sum_{e\in\mathcal{E}'} \theta_{7,c} f_{e,c,t} \quad \forall t \in \mathcal{T}, \forall \theta_{2,c} \in \Theta_2, \forall \theta_{7,c} \in \Theta_7 \tag{A.7}$$

Worst-Case. The worst case of this constraint is when the left side is maximized and the right side is minimized over the uncertain parameter theta.

$$0.58 \max_{\theta_{2,c}\in\Theta_2} \sum_{c\in\mathcal{C}} \sum_{e\in\mathcal{E}'} \theta_{2,c} f_{e,c,t} \quad \leq \quad \min_{\theta_{7,c}\in\Theta_7} \sum_{c\in\mathcal{C}} \sum_{e\in\mathcal{E}'} \theta_{7,c} f_{e,c,t} \quad \forall t \in \mathcal{T} \tag{A.8}$$

Robust Counterpart. The same auxiliary optimization problems can be formulated as above. The same dual auxiliary problem can then be used and substituted in the formulation. This results in the robust counterpart as formulated in equation (A.9).

$$0.58 \sum_{c\in\mathcal{C}} \sum_{e\in\mathcal{E}'} \overline{\theta_{2,c}} f_{e,c,t} + \delta(\Gamma q_2 + \sum_{c\in\mathcal{C}} s_{2,c}) \leq \quad \sum_{c\in\mathcal{C}} \sum_{e\in\mathcal{E}'} \overline{\theta_{7,c}} f_{e,c,t} - \delta(\Gamma q_7 + \sum_{c\in\mathcal{C}} s_{7,c}) \quad \forall t \in \mathcal{T} \tag{A.9}$$

Interdependency between elements constraints

Open Form Robust Constraint. The derivation of the robust counterpart for the interdependency constraints for the elemental flows is as follows. First, the robust constraint in open form is formulated as in equation (A.10).

$$U_k \sum_{k'\in\mathcal{K}} (K_{k'} \sum_{c\in\mathcal{C}} \sum_{e\in\mathcal{E}'} \theta_{k',c}) f_{e,c,t} \quad \geq \quad K_k \sum_{c\in\mathcal{C}} \sum_{e\in\mathcal{E}'} f_{e,c,t}\theta_{k,c} \quad \forall k \in \mathcal{K}, \forall t \in \mathcal{T}, \forall \theta_{k,c} \in \Theta_k \tag{A.10}$$

Worst-Case. Because it is preferred to be able to define a dual variable per element k', the constraint is reformulated, and then the worst case constraint is defined.

$$\begin{aligned} &U_k \min_{\theta_{k,c}\in\Theta_k} \left(\sum_{k'\in\mathcal{K}, k'\neq k} \sum_{c\in\mathcal{C}} \sum_{e\in\mathcal{E}'} \theta_{k',c} f_{e,c,t} K_{k'} \right) \\ &\geq K_k(1-U_k) \max_{\theta_{k,c}\in\Theta_k} \sum_{c\in\mathcal{C}} \sum_{e\in\mathcal{E}'} \theta_{k,c} f_{e,c,t} \quad \forall k \in \mathcal{K}, \forall t \in \mathcal{T} \end{aligned} \tag{A.11}$$

Auxiliary problem. There are two auxiliary optimization problems. The dual reformulation of the right maximization problem is already known. The derivation of the dual formulation of the left minimization optimization problem remains to be done. First, the minimization problem is rewritten to a maximization

problem.

$$
\begin{aligned}
&\min_{\theta_{k,c}\in\Theta_k}\left(\sum_{k'\in\mathcal{K}}\sum_{c\in\mathcal{C}}\sum_{e\in\mathcal{E}'}\theta_{k',c}f_{e,c,t}K_{k'}\right)\\
&\equiv \min_{\theta_{k,c}\in\Theta_k}\left(\sum_{k'\in\mathcal{K}}\sum_{c\in\mathcal{C}}\sum_{e\in\mathcal{E}'}\overline{\theta_{k',c}}f_{e,c,t}K_{k'}(1-\delta p_{k',c})\right)\\
&\iff \min\left(-\sum_{k'\in\mathcal{K}}\sum_{c\in\mathcal{C}}\sum_{e\mathcal{E}}\overline{\theta_{k',c}}f_{e,c,t}K_{k'}p_{k',c}\right)\\
&\equiv -\max\left(\sum_{k'\in\mathcal{K}}\sum_{c\in\mathcal{C}}\sum_{e\in\mathcal{E}'}\overline{\theta_{k',c}}f_{e,c,t}K_{k'}p_{k',c}\right) && \text{(A.12)}\\
&\text{s.t.}\quad 0\le p_{k',c}\le 1 && \forall k'\in\mathcal{K},k'\neq k,\forall c\in\mathcal{C} && \text{(A.13)}\\
&\qquad\sum_{c\in\mathcal{C}}p_{k',c}\le\Gamma && \forall k'\in\mathcal{K},k'\neq k && \text{(A.14)}
\end{aligned}
$$

Dual Auxiliary problem. The dual variable $s'_{k',c}$ is introduced for constraint (A.13) and the dual variable $q'_{k'}$ is introduced for constraint (A.14). For each problem with $(k\in\mathcal{K},t\in\mathcal{T})$ the dual auxiliary problem is then formulated as follows.

$$
\begin{aligned}
&\min \sum_{k'\in\mathcal{K},k'\neq k}\Gamma q'_k+\sum_{c\in\mathcal{C}}\sum_{k'\in\mathcal{K},k'\neq k}s'_{k,c} && && \text{(A.15)}\\
&\qquad\text{s.t.}s'_{k',c}+q'_{k'}\ge\sum_{e\in\mathcal{E}'}\overline{\theta_{k',c}}f_{e,c,t}K_{k'} && \forall c\in\mathcal{C},k'\in\mathcal{K},k'\neq k\\
&\qquad\qquad s'_{k',c}\ge 0 && \forall c\in\mathcal{C},k'\in\mathcal{K},k'\neq k\\
&\qquad\qquad q'_{k'}\ge 0 && k'\in\mathcal{K},k'\neq k && \text{(A.16)}
\end{aligned}
$$

Robust Counterpart. By strong duality, the initial optimization problem (A.12) which is a $-$ max problem is equivalent to a $-$ min problem and this is equal to a max $-$ problem. This is substituted into constraint (A.11), providing the following inequality. Because the primal problem is feasible, the dual problem will be bounded and thus for general dual variables, it will be definitely feasible for the optimal dual variables. So the minimum sign can be dropped. This results in the following robust counterpart.

$$
\begin{aligned}
&U_k\left(\sum_{c\in\mathcal{C}}\sum_{e\in\mathcal{E}'}\overline{\theta_{k',c}}f_{e,c,t}K_{k'}-\delta(\Gamma q'_k+\sum_{c\in\mathcal{C}}s'_{k,c})\right)\\
&\quad\ge K_k(1-U_k)\sum_{c\in\mathcal{C}}\sum_{e\in\mathcal{E}'}\overline{\theta_{k,c}}f_{e,c,t}+\delta(\Gamma q_k+\sum_{c\in\mathcal{C}}s_{k,c}) && \forall k\in\mathcal{K},\forall t\in\mathcal{T} && \text{(A.17)}\\
&\quad\text{s.t.}\quad s'_{k',c}+q'_{k'}\ge\sum_{e\in\mathcal{E}'}\overline{\theta_{k',c}}f_{e,c,t}K_{k'} && \forall c\in\mathcal{C},k'\in\mathcal{K},k'\neq k\\
&\qquad s'_{k',c}\ge 0 && \forall c\in\mathcal{C},k'\in\mathcal{K},k'\neq k\\
&\qquad q'_{k'}\ge 0 && \forall k'\in\mathcal{K},k'\neq k
\end{aligned}
$$

B

Additional results optimization models

This appendix presents additional numerical results for the formulated optimization models for the SBCP. Sections B.1 and B.2 present the optimization results for the robust mass fraction model for varying values of the normalized perturbation factor λ_k for different elements. Section B.3 presents the results for the one-stage stochastic model utilizing the scenario tree $\overline{\mathcal{Z}}_{sampled}$. Section B.4 presents the performance of the double robust model evaluated for both mass and mass fraction uncertainty.

B.1. Optimization results robust mass fraction model for varying lambda

Table B.1 presents the optimization results of the robust mass fraction model, which utilizes a budgeted uncertainty set for the mass fraction parameters for all the elements $k \in \mathcal{K}$. The normalized perturbation factor λ that denotes the maximum percentage deviation of the nominal mass fraction in the budgeted uncertainty set is varied between 0.01 and 0.05. The budget parameter is set to $\Gamma = \frac{1}{2}CC$ and the results are presented across instance A till instance E. The table illustrates that from a value $\lambda = 0.01$ applied to the budgeted uncertainty sets of all elements simultaneously, the model is not able to find a feasible solution across all instances.

Table B.1: Optimization results of the robust model for uncertainty in the mass fraction of elements in a copper concentrate. A budgeted uncertainty set has been implemented with a varying normalized perturbation factor λ across the budgeted uncertainty sets for all elements. The budget parameter is $\Gamma = \frac{1}{2}CC$. The results are shown for instance A till instance E.

	Output	$\lambda = 0.0$ (deterministic)	$\lambda = 0.01$	$\lambda = 0.02$	$\lambda = 0.03$	$\lambda = 0.04$	$\lambda = 0.05$
Instance A	Feasibility status	feasible	feasible	feasible	infeasible at p7	infeasible at p7	infeasible at p7
	Computational time (s)	0.23	0.28	0.25	*	*	*
	Objective value (million euros)	9.5	9.4	9.2	*	*	*
Instance B	Feasibility status	feasible	feasible	feasible	feasible	infeasible at p5	infeasible at p5
	Computational time (s)	0.76	1.04	1.29	1.02	*	*
	Objective value (million euros)	17.5	17.3	17.1	16.2	*	*
Instance C	Feasibility status	feasible	feasible	feasible	feasible	infeasible at p5	infeasible at p5
	Computational time (s)	0.32	0.57	0.99	0.65	*	*
	Objective value (million euros)	36.9	36.0	34.7	33.3	*	*
Instance D	Feasibility status	feasible	feasible	infeasible at p5	infeasible at p5	infeasible at p5	infeasible at p5
	Computational time (s)	0.53	10.92	*	*	*	*
	Objective value (million euros)	63.2	62.4	*	*	*	*
Instance E	Feasibility status	feasible	infeasible at p5	infeasible at p5	infeasible at p5	infeasible at p5	infeasible at p5
	Computational time (s)	3.16	*	*	*	*	*
	Objective value (million euros)	199.0	*	*	*	*	*

Table B.1 presents again the optimization results of the robust mass fraction model, which has a budgeted uncertainty set for the mass fraction parameter for all the elements $k \in \mathcal{K}$. Now, the normalized perturbation factor for the budgeted uncertainty sets applied to the mass fraction parameter of element 2 and element 7 are set to $\lambda_2 = \lambda_7 = 0.001$ because we know that these the SBCP reacts more sensitively to uncertainty in these parameters. The normalized perturbation factors for the other elements are varied between 0.01 and 0.05. The budget parameter is set again to $\Gamma = \frac{1}{2}CC$ and the results are shown across instance A till instance E. The table illustrates that from $\lambda = 0.03$ for the budgeted uncertainty sets for the remaining elements, not for every instance a feasible solution can be found.

Table B.2: Optimization results of the robust model for uncertainty in the mass fraction of elements in a copper concentrate. A budgeted uncertainty set has been implemented with a varying normalized perturbation factor λ across the budgeted uncertainty sets for the elements $k \in \mathcal{K} \setminus \{2, 7\}$. The normalized perturbation factor for elements 2 and 7 is set to $\lambda_2 = \lambda_7 = 0.001$. The budget parameter is $\Gamma = \frac{1}{2}CC$. The results are shown for instance A till instance E.

	Output	$\lambda = 0.0$ (deterministic)	$\lambda = 0.01$	$\lambda = 0.02$	$\lambda = 0.03$	$\lambda = 0.04$	$\lambda = 0.05$
Instance A	Feasibility status	feasible	feasible	feasible	infeasible at p7	infeasible at p7	infeasible at p7
	Computational time (s)	0.23	0.28	0.22	*	*	*
	Objective value (million euros)	9.5	9.4	9.2	*	*	*
Instance B	Feasibility status	feasible	feasible	feasible	feasible	feasible	feasible
	Computational time (s)	0.76	1.098	1.235	1.358	0.991	1.543
	Objective value (million euros)	17.5	17.31745185356401	17.12453134699347	16.90182473326156	16.67941015644814	16.45761145695507
Instance C	Feasibility status	feasible	feasible	feasible	feasible	feasible	feasible
	Computational time (s)	0.32	0.57	0.632	0.728	0.737	0.685
	Objective value (million euros)	36.9	36.7	36.52797871869253	36.33309999745168	36.14162223127252	35.874036888419454
Instance D	Feasibility status	feasible	feasible	feasible	feasible	feasible	feasible
	Computational time (s)	0.53	4.80	14.51	8.83	6.38	9.87
	Objective value (million euros)	63.2	62.9	62.1	61.2	60.1	59.1
Instance E	Feasibility information	feasible	feasible	feasible	infeasible at p5	infeasible at p5	infeasible at p5
	Computational time (s)	3.16	635.93	801.75	*	*	n*
	Objective value (million euros)	199.0	189.8	181.3	*	*	*

B.2. Optimization results robust mass fraction model individual uncertainty sets

The sensitivity of the SBCP to mass fraction uncertainty is studied in detail by creating different robust models, each incorporating a budgeted uncertainty set implemented for an individual element k as opposed to an uncertainty set applied to all elements simultaneously. The normalized perturbation factor λ_k is varied between 0 and 0.1 with steps of 0.01. This allows us to analyze the size of the uncertainty set for an individual element for which the robust model still finds feasible solutions across the instances. The budget parameter $\Gamma = \frac{1}{2}CC$ is used and the study is performed on instance A till instance C. Figure B.1a till B.4b show the results, where the objective value of each instance is scaled between 0.0 and 1.0, denoted as the uniform objective value.

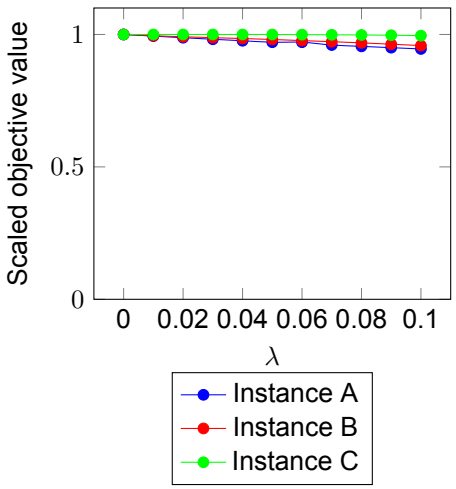

(a) Robust model with budgeted uncertainty set for element 1.

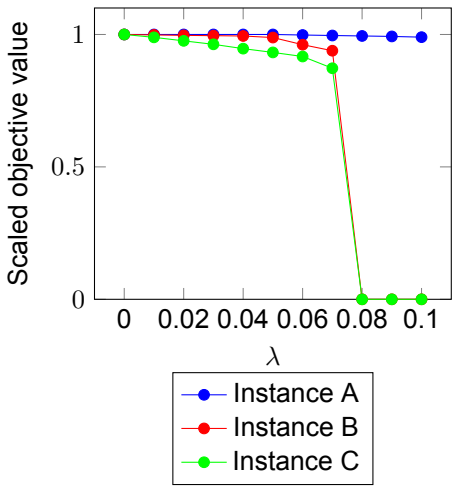

(b) Robust model with budgeted uncertainty set for element 2.

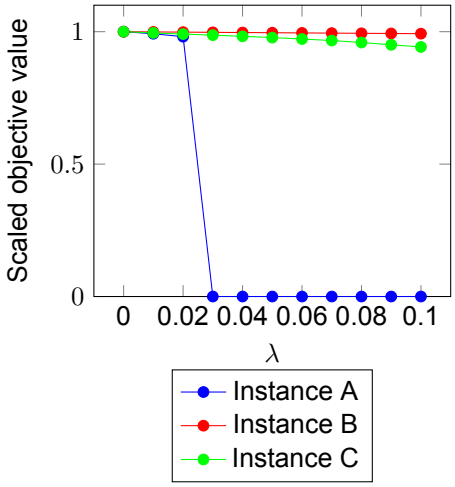

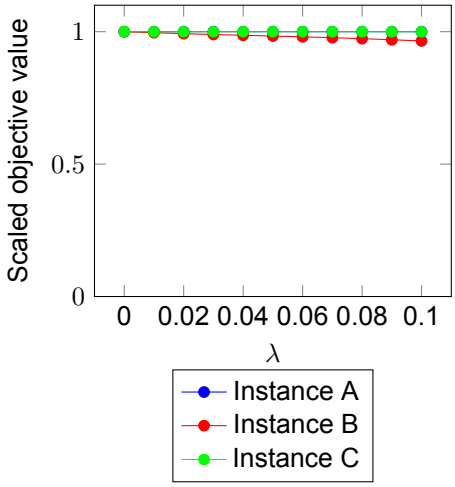

Figure B.2: Optimization results for robust model with a budgeted uncertainty set for respectively element 3 or element 4

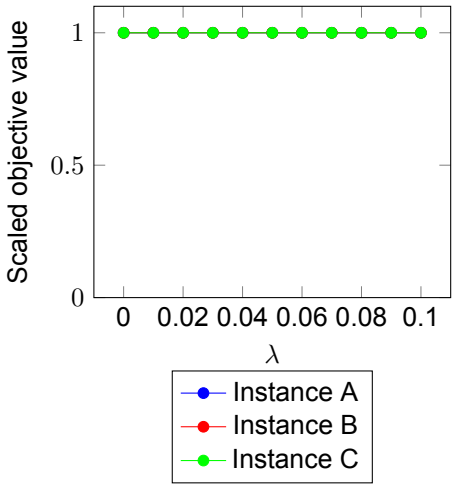

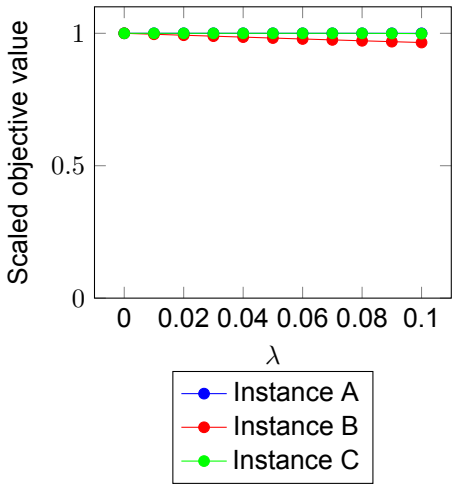

(a) Robust model with budgeted uncertainty set for element 6.

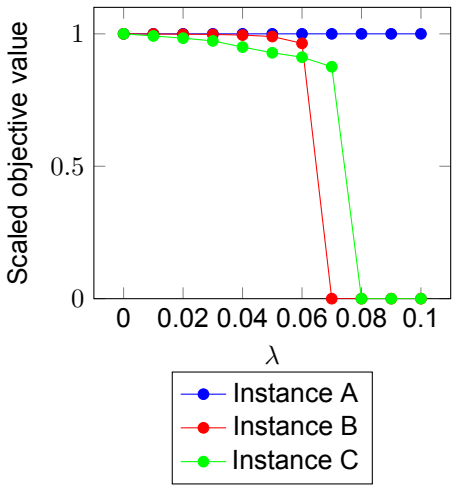

(a) Robust model with budgeted uncertainty set for element 7.

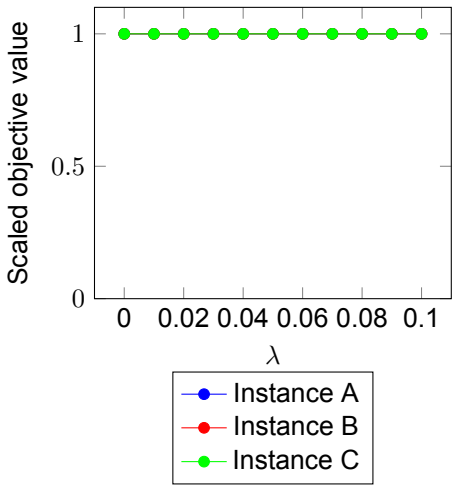

(b) Robust model with budgeted uncertainty set for element 8.

Figure B.4: Optimization results for robust model with a budgeted uncertainty set for respectively element 7 or element 8

B.3. Result one-stage stochastic model with sampled scenario set

Optimization results

Table B.3 shows the optimization results of the one-stage stochastic model with a reduced scenario set $\overline{\mathcal{Z}}_{sampled}$ that is constructed by sampling X random scenarios from the probability distribution that describes the delay of a copper concentrate, as discussed in Section 4.5.2. This probability distribution is described in Section 4.2.3. We exclude instance E due to memory constraints.

Table B.3: Optimization results of the one-stage stochastic model with the reduced set of scenarios $\overline{\mathcal{Z}}_{sampled}$. The reduced set of scenarios $\overline{\mathcal{Z}}_{sampled}$ is generated by sampling random scenarios from the probability distribution which describes the uncertain delay of a copper concentrate. The parameter X denotes the size of the set of sampled scenarios.

	Output	Deterministic	$X = 10$	$X = 100$	$X = 1000$
Instance A	Feasibility status	feasible	infeasible at p8	infeasible at p6	infeasible at p6
	Computational time (s)	0.02	*	*	*
	Objective value (million euros)	9.5	*	*	*
Instance B	Feasibility status	feasible	feasible	feasible	feasible
	Computational time (s)	0.07	0.32	0.32	5.57
	Objective value (million euros)	17.5	12.3	11.5	9.8
Instance C	Feasibility status	feasible	feasible	feasible	feasible
	Computational time (s)	0.07	0.13	0.22	2.34
	Objective value (million euros)	36.9	32.3	24.7	24.7
Instance D	Feasibility status	feasible	infeasible at p30	infeasible at p18	infeasible at p15
	Computational time (s)	0.04	*	*	*
	Objective value (million euros)	63.2	*	*	*

The table presents that the one-stage model with the reduced scenario set $\overline{\mathcal{Z}}_{sampled}$ feasible stochastic solutions are found for instances B and C, regardless of the sampling size X. This illustrates that for these instances the model is capable of finding a solution that is feasible for a large part of the probability space. However, for instances A and B, solutions are consistently infeasible, independent of the sampling size. This shows that the model has difficulty in finding feasible solutions for the sampled scenarios of arrival time uncertainty. The sensitivity of the SBCP to arrival time uncertainty appears thus to be instance-specific, influenced by factors such as the availability of start inventory, the number of expected copper concentrates, and the scheduling horizon's length. We conclude that the one-stage stochastic model can not find feasible solutions for scenarios that represent the majority of the probability space of the arrival time uncertainty across all instances. When a feasible solution is found this is accompanied by a significantly lower objective value compared with the nominal solution. The computation time of the one-stage stochastic model is not significantly larger than the deterministic model. However, the infeasibility of the solutions and the large decrease in objective value indicate that the one-stage model may be too conservative for the SBCP and the implementation of a multistage model would provide a more sufficient solution.

Performance results

Table B.4 shows the simulation results of the one-stage stochastic model with the reduced set of scenarios $\overline{\mathcal{Z}}_{sampled}$. The number of sampled scenarios is $X = 10$. For a larger number memory issues occurred during re-optimization. A re-optimization period of seven days is applied.

Table B.4: Performance of one-stage stochastic model with the reduced scenario set $\overline{\mathcal{Z}}_{sampled}$ where the scenarios are randomly generated from the probability distribution of the delay of a copper concentrate. The sample size is $X = 10$. A re-optimization period of seven days is applied.

	Number of simulations	Performance measures	Nominal Model	OSM: $\overline{\mathcal{Z}} = \overline{\mathcal{Z}}_{sampled}$, $X = 10$
Instance B	10	Feasibility ratio	0.0	*
		Average objective ratio	***	*
		Simulation time (s)	2.13	18.529
	100	Feasibility ratio	0.0	1.0
		Average objective ratio	***	80.0
		Simulation time (s)	15.10	162.24
Instance C	10	Feasibility ratio	0.0	10.0
		Average objective ratio	***	89.0
		Simulation time (s)	1.36	11.18
	100	Feasibility ratio	0.0	16.0
		Average objective ratio	***	88.8
		Simulation time (s)	13.25	129.018

The table illustrates a low feasibility ratio for the one-stage stochastic model with the reduced scenario set $\overline{\mathcal{Z}}_{sampled}$ varying from 1.0 (instance B, $N = 10$) to 16.0 (instance C, $N = 100$). The feasibility ratios are low primarily because for the majority of the realizations, only infeasible solutions could be found by the model. This indicates that the stochastic model does not yet capture the whole probability space of the arrival time uncertainty. This is expected for a sample size of $X = 10$, enlarging the sample size may result in higher feasibility ratios. The SBCP is sensitive to uncertainty in the arrival time of a copper concentrate and we can conclude that the one-stage stochastic model with $\overline{\mathcal{Z}}_{sampled}$ and $X = 10$ is not sufficient for providing a robust solution across all instances.

B.4. Performance results of double robust model

Table B.5 presents the simulation results of the double robust model (DRM) for simulated uncertainty both in the mass of a copper concentrate and the mass fraction of the elements in a copper concentrate. For comparison, also the performances of the robust mass model (RMM) and the robust mass fraction model (RMFM) in addition to the performance of the nominal model for simulated uncertainty for both the mass and mass fraction of elements of a copper concentrate are presented. The results are presented for instance A till instance C.

The above table illustrates that the nominal model evaluated for both mass uncertainty and mass fraction uncertainty performs worse than only evaluated for mass uncertainty (refer to Table 6.2). Instance A has a feasibility ratio of 40.0, which lies between the score of the evaluation for mass uncertainty (100.0) and the feasibility ratio during the evaluation of mass fraction uncertainty (20.0). Both uncertainties seem to level each other out for instance A. For instance B and C the feasibility ratio is 0.0, indicating that the nominal solution is not feasible against realizations of the mass and mass fraction uncertainty combined.

The performance of the robust mass model (RMM) is poor, indicated by feasibility ratios varying between 0.0 and 40.0. The robust mass model worked well to provide robust models for uncertainty in the mass of a copper concentrate. However, when also uncertainty in the mass fraction of the elements is applied to these solutions the table shows that the solutions perform the same as the nominal model. The robust mass fraction model (RMFM) performs better for the uncertainties in both mass and mass fraction. The feasibility ratios for instance A and instance B are high varying between 90.0 (instance B, $N = 10$) and 100.0 (instance A, $N = 10$). However, as can be seen in Table 6.2 these instances already performed well for mass uncertainty with the nominal solution. Therefore the addition of mass uncertainty has not a large negative influence on the feasibility ratio of these instances. Instance C however did not perform well under mass uncertainty with the nominal solution, and the solution from the robust mass fraction model performed poorly under the addition of mass uncertainty (40.0). Both robust models perform thus well for their uncertainty individually, however when the other uncertainty is added the feasibility ratios drop.

Table B.5: Performance of the models for simulated uncertainty in the mass of a copper concentrate and the mass fraction of elements in a copper concentrate. The performances of the nominal model, the robust mass model (RMM), the robust mass fraction model (RMFM), and the double robust model (DRM) across instances A till C are presented.

	Number of simulations	Performance measures	Nominal Model	RMM	RMFM	DRM
Instance A	10	Feasibility ratio	40.0	40.0	100.0	100.0
		Average objective ratio	100.25	98.7	97.8	96.9
		Simulation time (s)	0.97	1.43	1.69	1.86
	100	Feasibility ratio	47.0	49.0	93.0	97.0
		Average objective ratio	100.2	98.8	97.7	96.8
		Simulation time (s)	6.14	8.80	10.91	11.0
Instance B	10	Feasibility ratio	0.0	0.0	90.0	90.0
		Average objective ratio	*	*	98.9	98.9
		Simulation time (s)	2.41	4.55	18.92	15.89
	100	Feasibility ratio	3.0	3.0	93.0	93.0
		Average objective ratio	100.3	100.0	92.2	99.1
		Simulation time (s)	18.74	31.74	141.32	159.28
Instance C	10	Feasibility ratio	0.0	0.0	40.0	80.0
		Average objective ratio	*	*	99.3	97.5
		Simulation time (s)	1.84	4.30	9.87	9.57
	100	Feasibility ratio	0.0	0.0	42.0	80.0
		Average objective ratio	*	*	99.5	97.5
		Simulation time (s)	12.25	26.89	87.84	92.82

Notably, the combination of above models, denoted as the combined robust model (CRM) can provide robust solutions that remain feasible both under mass and mass fraction uncertainty, indicated by high feasibility ratios (varying from 80.0 to 100.0). We can conclude that the robust models are sufficient for capturing the uncertainty and yielding a feasible solution under mass and mass fraction uncertainty under minor profit reductions in reasonable computation time.

C

SBCP data instances

This chapter presents the nummerics of the SBCP instances which are used to evaluate the various optimization models for the SBCP. Specifically, we present the list of expected copper concentrates which corresponding copper concentrate parameters and similarly the parameters for the non copper concentrates in each instance. The general blending system parameters and element constraint parameters have been already presented in Chapter 5. In total five data instances are studied, denoted instance A until instance E respectively. Refer also to Chapter 5 for a description of the construction of these instances.

C.1. Data of SBCP Instance A

Table C.1: Expected copper concentrates for SBCP instance A.

c	t'	j	$\overline{g_{m,j,c,t'}}$	α_c	$\theta_{1,c}$	$\theta_{2,c}$	$\theta_{3,c}$	$\theta_{7,c}$
1	1	1	11380	146	0.254	0.297	0.329	0.12
2	7	1	10800	1172	0.7	0.00507	0.185	0.11
3	0	1	5017	319	0.25	0.22	0.27	0.26
4	0	1	5009	216	0.221	0.37	0.355	0.055
5	0	1	4719	264	0.241	0.255	0.315	0.189

Table C.2: The non-copper concentrates which arrive daily for instance A.

c	j	$h_{j,c,t}$	α_c	$\theta_{1,c}$	$\theta_{2,c}$	$\theta_{3,c}$	$\theta_{7,c}$
1	S+1	38.14	0	0.207	0.35	0.121	0.322

C.2. Data of SBCP instance B

Table C.3: Expected copper concentrates for SBCP instance B.

c	t'	j	$\overline{g_{m,j,c,t'}}$	α_c	$\theta_{1,c}$	$\theta_{2,c}$	$\theta_{3,c}$	$\theta_{4,c}$	$\theta_{5,c}$	$\theta_{6,c}$	$\theta_{7,c}$	$\theta_{8,c}$
1	0	1	11360	146	0.254	0.297	0.0000806	0.0000206	0.000112	0.000023	0.053	0.329
2	3	2	12590	1130	0.303	0.307	0.0000706	0.0000455	0.0000349	0.00457	0.0132	0.345
3	6	3	10800	1172	0.700	0.005	0.0005	0.0000015	0	0.06	0.00	0.185
4	7	4	15600	412	0.0372	0.176	0.000285	0.0000202	0.000184	0.0000597	0.136	0.130
5	10	5	183	766	0.002	0.0275	0.005	0.000370	0	0.00002	0.730	0.00200
6	0	6	5017	319	0.25	0.22	0.0100	0.0000001	0.00005	0.0001	0.0580	0.270
7	0	7	5009	216	0.221	0.37	0.000538	0.000000669	0.00000885	0.0000338	0.00467	0.355
8	0	8	4719	264	0.241	0.255	0.00157	0.000000157	0	0.0000243	0.0775	0.315
9	0	9	3543	214	0.236	0.0699	0.00155	0.000000075	0	0.0000135	0.125	0.118
10	0	10	2609	437	0.00219	0.280	0.00930	0.000129	0	0.000422	0.365	0.155

Table C.4: The non-copper concentrates which arrive daily for instance B.

c	j	$h_{j,c,t}$	α_c	$\theta_{1,c}$	$\theta_{2,c}$	$\theta_{3,c}$	$\theta_{4,c}$	$\theta_{5,c}$	$\theta_{6,c}$	$\theta_{7,c}$	$\theta_{8,c}$
1	S + 1	1000	0	0	0	0	0	0	0	1	0
2	S + 1	1 6.26	0	0.241	0.309	0.00113	0.00000514	0	0.00322	0.183	0.2627
3	S + 1	36.05	0	0.207	0.350	0.000774	0.00000429	0	0.00211	0.240	0.1997
4	S + 1	37.34	0	0.428	0.00	0.0168	0.0000278	0	0	0	0.5556

C.3. Data of SBCP instance C

Table C.5: Expected copper concentrates for SBCP instance C.

c	t'	j	$\overline{g_{m,j,c,t'}}$	α_c	$\theta_{1,c}$	$\theta_{2,c}$	$\theta_{3,c}$	$\theta_{4,c}$	$\theta_{5,c}$	$\theta_{6,c}$	$\theta_{7,c}$	$\theta_{8,c}$
1	0	1	13960.0	448.0	0.17003871621971953	0.2567798830132928	0.001132613157673963	3.588290077199732E-5	0.0	3.89251771615203E-4	0.18391073041338413	0.561672431273802
2	0	2	7675.0	1241.0	0.1249883722283784	0.1286097062515374	7.805724288560929E-4	4.2332596562691696E-5	0.0	8.262286490755191E-4	0.28934605820305503	0.23818391974623285
3	0	3	7002.0	362.0	0.28884769317561776	0.31164335505359836	0.0019821005427581024	2.9272428358281307E-5	1.8049391053467958E-4	8.608559980975405E-4	0.0038419954727158755	0.35151979514931736
4	0	4	8146.0	207.0	0.6893054635920309	0.22072033282830786	4.294484551856119E-4	1.8464254066903144E-5	1.3156570654848734E-4	2.263971027493371E-4	0.13888734552672685	0.20135204728395661
5	0	5	11157.0	551.0	0.2453211205509214	0.1388140131466227	0.001728642530183658	5.829495330693889E-5	9.822733224503581E-5	8.03097077692396E-5	0.09341354914413576	0.27461360803257856
6	1	1	8368.0	1014.0	0.48527898318182633	0.30966862163741843	0.001445659123864293	1.2733279842674029E-5	7.271809658320718E-5	0.0011551635748097647	0.18555232909710803	0.4249709704376927
7	6	1	5798.0	1021.0	0.695444664922607	0.35382624036268423	3.991604784599199E-4	5.772697992358675E-5	1.663948327993328E-4	4.403512993489768E-4	0.1970254023734932	0.3177650086132736
8	9	2	7549.0	245.0	0.35237537682206393	0.3968174772620357	0.0019407093642390388	2.1234881375333655E-5	0.0	0.0011844529727692682	9.397165288366871E-4	0.24117593307548357
9	12	1	6386.0	1093.0	0.6924058389658382	0.3081396306911185	0.0010379960490429965	1.5387354255469374E-5	0.0	0.0011172636695946597	0.21798857622780446	0.2692426436878386
10	11	2	741.0	1006.0	0.06271654271319631	0.34087304852940076	7.769421540508834E-5	1.8525498070495776E-5	5.56667930045994E-5	4.779619248371226E-4	0.28166448566732794	0.48337729117005107

Table C.6: The non-copper concentrates which arrive daily for instance C.

c	j	$h_{j,c,t}$	α_c	$\theta_{1,c}$	$\theta_{2,c}$	$\theta_{3,c}$	$\theta_{4,c}$	$\theta_{5,c}$	$\theta_{6,c}$	$\theta_{7,c}$	$\theta_{8,c}$
1	S + 1	1000	0	0	0	0	0	0	0	1	0
2	S + 1	32.0	0.0	0.6362475269184792	0.02257379496193405	0.0013183890946644335	2.9845965535087666E-5	9.041446268270526E-5	3.115676850616224E-4	0.11355855380432417	0.40317663066941556
3	S + 1	30.0	0.0	0.22742059729210226	0.009603661119236375	0.0014231845273291314	4.474027015896369E-5	8.861199085794442E-5	8.606617059083683E-4	0.028568252525337144	0.3231628968022674
4	S + 1	10.0	0.0	0.40754428224669237	0.0	0.0	3.5667508659495156E-5	0.0	0.0	0.0	0.0

C.4. Data of SBCP instance D

Table C.7: Expected copper concentrates for SBCP instance D.

c	t'	j	$\overline{g_{m,j,c,t'}}$	α_c	$\theta_{1,c}$	$\theta_{2,c}$	$\theta_{3,c}$	$\theta_{4,c}$	$\theta_{5,c}$	$\theta_{6,c}$	$\theta_{7,c}$	$\theta_{8,c}$
1	0	1	13960.0	448.0	0.17003871621971953	0.2567798830132928	0.001132613157673963	3.588290077199732E-5	0.0	3.89251771615203E-4	0.18391073041338413	0.561672431273802
2	0	2	7675.0	1241.0	0.1249883722283784	0.1286097062515374	7.805724288560929E-4	4.2332596562691696E-5	0.0	8.262286490755191E-4	0.28934605820305503	0.23818391974623285
3	0	3	7002.0	362.0	0.28884769317561776	0.31164335505359836	0.0019821005427581024	2.9272428358281307E-5	1.8049391053467958E-4	8.608559980975405E-4	0.0038419954727158755	0.35151979514931736
4	0	4	8146.0	207.0	0.6893054635920309	0.22072033282830786	4.294484551856119E-4	1.8464254066903144E-5	1.3156570654848734E-4	2.263971027493371E-4	0.13888734552672685	0.20135204728395661
5	0	5	11157.0	551.0	0.2453211205509214	0.1388140131466227	0.001728642530183658	5.829495330693889E-5	9.822733224503581E-5	8.03097077692396E-5	0.09341354914413576	0.27461360803257856
6	1	1	8368.0	1014.0	0.48527898318182633	0.30966862163741843	0.001445659123864293	1.2733279842674029E-5	7.271809658320718E-5	0.0011551635748097647	0.18555232909710803	0.4249709704376927
7	6	2	5798.0	1021.0	0.695444664922607	0.35382624036268423	3.991604784599199E-4	5.772697992358675E-5	1.663948327993328E-4	4.403512993489768E-4	0.1970254023734932	0.3177650086132736
8	4	3	7549.0	245.0	0.35237537682206393	0.3968174772620357	0.0019407093642390388	2.1234881375333655E-5	0.0	0.0011844529727692682	9.397165288366871E-4	0.24117593307548357
9	12	1	6386.0	1093.0	0.6924058389658382	0.3081396306911185	0.0010379960490429965	1.5387354255469374E-5	0.0	0.0011172636695946597	0.21798857622780446	0.2692426436878386
10	11	2	741.0	1006.0	0.06271654271319631	0.34087304852940076	7.769421540508834E-5	1.8525498070495776E-5	5.56667930045994E-5	4.779619248371226E-4	0.28166448566732794	0.48337729117005107
11	13	3	8160.0	373.0	0.033235999651613155	0.2604559409103614	0.0010291331815335527	3.0439093137474696E-5	3.6895024588858746E-5	5.761826341004262E-4	0.16574257181869315	0.27923767863773374
12	27	1	2073.0	862.0	0.4913819814530637	0.2994143798546626	0.0012423019467767147	1.4162272422410154E-5	0.0	1.5505569126304556E-4	0.10056711659158354	0.41364359804453477
13	23	2	5270.0	1443.0	0.6252066008731575	0.12253946463975869	8.981283024187955E-4	4.1276531918168036E-5	0.0	0.0010255627543749293	0.05099853279482679	0.3275594863339609
14	27	3	1519.0	1443.0	0.40689034074270863	0.2067484145795626	6.725144104400573E-4	3.2448247044972334E-5	3.6910038129883872E-6	6.278524091524897E-4	0.26339000920512157	0.4490291374688676
15	30	4	10543.0	253.0	0.5193497933254405	0.2544148818890922	6.781532972131784E-4	4.503982190385099E-5	0.0	6.239992520972819E-4	0.2782007517514631	0.2835382486170498

Table C.8: The non-copper concentrates which arrive daily for instance D.

c	j	$h_{j,c,t}$	α_c	$\theta_{1,c}$	$\theta_{2,c}$	$\theta_{3,c}$	$\theta_{4,c}$	$\theta_{5,c}$	$\theta_{6,c}$	$\theta_{7,c}$	$\theta_{8,c}$
1	S + 1	1000	0	0	0	0	0	0	0	1	0
2	S + 1	32.0	0.0	0.21928481551326517	0.21416544636693283	4.1592004615343076E-4	6.899380326411973E-6	1.4673430618318922E-4	0.0012300680644086865	0.015336477491002953	0.294204172161606
3	S + 1	32.0	0.0	0.15165719975009348	0.13682322248791082	5.539844989171829E-4	4.415225637149414E-5	0.0	3.52949145447458E-4	0.13411452854574435	0.3660892772714125
4	S + 1	10.0	0.0	0.05593109469411624	0.0	0.0	7.917444591101817E-6	0.0	0.0	0.0	0.0

C.5. Data of SBCP instance E

Table C.9: The non-copper concentrates which arrive daily for instance E.

c	j	$h_{j,c,t}$	α_c	$\theta_{1,c}$	$\theta_{2,c}$	$\theta_{3,c}$	$\theta_{4,c}$	$\theta_{5,c}$	$\theta_{6,c}$	$\theta_{7,c}$	$\theta_{8,c}$
1	S + 1	1000	0	0	0	0	0	0	0	1	0
2	S + 1	36.0	0.0	0.6138607907800575	0.33581503315727707	8.085552158124025E-4	2.0818647696045746E-5	1.5362533676094797E-4	0.0010176019096367296	0.18360816151519999	0.20614580465932109
3	S + 1	32.0	0.0	0.4997748726214602	0.3434882414160816	6.769526701096945E-4	1.4942692518273655E-6	0.0	5.762170851756262E-4	0.057350780463013395	0.5593032329452856
4	S + 1	10.0	0.0	0.27901990591219444	0.0	0.0	4.815185568842242E-6	0.0	0.0	0.0	0.0

Table C.10: Expected copper concentrates for SBCP instance E.

c	t'	j	$\overline{g_{m,j,c,t'}}$	α_c	$\theta_{1,c}$	$\theta_{2,c}$	$\theta_{3,c}$	$\theta_{4,c}$	$\theta_{5,c}$	$\theta_{6,c}$	$\theta_{7,c}$	$\theta_{8,c}$
1	0	1	13960.0	448.0	0.17003871621971953	0.2567798830132928	0.001132613157673963	3.588290077199732E-5	0.0	3.89251771615203E-4	0.18391073041338413	0.561672431273802
2	0	2	7675.0	1241.0	0.1249883722283784	0.1286097062515374	7.805724288560929E-4	4.2332596562691696E-5	0.0	8.262286490755191E-4	0.28934605820305503	0.23818391974623285
3	0	3	7002.0	362.0	0.28884769317561776	0.31164335505359836	0.0019821005427581024	2.9272428358281307E-5	1.8049391053467958E-4	8.608559980975405E-4	0.0038419954727158755	0.35151979514931736
4	0	4	8146.0	207.0	0.6893054635920309	0.22072033282830786	4.294484551856119E-4	1.8464254066903144E-5	1.3156570654848873E-4	2.263971027493371E-4	0.13888734552672685	0.20135204728395661
5	0	5	11157.0	551.0	0.2453211205509214	0.1388140131466227	0.001728642530183658	5.829495330693889E-5	9.822733224503581E-5	8.03097077692396E-5	0.09341354914413576	0.27461360803257856
6	0	6	4580.0	168.0	0.291624461211845	0.10444340578717912	0.0019000276358941066	4.14195844774437E-5	0.0	0.001177566986038912	0.2835999716878887	0.20494324958468088
7	0	7	13888.0	463.0	0.5979737409177263	0.3154867680717483	0.0019874047899882175	5.299503152844013E-5	0.0	2.2717703788899545E-4	0.0571850525928811 5	0.5327609615217079
8	0	8	4404.0	484.0	0.460477653434157 64	0.13162416074461877	2.5608506012328436E-4	2.8328903605750995E-5	1.8251750839547992E-4	0.0014543197211264285	0.10593182165373545	0.21710801962493445
9	0	9	9977.0	778.0	0.022501513452284683	0.19604972509151458	0.001945880563368156	5.9347845258777975E-5	1.3232185334350336E-4	9.634329556798693E-4	0.10125214446704768	0.47317202119859614
10	0	10	13029.0	215.0	0.13395093454197848	0.08187094606119273	0.0016530515547834633	5.556366300143178E-5	6.765500334488727E-7	4.711831936886437E-4	0.1594825668746393	0.5380992705371465
11	29	1	1701.0	784.0	0.5396671940031859	0.2208446785645558	3.573198759204177E-4	5.864437787167624E-5	0.0	7.519987946250782E-4	0.1520104787858558	0.39146969236657325
12	26	2	12282.0	969.0	0.3877127468026742	0.09030378241081952	6.028901634020631E-4	5.741380779608724E-5	1.3714492631204537E-4	9.162339814883313E-4	0.07052451775924982	0.3429846045028013
13	14	3	15060.0	817.0	0.40754428224669237	0.2396106119399347	1.8380830106438738E-4	4.529969352940885E-5	0.0	6.510665085236548E-4	0.20626549145515913	0.3501492369003878
14	18	4	13720.0	46.0	0.2444425879953877	0.3396639905616926	0.0016878339986498739	2.6187389652463945E-7	0.0	4.7724301395208105E-4	0.16206882125142594	0.5580955479277375
15	29	5	6935.0	1096.0	0.6148439410780863	0.2724043152326981	6.50970090209479E-4	5.819990926998133E-5	0.0	9.521208150079381E-4	0.09446770455268659	0.4760545082551242
16	2	6	5457.0	1084.0	0.6492942219322949	0.09491612327921445	0.0013414412290163823	3.537208909291405E-5	0.0	2.795507145263164E-4	0.034164607391298986	0.45159559237968694
17	7	7	2092.0	685.0	0.03786315785998923	0.10635527560096218	1.5488918813269197E-4	3.7282400957476354E-5	4.6098656473909844E-5	0.001106880752544448	0.02734396857777812	0.29713280170631307
18	30	8	12418.0	1211.0	0.05593109469411624	0.05669404444697902	0.0014360090969213943	4.9079389680422915E-5	9.837353213376391E-5	1.4080730713951167E-4	0.15940576370841805	0.22672974360718962
19	28	9	8220.0	63.0	0.6124077065382231	0.3725725155239225	8.811196828673872E-5	2.5123766539175584E-6	5.025198882761118E-5	7.763522489647886E-4	0.28342207798472696	0.279897490831651
20	19	10	3367.0	1107.0	0.5256579107190078	0.26170738017817474	0.00189664152829989	5.2814592330302956E-5	0.0	3.498386210699549E-4	0.042020098192374934	0.42202457995871856
21	19	11	497.0	1032.0	0.33075279879606634	0.052999504642756975	5.071297687057466E-4	1.5035100512627715E-5	0.0	0.0010698462429556735	0.13024258066851688	0.501465687751003
22	37	1	11198.0	411.0	0.24955053458112167	0.18495174022170166	0.0014804035623128754	3.355597654734468E-5	3.7934160053218664E-5	2.3577787940850668E-4	0.27611166184556596	0.4529775803316598
23	40	2	10528.0	168.0	0.1435116463979041	0.09900060568038525	0.0016206676729089257	9.119394962567728E-6	2.5427493262224362E-5	1.581385893518446E-4	0.24590806847267174	0.4464321293885303
24	34	3	6889.0	1078.0	0.30821760680211463	0.08178699572559345	0.0012319031098268851	5.2460282813734334E-5	0.0	5.700205258883152E-4	4.921880189225236E-4	0.45364595213730635
25	55	4	10565.0	299.0	0.6754261856770654	0.3236716925068165	0.0017295045754087796	5.737453042407149E-5	6.283941249675381E-5	1.082732287383757E-4	0.10478549434793497	0.39154611743337675
26	51	5	5117.0	640.0	0.25697254358138416	0.3924125490280354	7.338825879732145E-5	3.672127686244973E-5	0.0	5.328301714878265E-4	0.20854688346652642	0.21164597642271987
27	55	6	301.0	656.0	0.5853933205033618	0.09241809447498568	0.0015279304546072362	2.9282212173592072E-5	0.0	2.639166778164546E-4	0.11152169064868725	0.2861210729977949
28	54	7	15620.0	1471.0	0.6217294658907725	0.11414171205155058	0.0011129419305534044	2.72664679718948E-5	0.0	0.0014043158120438505	0.26259223690140227	0.5134917001007198
29	47	8	12025.0	423.0	0.5453498397097957	0.2537197595325915	6.430178783501605E-4	4.494984784090452E-5	4.9920641623925265E-5	0.0010863133541187569	0.12584872926667898	0.3068029214560 48
30	32	9	11311.0	754.0	0.6315307568195456	0.259214827766231	0.001204979610785949	4.19485832522497E-5	4.8031474345375846E-5	9.354826937550293E-4	0.14721665333313642	0.3526667193811865
31	45	10	4664.0	815.0	0.3398588215568121	0.3128460405503276	0.0013382688498249152	2.08811634571409E-5	0.0	0.0011152664042792925	0.2629027541526534	0.30748546287458256
32	54	11	6000.0	333.0	0.5304931940354335	0.3079878120678261	0.0017238421852158361	1.3839631602310072E-5	0.0	3.883507860847146E-4	4.3027259950628727E-4	0.29865500971093695
33	34	12	8769.0	891.0	0.45453952718851265	0.22133722767695155	1.0861451573940455E-4	3.7173838153620006E-5	0.0	8.271987829804725E-5	0.291699153320518	0.3500757460477104
34	84	1	2875.0	712.0	0.12936461100567404	0.28664818937510383	8.027484586291066E-4	1.3465496239446769E-5	0.0	2.245079513484386E-4	0.2433252701678542	0.31618213861537553
35	79	2	9519.0	496.0	0.6805420279431091	0.18849777147888908	8.678447994672152E-4	3.7400533056955816E-5	0.0	5.725011704586867E-4	0.2738874134119105	0.40916822191879954
36	67	3	7965.0	120.0	0.4116120863106623	0.14321115866010212	8.860452209154284E-4	5.064988802134722E-5	3.0336272505827056E-5	0.001118190507473566	0.278494937357977	0.34317649350776397
37	69	4	9245.0	101.0	0.6578988131598 61	0.12595547086547704	0.0016494344175225632	2.9880783352595676E-5	0.0	5.01398021581993E-4	0.1747840814462245	0.3324764576238844
38	76	5	2224.0	871.0	0.285903199307652	0.30452135416158455	3.5793370467663535E-4	3.814400715138 73E-5	1.1263759927153185E-4	3.721526622879377E-4	0.11824954875314447	0.5661194940785389
39	66	6	2566.0	1076.0	0.49324915834663824	0.20720094798318242	4.037083144668818E-4	2.0538967654955078E-5	0.0	7.523782215897747E-4	0.15935274543966643	0.4583134270588869
40	66	7	2800.0	309.0	0.088266204851968	0.0528592247212124	2.947722499294059E-4	9.617878392230766E-6	0.0	9.80315689097683E-4	0.2134891288463723	0.5467222951263915
41	85	8	6313.0	1406.0	0.1538437819289439	0.24687498422052725	7.617515336472334E-4	2.9005381415655954E-5	0.0	0.00141044423848092	0.2257365374037753	0.268927254623615
42	79	9	15494.0	1103.0	0.4833457220597779	0.2696208571601767	0.0014431185775010907	8.48436943523324E-6	2.7392963411772774E-5	8.823129550800255E-4	0.2499956842774835	0.44693908909218616
43	68	10	10687.0	266.0	0.2704926561564325	0.2787818314504935	9.845553725061794E-4	6.533881634561765E-6	1.5286019907112018E-4	1.3949597008414168E-4	0.23088531973854468	0.4007415888967119
44	63	11	682.0	361.0	0.3117249275762517	0.07824114745186324	0.0017411417564300467	1.7350617029958877E-5	0.0	0.0012249683954947922	0.0877017057542281	0.36279238230541305
45	77	12	15921.0	756.0	0.41211696983017565	0.33745802056038465	1.9521220974978194E-4	4.6481029959561935E-5	4.3121393653917524E-5	0.0011185287156553984	0.20663927717377414	0.2372484904233098